

# **Magnesium stable isotopes as a proxy for biogeochemical processes in terrestrial environment**

Von der Fakultät für Mathematik, Informatik und Naturwissenschaften der RWTH  
Aachen University zur Erlangung des akademischen Grades eines Doktors der  
Naturwissenschaften

vorgelegt von

**Yi Wang**

Master – Environmental Engineering

Aus Hebei, China

Berichter: *Universitätsprofessor Dr. Erwin Klumpp*  
*Universitätsprofessor Dr. Andreas Schäffer*

Tag der mündlichen Prüfung: 12.11.2019

Diese Dissertation ist auf den Internetseiten der Universitätsbibliothek verfügbar.

# Abstract

Magnesium (Mg) is the fourth most abundant element in the Earth and plays a significant role in biological activities. Processes involved in Mg cycle can fractionate Mg stable isotopes, which makes Mg isotope systematics as a novel and promising proxy in biogeochemistry. To improve our understanding of Mg isotope fractionations in different ecosystems, studies performed in this doctoral work include: i) Mg isotope fractionation of plants under Mg deficient environment, ii) Mg isotope fractionation in agricultural system impacted by long-term anthropogenic soil practices, and iii) Soil Mg isotope signatures in the Atacama Desert as extreme environment of hyper-aridity.

Magnesium deficiency is detrimental to plant growth. However, an integrative tracer revealing plant responses to Mg deficiency is still lack. Here, Mg isotopes were used as an indicator with the hypothesis that Mg deficiency could promote increased Mg isotope fractionation in plants during uptake and subsequent translocation processes. To test this hypothesis, wheat plants (*Triticum aestivum*) were grown in a greenhouse under Mg-sufficient and deficient conditions, and Mg concentrations as well as their  $\delta^{26}\text{Mg}$  isotope compositions in roots, stems, leaves and spikes at different growth stages were analyzed. The results confirmed previous studies that plants were systematically enriched in heavy isotopes relative to the nutrient solution. This enrichment, however, was more pronounced under low-Mg supply, which was attributed to the increased contribution from active transport system for Mg. With crop growth, the  $\delta^{26}\text{Mg}$  of shoots shifted towards higher values under control but not under low-Mg supply, reflecting a reduced root-shoot upward translocation under low-Mg supply. At reproduction state, light Mg was redistributed into the stems. Overall, initial Mg supply can impact Mg isotope fractionation in plants and assessing the Mg isotope compositions of plant organs provides a useful indicator for different plant responses to Mg supply from external environment.

Liming is widely used to alleviate soil acidity in western and central Europe. However, its role on the cycling of Mg in arable soil-plant systems is still not fully clarified. In the second part of work, Mg concentrations and natural isotope compositions with soil profiles and its vegetation (winter rye) from a long-term agricultural experimental field with and without liming practice were systematically analyzed. The results showed that the  $\delta^{26}\text{Mg}$  signatures of the bulk Mg pool in soil in the studied Albic Luvisol displayed limited variation with depth and between trials. In contrast, the exchangeable Mg pool in soil exhibited an apparent increase of  $\delta^{26}\text{Mg}$  values along profile down to 50 cm depth, especially in limed field with more negative shift of  $\delta^{26}\text{Mg}$  than non-limed field. The observed enrichment of light Mg isotopes in upper layers mainly resulted from the lime deposition and plant uptake. An isotope-mixing model was used to assess the respective contribution from lime application and plant uptake to the Mg isotope compositions in the exchangeable Mg pool in soil. The results indicated that decades of liming practice presumably enhanced Mg uptake by vegetation when comparing limed and non-limed fields. However, no evidenced effects of liming on the isotope compositions of plant Mg were observed. Winter ryes grown on both limed and non-limed fields displayed identical Mg isotope compositions with roots and spikes enriched isotopically heavy Mg most.

Silicate weathering is confirmed to fractionate Mg isotopes in nature. However, how Mg isotopes are fractionated under extreme climate is still not reported. In the third part of this work, Mg isotope compositions of surface soil layer with altitudinal gradient (from 1300 to 2700 m a.s.l.) in the Aroma transect of the Atacama Desert were analyzed. The surface soil Mg in the Aroma transects is considered to stem from the mixing deposition of both oceanic aerosols and the Andean inputs. With elevation decreased, soils Mg became isotopically lighter. Enrichment of  $^{26}\text{Mg}$  at the site 2000 and 1300m a.s.l indicated another Mg input or loss process. The  $\delta^{26}\text{Mg}$  values in the pit soils from both the Aroma transect and well-known Yungay site were positively related to the weathering degree. Climatic aridity is assumed to change the Mg isotope signatures by influencing weathering degree. The present study for the first time reported soil Mg isotope composition in such hyper-arid environment and suggested a potential use of Mg isotopes to reconstruct the paleoclimatic changes.

To conclude, studies in this doctoral work provided novel and comprehensive insights into Mg isotope signatures and fractionations in biogeochemistry, and improved the knowledge of Mg stable isotopes as a proxy for biogeochemical processes in terrestrial environment.

# Zusammenfassung

Magnesium (Mg) ist das vierthäufigste Element der Erde und spielt eine wichtige Rolle bei biologischen Aktivitäten. Einige am Mg-Zyklus beteiligte Prozesse können Mg stabile Isotope fraktionieren, was die Mg Isotopensystematik zu einem neuen und vielversprechenden Proxy in der Biogeochemie macht. Um unser Verständnis der Mg-Isotopenfraktionierung in verschiedenen Ökosystemen zu verbessern, umfassen die in dieser Doktorarbeit durchgeführten Studien: i) Mg-Isotopenfraktionierung von Pflanzen unter Mg-Mangel, ii) Mg-Isotopenfraktionierung in landwirtschaftlichen Systemen, die von langfristigen anthropogenen Bodenpraktiken beeinflusst werden, und iii) Soil Mg-Isotopensignaturen in der Atacama-Wüste als extreme Umgebung von Hyperaridität.

Magnesiummangel behindert das Pflanzenwachstum. Ein integrativer Tracer, der Pflanzenreaktionen auf Mg-Mangel aufzeigt, fehlt jedoch noch. Hier wurden Mg-Isotope als Indikator mit der Hypothese verwendet, dass Mg-Mangel eine erhöhte Mg-Isotopenfraktionierung in den Pflanzen während der Aufnahme und nachfolgender Translokationsprozesse fördern könnte. Um diese Hypothese zu testen, Weizenpflanzen (*Triticum aestivum*) wurden in einem Treibhaus angebaut unter Mg-genügenden und mangelhaften Bedingungen, und Mg-Konzentrationen sowie deren  $\delta^{26}\text{Mg}$  Isotopenzusammensetzungen in Wurzeln, Stängeln, Blättern und Ähren in verschiedenen Wachstumsphasen wurden analysiert. Die Ergebnisse bestätigten die Resultate früherer Studien, dass Pflanzen im Verhältnis zur Nährlösung systematisch mit schweren Isotopen angereichert wurden. Diese Anreicherung war jedoch bei niedrigem Mg-Angebot stärker ausgeprägt, was auf den erhöhten Beitrag des aktiven Transportsystems für Mg zurückzuführen ist. Mit dem Pflanzenwachstum verlagerte sich die  $\delta^{26}\text{Mg}$  der Triebe in Richtung höherer Werte unter der Kontrolle, aber nicht unter niedriger Mg-Versorgung, was auf eine reduzierte Wurzelschussaufwärts-Translokation unter niedriger Mg-Versorgung hinweist. Im Reproduktionszustand wurde das leichte Mg in den Stielen neu verteilt. Insgesamt kann die anfängliche Mg-Versorgung die Mg-Isotopenfraktionierung in Pflanzen beeinflussen und die Beurteilung der Mg-Isotopenzusammensetzung von Pflanzenorganen ist ein nützlicher Indikator für unterschiedliche Reaktionen der Pflanze auf die Mg-Versorgung aus der externen Umgebung.

Kalkung ist in West- und Mitteleuropa weit verbreitet, um den Säuregehalt des Bodens zu verringern. Seine Rolle beim Kreislauf von Mg in Ackerbausystemen ist jedoch noch nicht vollständig geklärt. Im zweiten Teil der Arbeit Mg-Konzentrationen und natürliche Isotopenzusammensetzungen mit Bodenprofilen und deren Vegetation (Winterroggen) aus einem landwirtschaftlichen Versuchsfeld für Langzeitstudien mit und ohne Äscherpraxis wurden systematisch analysiert. Die  $\delta^{26}\text{Mg}$ -Signaturen des Bulk-Mg-Pools im Boden im untersuchten Albic-Luvisol zeigten eine begrenzte Variation mit der Tiefe und zwischen den Versuchen. Im Gegensatz dazu zeigte der bodenaustauschbare Mg Pool einen scheinbaren Anstieg der  $\delta^{26}\text{Mg}$ -Werte entlang des Profils bis in eine Tiefe von 50 cm, insbesondere im gekalkten Feld mit einer stärkeren negativen Verschiebung von  $\delta^{26}\text{Mg}$  als im ungekalkten Feld. Die beobachtete Anreicherung von leichten Mg-Isotopen in den oberen Schichten resultierte hauptsächlich aus der Kalkablagerung und der Pflanzenaufnahme. Ein Isotopenmischmodell wurde verwendet, um den jeweiligen Beitrag von Kalkanwendung und Pflanzenaufnahme zu den Mg-Isotopenzusammensetzungen im austauschbaren Mg-Pool zu bewerten. Die Ergebnisse zeigten, dass die jahrzehntelange Äscherpraxis vermutlich die Mg-Aufnahme durch die Vegetation beim Vergleich von kalkhaltigen und ungeklärten Feldern erhöht hat. Es wurden jedoch keine nachgewiesenen Effekte der Äsche auf die Isotopenzusammensetzung des Pflanzen-Mg beobachtet. Winterroggen, der sowohl auf kalkhaltigen als auch auf nicht kalkhaltigen Feldern angebaut wurden, zeigten identische Mg-Isotopenzusammensetzungen in den Wurzeln und Ähren, die am meisten mit isotopisch schwerem Mg angereichert waren.

Die Silikatverwitterung hat sich als Grund für die Fraktionierung von Mg-Isotopen in der Natur erwiesen. Wie Mg-Isotope unter extremen klimatischen Bedingungen fraktioniert werden ist unklar. Im dritten Teil dieser Arbeit wurden Mg-Isotopenzusammensetzungen von Oberflächenbodenschichten mit Höhengradienten (von 1300 bis 2700 m ü.d.M.) im Aroma-Transekt der Atacama Wüste analysiert. Es wird angenommen, dass das Mg in der oberen Bodenschicht im Aromatransekt aus der Mischabscheidung sowohl von ozeanischen Aerosolen als auch von den Andeneinträgen stammt. Mit abnehmender Höhe wurden die Böden Mg isotopisch leichter. Die Anreicherung von  $^{26}\text{Mg}$  am Standort Ar2000 und Ar1300 deutete auf einen weiteren Mg-Eingangs- oder Verlustprozess hin. Die  $\delta^{26}\text{Mg}$ -Werte in den tieferen Bodenschichten vom Aroma-Transekt als auch von Yungay als Vergleichsstandort waren positiv auf den Verwitterungsgrad bezogen. Es wird davon ausgegangen, dass die klimatische Trockenheit die Mg-Isotopensignaturen verändert, indem sie den Verwitterungsgrad beeinflusst. Die vorliegende Studie berichtete zum ersten Mal über die Zusammensetzung der Boden-Mg-Isotope in einer solchen hyperariden Umgebung und schlug eine mögliche Verwendung von Mg-Isotopen zur Rekonstruktion der paläoklimatischen Veränderungen vor.

Abschließend lieferten die Studien in dieser Doktorarbeit neue und umfassende Einblicke in die Signaturen und Fraktionierungen von Mg-Isotopen in biogeochemischen Prozessen in der terrestrischen Umwelt.

# Table of contents

Abstract .....	I
Zusammenfassung .....	II
Table of contents .....	III
1 General introduction .....	1
1.1 Magnesium cycling in the environment .....	1
1.2 Biological functions of Mg .....	2
1.3 Magnesium isotope geochemistry .....	4
1.4 Magnesium isotope fractionation law .....	6
1.5 Magnesium isotope fractionation in terrestrial environment .....	11
1.6 Objectives and scopes of the thesis .....	21
2 Materials and methods .....	23
2.1 Plant culture experiment in greenhouse .....	23
2.2 Field sites description and sampling .....	25
2.2.1 Berlin-Dahlem site .....	25
2.2.2 The Atacama Desert .....	29
2.3 Bulk soil digestion .....	30
2.4 Extraction of exchangeable Mg in soil .....	31
2.5 Digestion of plant material .....	32
2.6 Magnesium purification .....	32
2.7 Magnesium isotope measurement .....	34
2.8 Data calculation .....	36
3 Results and discussion .....	38
3.1 Wheat plants response to Mg deficiency reflected from Mg isotope fractionation .....	38
3.1.1 Plant biomass and Mg concentration in wheat under different Mg conditions .....	38
3.1.2 Magnesium isotope composition in plants .....	40
3.1.3 Magnesium isotope fractionation during root uptake .....	41
3.1.4 Magnesium isotope fractionation during translocation .....	49
3.1.5 Implications for Mg homeostasis in plant .....	53
3.2 Mg isotope signatures in an agricultural field with long-term liming practice .....	54

3.2.1	Magnesium concentrations, stocks and isotope compositions in bulk soil.....	54
3.2.2	Magnesium concentrations, stocks and isotope compositions in exchangeable pool .....	55
3.2.3	Magnesium concentration and isotope composition in plants .....	58
3.2.4	Magnesium isotope fractionation in the soil profile.....	60
3.2.5	Estimating Mg isotope composition in exchangeable Mg pool.....	67
3.2.6	Magnesium isotope fractionation in plants.....	71
3.3	Weathering degree in hyper-arid area of the Atacama Desert, Chile as revealed by magnesium isotope signatures.....	74
3.3.1	Magnesium isotope compositions of surface soil in the Aroma transect .....	74
3.3.2	Soil Mg isotope compositions along with profile at different elevation .....	82
4	Summary and conclusions .....	88
	Reference .....	92
	List of Figures.....	107
	List of Tables .....	111
	List of Abbreviations .....	112
	Acknowledgement .....	114

# Chapter 1

## General introduction<sup>1</sup>

### 1.1 Magnesium cycling in the environment

Magnesium (Mg) is located in the alkaline earth element group in the Periodic Table with an atomic number of 12. As the fourth most abundant element in the Earth (MgO = 25.5 wt%), the fifth most abundant element in the continental crust (MgO = 4.66 wt%) and the second most abundant cation in seawater (Mg = 0.128 wt%), Mg is widely distributed in the hydrosphere lithosphere and biosphere (Teng, 2017). Magnesium plays a vital role in both abiotic and biotic processes during Mg cycling because of its high mobility and redox state of stability (Mikkelsen 2010; Senbayram et al., 2016). Moreover, Mg cycling is also found to participate in the long-term regulation of CO<sub>2</sub> in atmosphere (Maroto-Valer et al., 2005; Saenger and Wang, 2014). Therefore, understanding the Mg cycling in biogeochemical environment is of great significance. Generally, Mg in the terrestrial environment originates primarily from the dissolution of silicate and carbonate minerals,

---

<sup>1</sup> Contains parts from “*Magnesium isotope fractionation reflects plant response to magnesium deficiency: a greenhouse study with wheat*, by Yi Wang\*, Bei Wu, Anne E. Berns, Ying Xing, Arnd J. Kuhn, and Wulf Amelung. Submitted to Plant and Soil, 2019” and “*Magnesium isotope signatures trace liming effects on crop nutrient uptake in long-term agricultural field trial*, by Yi Wang\*, Bei Wu, Anne E. Bern, Roland Bol, Frank Wombacher, Frank Ellmer, and Wulf Amelung. Submitted to Geoderma, 2019”

which is more typical in the riverine systems. A proportion of Mg released from silicate-weathering in the water-rock interface is then incorporated into the structure during the formation of secondary minerals like clay mineral, as well as taken up by vegetation and microbes as essential nutrient for a series of biological processes like photosynthesis and enzyme activities (Pasternak et al., 2010; Maschner 2011). Biotic effects on silicate weathering are well studied by reporting that the presence of microbes and vegetation can enhance Mg release process (Drever, 1994; Derry 2005; Balogh-Brunstad et al., 2008). The biologically-consumed part of Mg in the organisms after uptake is then released back to soil or catchment as plant debris (e.g. Bolou-Bi et al., 2012; Uhlig et al., 2017; Kimmig et al., 2018). Magnesium in the river body can be transported to lake and ocean, where Mg eventually reacts with dissolved carbonate ions from atmospheric CO<sub>2</sub> and deposits as carbonate minerals with reserved back into the lithosphere (e.g. Bolou-Bi et al., 2012; Opfergelt et al., 2014; Uhlig et al., 2017). In agricultural fields, cycling of Mg is also characterized as farming practices play an important role of controlling Mg composition in such a soil-plant system. Details on Mg cycling in an agricultural soil-plant system are outlined in Chapter 3.

### **1.2 Biological functions of Mg**

Magnesium is one of the essential macronutrients for plants, playing a key role in many biochemical processes. The role of Mg known most widely is its occurrence at the center of the chlorophyll molecule which is crucial for photosynthesis (Maguire and Cowan, 2002; Willows, 2007). Moreover, Mg is necessary for a series of enzyme activities and for protein synthesis, functioning as bridge element between enzymes and substrates, for example,

in the synthesis of ATP (Shaul, 2002; Marschner, 2011). Recent studies have also revealed a role of Mg in alleviating negative effects in adverse growth conditions, such as aluminum and manganese toxicity (Bose et al., 2011; Gransee and Führs, 2013), photooxidative damage (Cakmak and Kirkby, 2008), and heat stress (Mengutay et al., 2013). Therefore, Mg availability significantly affects both productivity and quality of agricultural and horticultural crops, especially under environmental stress conditions (Hermans et al., 2005; Verbruggen and Hermans, 2013). Nevertheless, Mg depletion is increasingly observed worldwide in forest and agriculture ecosystems, particularly in soils intensively fertilized with  $K^+$  and  $NH_4^+$ , or in soils with low pH (Cakmak and Yazici, 2010; Guo et al., 2016). The presence of other cations like  $K^+$ ,  $NH_4^+$ ,  $Ca^{2+}$  can strongly depress the Mg uptake due to the antagonistic effect (Barber, 1995). In addition, Mg bonds less strong to the soil particles compared with Ca, K and Na because its hydrated radius is substantially larger (Gransee and Führs, 2013). Thus the potential loss of Mg by leaching is relatively heavier in acidic soils.

When Mg is not supplied in sufficient amounts, a series of Mg-deficiency symptoms (e.g. yellowing of leaves, interveinal chlorosis) appear: the photosynthetic rate and the export of sucrose from leaves via phloem decreases, leading to accumulation of carbohydrates in source leaves and growth inhibition of sink organs. Consequently, a decline of both productivity and quality in crop plants may be observed at insufficient Mg supply (Verbruggen and Hermans, 2013; Chen et al., 2018). In order to obtain and preserve high contents of Mg in plants, in particular when Mg supplies are limited, plants have developed efficient physiological systems for Mg uptake and internal translocation (Hermans et al., 2013). For example, The MGT/MRS2 family of Mg transporters are discovered to be the



primary Mg transporters play a key role in active Mg uptake by plants, e.g. *Arabidopsis*, rice and maize (Gebert et al., 2009; Li et al., 2016; Li et al., 2001; Saito et al., 2013). On the other hand, Mg is also thought to enter into root cells via passive pathways such as non-selective cation channels (Marschner, 2011). However, our knowledge on how plants react to the Mg-deficient environment still remains to be improved.

### **1.3 Magnesium isotope geochemistry**

Magnesium has three stable isotopes in nature,  $^{24}\text{Mg}$ ,  $^{25}\text{Mg}$  and  $^{26}\text{Mg}$ , with relative natural abundances of approximate 78.99%, 10.00% and 11.01%, respectively (Rosman and Taylor, 1998). The relative mass difference between  $^{26}\text{Mg}$  and  $^{24}\text{Mg}$  could reach approximate 8%, which means a great potential to produce significant Mg isotope fractionations during geochemical and biological processes in the natural environment (An and Huang, 2014). To express the Mg isotope ratios and better relate isotope data of different laboratories, a delta notion ( $\delta$ ) in per mil (‰) unit is introduced with the definition of the deviation of the measured  $^{25}\text{Mg}/^{24}\text{Mg}$  or  $^{26}\text{Mg}/^{24}\text{Mg}$  ratios in unknown samples relative to those in the international reference material. In case of Mg, the material DSM3 (Dead Sea Magnesium, Galy et al., 2003) is commonly used as the isotope standard with a  $\delta$  value of zero. The Mg isotope composition of a given sample is therefore expressed following the equation:

$$\delta^x\text{Mg} (\text{‰}) = \left[ \frac{(\text{}^x\text{Mg}/^{24}\text{Mg})_{\text{sample}}}{(\text{}^x\text{Mg}/^{24}\text{Mg})_{\text{standard}}} - 1 \right] \times 1000 \quad (1.1)$$

where x represents the mass 25 or 26. Thus positive values of  $\delta^x\text{Mg}$  means the relative higher abundance of heavy Mg isotopes ( $^{25}\text{Mg}$ ,  $^{26}\text{Mg}$ ) in samples compared with the reference standard whose  $\delta^x\text{Mg}$  is 0‰ and negative values of  $\delta^x\text{Mg}$  indicate a relative enrichment of light Mg isotopes. Likewise, the increased values of  $\delta^{25}\text{Mg}$  or  $\delta^{26}\text{Mg}$  in products indicate an enrichment of  $^{25}\text{Mg}$  or  $^{26}\text{Mg}$  isotope in a certain compartment, and vice versa. Thus far, investigated terrestrial samples have shown an extent over 7‰ of Mg isotope fractionation in  $^{26}\text{Mg}/^{24}\text{Mg}$  ratio. The lightest Mg isotope composition has been found in carbonate with  $\delta^{26}\text{Mg}$  of -5.6‰, while the heaviest one belongs to the weathered silicates with  $\delta^{26}\text{Mg}$  up to 1.8‰ (see review of Teng 2017; Figure 1.1). In recent years, Mg isotope systematics have been used as a powerful tool to trace the elemental cycle in a variety of terrestrial systems (e.g. Bolou-Bi et al., 2012; Huang et al., 2012; Opfergel et al., 2014; Uhlig et al., 2017). A series of abiotic and biotic processes have been identified to induce Mg isotope fractionation, such as silicate weathering, water-rock interaction, plant growth, etc. (Schmitt et al., 2012), which will be introduced in the following parts.

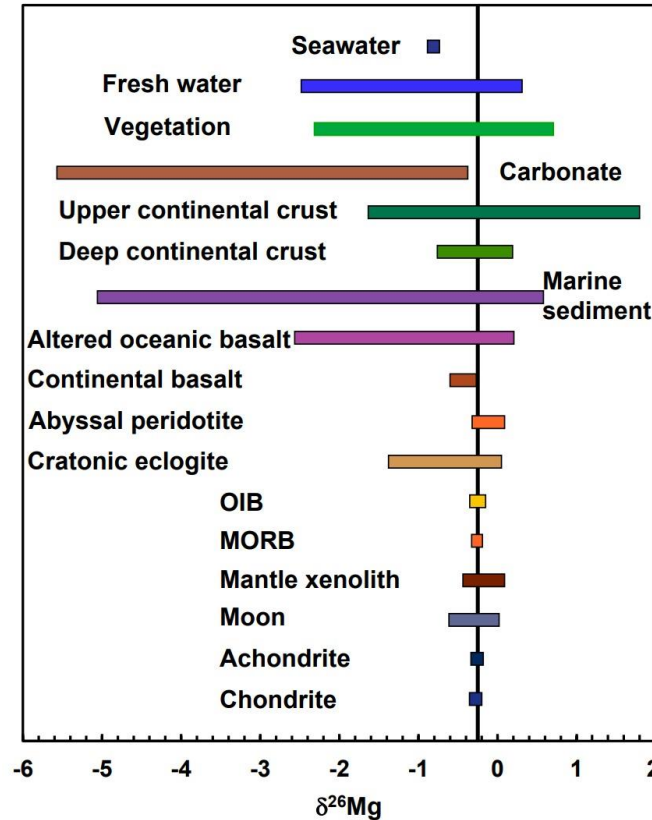


**Figure 1.1** Magnesium isotope signatures in major extraterrestrial and terrestrial reservoirs. The vertical line represents the average Mg isotope composition of the bulk Earth ( $\delta^{26}\text{Mg} = -0.25 \pm 0.04\text{‰}$ , 2SD), adapted from Teng (2017).

## 1.4 Magnesium isotope fractionation law

Isotope fractionation is always caused by different level of isotope-engagement in chemical reactions and/or physical processes, which can result in the variations of isotopic abundance by enriching one isotope in a compartment over another (Vanhaecke and Degryse, 2012). Practically, almost all variations of isotope ratios in natural samples are resulted from mass-dependent isotope fractionation, even though mass-independent fractionation in rare cases has also been observed (Buchachenko, 2013; Wiederhold,

2015), such as the nuclear volume effect (Wiederhold, 2015) and/or the instrumental mass discrimination during isotope ratio measurements induced by the existence of matrix elements (Wombacher et al., 2009). In this section only the theoretical basis for the type of mass-dependent isotope fractionation is briefly introduced (for details see Young et al., 2002; Dauphas and Schauble, 2016), using Mg as an example.

Mass-dependent fractionation in natural samples can be influenced by two types of process: equilibrium effects and kinetic effects. The equilibrium isotope effects are observed in two phases between which the bidirectional reaction proceeds at equal rates. In an equilibrium reaction process different binding energy between reactant and product is considered to control isotope fractionation with the heavier isotopes preferring to accumulate in compounds of stronger chemical bond (Johnson et al., 2004; Pokharel 2018). The kinetic isotope effects are resulted from different rates between light and heavy isotopes when participating in a unidirectional or incomplete chemical reaction, like adsorption, precipitation, synthesis and decomposition reactions. Different transport velocity or required energy due to mass discrimination in a kinetic reaction can induce the enrichment of lighter or heavier isotopes in product (Schauble, 2004; Bindeman et al., 2013). Figure 1.2 gives a schematic illustration of these two types of processes (Wiederhold, 2015). The partitioning of isotopes in kinetic or equilibrium reactions can be described by mass-dependent fractionation laws.

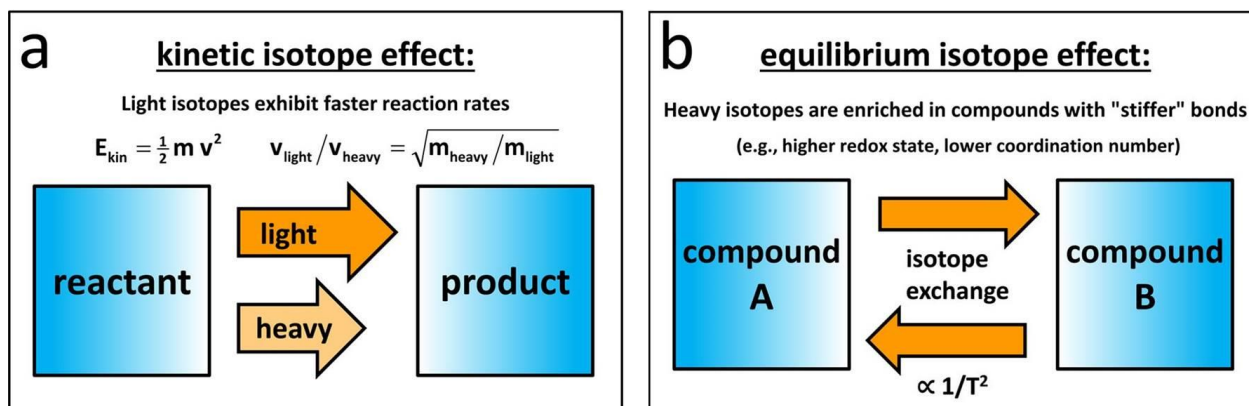


**Figure 1.2** Schematic illustration of kinetic (a) and equilibrium (b) isotope fractionation, adapted from Wiederhold (2015).

To express the isotope fractionation between two compounds in a certain reaction, the fractionation factor ( $\alpha$ ), defined as the quotient of isotope ratios in different compounds, is always used:

$$\alpha_{A-B} = \frac{R_A}{R_B} \quad (1.2)$$

where  $R$  is the isotope ratio of  $^{25}\text{Mg}/^{24}\text{Mg}$  or  $^{26}\text{Mg}/^{24}\text{Mg}$  in compounds A and B. In a kinetical reaction, A and B mean the reactant and product, and in an equilibrium process they can represent two phases.

To compare the isotope composition of A and B, the apparent difference of  $\delta$  values between A and B is used:

$$\Delta_{A-B} = \delta_A - \delta_B \quad (1.3)$$

The  $\Delta_{A-B}$  and the  $\alpha_{A-B}$  can be linked by a convenient approximate conversion with the following equation:

$$\Delta_{A-B} \approx 1000 \ln \alpha_{A-B} \quad (1.4)$$

For element with three or more stable isotopes, such as  $^{24}\text{Mg}$   $^{25}\text{Mg}$   $^{26}\text{Mg}$ , an exponential law can be used to describe the relationship between the fractionation factors ( $\alpha$ ) and the isotope ratios ( $^{25}\text{Mg}/^{24}\text{Mg}$  and  $^{26}\text{Mg}/^{24}\text{Mg}$ ) in a mass-dependent isotope fractionation:

$$\alpha_{^{25}\text{Mg}/^{24}\text{Mg}} = \left( \alpha_{^{26}\text{Mg}/^{24}\text{Mg}} \right)^\beta \quad (1.5)$$

For the kinetic mass-dependent isotope fractionation, the scaling factor  $\beta_{\text{kin}}$  follows the relation:

$$\beta_{\text{kin}} = \frac{\ln\left(\frac{m_{^{24}\text{Mg}}}{m_{^{26}\text{Mg}}}\right)}{\ln\left(\frac{m_{^{24}\text{Mg}}}{m_{^{25}\text{Mg}}}\right)} \quad (1.6)$$

where  $m$  is the atomic mass of corresponding Mg isotopes:  $^{24}\text{Mg}$  (23.985042),  $^{25}\text{Mg}$  (24.985837),  $^{26}\text{Mg}$  (25.982593) (Young and Galy, 2004).

Equilibrium mass-dependent isotope fractionation conforms to another fractionation law different from the kinetic process. The scaling factor in equilibrium process  $\beta_{\text{equil}}$  obeys the relation:

$$\beta_{\text{equil}} = \frac{\left( \frac{1}{m_{^{24}\text{Mg}}} - \frac{1}{m_{^{25}\text{Mg}}} \right)}{\left( \frac{1}{m_{^{24}\text{Mg}}} - \frac{1}{m_{^{26}\text{Mg}}} \right)} \quad (1.7)$$

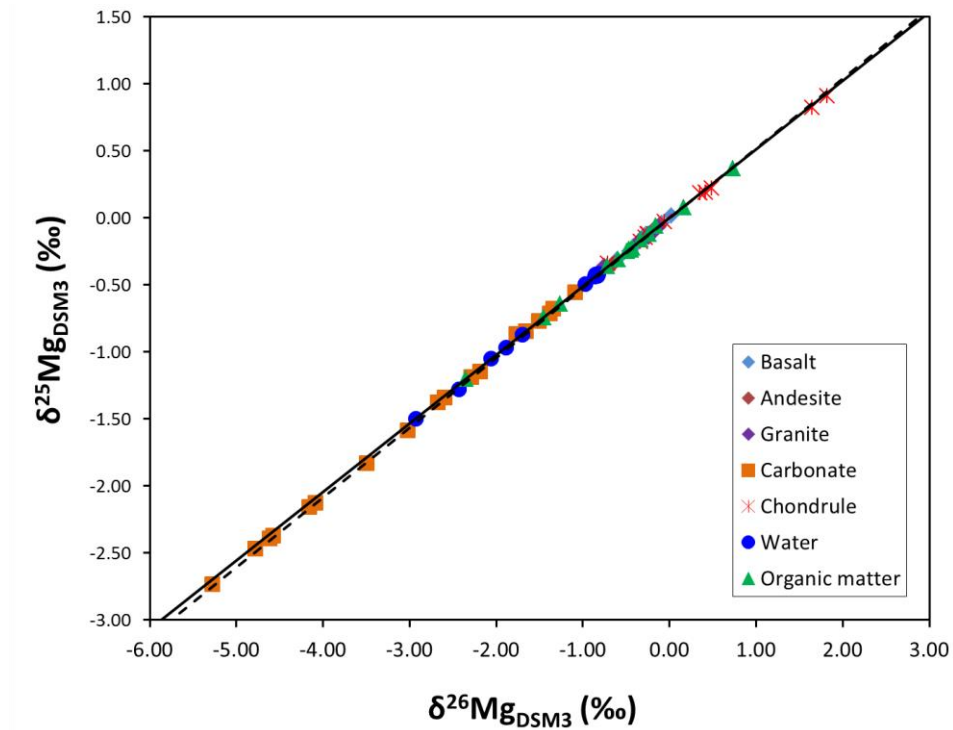


**Figure 1.3** Magnesium three-isotope plot from terrestrial and extraterrestrial samples. Solid line (slope = 0.511) and dashed line (slope = 0.521) represents the predicted kinetic and equilibrium fractionation laws, respectively. Data are adapted from Young and Galy (2004), Bolou-Bi et al. (2012), Teng (2017) and Uhlig et al. (2017).

The relative extent of mass-dependent fractionation can be predicted simply with this relationship using the scaling factor  $\beta$ . In the terms of Mg, the theoretical value of  $\beta$  in kinetic processes should be close to 0.511 as calculated with equation 2.5, and for equilibrium processes the theoretical value of should be close to 0.521 according to equation 2.6 (Young and Galy, 2004; Figure 1.3). According to this isotope fractionation law, in a mass-dependent isotope fractionation the value of  $\delta^{26}\text{Mg}$  of a sample should be

around twice as large as that of  $\delta^{25}\text{Mg}$ , with which the absence of mass-independent fractionation could be verified during the measurement.

### 1.5 Magnesium isotope fractionation in terrestrial environment

Since the Mg cycling in the environment introduced in section 1.1 are always associated with Mg isotope fractionations, Mg isotopes geochemistry have been used recently as a powerful tool to trace the elemental cycle in a variety of terrestrial (e.g. Bolou-Bi et al., 2012; Huang et al., 2012; Opfergel et al., 2014; Uhlig et al., 2017). A series of abiotic and biotic processes have been identified to induce Mg isotope fractionation, such as silicate weathering, water-rock interaction, plant growth, etc. (Schmitt et al., 2012). In this section, both abiotic and biotic processes that fractionate Mg stable isotopes in terrestrial environment are briefly reviewed.

Dissolution of primary minerals fractionates Mg isotopes by preferentially releasing light Mg isotopes into the dissolved phase, which has been demonstrated in olivine and biotite dissolution experiments by Wimpenny et al. (2010) and Ryu et al. (2016), respectively. Similar results are also reported in largescale riverine catchments. For example, Tipper et al. (2006, 2008) found that the Mg isotope composition of stream water draining silicate rocks is isotopically lighter than their bedrock, which has been confirmed by a number of studies (e.g. Brenot et al., 2008; Teng et al., 2010; Wimpenny et al., 2011; Bolou-Bi et al., 2012; Pogge von Strandmann et al. 2012; Mavromatis et al., 2014; Dessert et al., 2015; Uhlig et al., 2017; Kimmig et al., 2018). Kimmig et al. (2018) reviewed the Mg isotope compositions of river samples and their silicate bedrock in these studies and yielded an apparent difference between river and bedrock  $\Delta^{26}\text{Mg}_{\text{river-silicate}}$  of  $-0.42 \pm 0.17\text{‰}$  (2SE). In



addition to the primary mineral dissolution, secondary mineral formation is suggested to be another process resulting in depletion of heavy Mg isotopes in dissolved phase during silicate weathering. Neoformation of clay minerals are found to incorporate heavy Mg isotopes into their structure (e.g. Tipper et al., 2008; Opfergelt et al., 2012; Ryu et al., 2016). However, contrary phenomenon is observed by Opfergelt et al. (2014) who reported isotopically lighter clays than parent basalt. To explain these contradictory studies, Wimpenny et al. (2014) investigated experimentally the behavior of Mg isotopes during the formation of clay minerals and confirmed the general consensus of preferential incorporation of isotopically heavy Mg into secondary silicates. They also concluded that the Mg isotope composition of freshly formed clay minerals depends on the proportion of Mg partitioning into the octahedral sheet ('structural' Mg), and into the interlayer and surface sites.

Biotic-induced Mg isotope fractionations are also found in recent years as Mg plays an important role in a series of biological processes, such as activating enzymes, building chlorophyll molecules for photosynthesis. Young and Galy (2004) firstly reported the Mg isotope composition in chlorophyll molecules of spinach. The Mg isotope fractionation during chlorophyll formation from experimentally cultivated cyanobacteria is firstly observed by Black et al. (2006), showing a depletion of heavy Mg isotopes in the chlorophyll molecules relative to the growth medium ( $\Delta^{26}\text{Mg}_{\text{chlo-medium}} = -0.71 \pm 0.35\text{‰}$ , 2SD). Similar results are also reported later in wheat by Black et al. (2008) and in coccoliths by Ra et al. (2010). In contrast, Ra and Kitagawa (2007) found a contrary fractionation of Mg isotope with the chlorophyll molecules of marine red algae enriching heavy Mg isotopes by up to 0.74‰ higher than seawater, which is consistent with the observation in English ivy (Black et al., 2007). The Mg isotope signature in chlorophyll is

thus thought to be species-dependent. Laboratory experiments of higher plant growth have also been performed to investigate how plant growth induces Mg isotope fractionation. Hydroponic culture of wheat (*Triticum aestivum* L.) shows an enrichment of heavy Mg isotopes in plant relative to its nutrient solution, with  $\Delta^{26}\text{Mg}_{\text{plant-nutrient}}$  around 0.2‰ (Black et al., 2008). Other plant species like bulk rye grass, clover, and sugar maple grown under hydroponic condition or solid media (e.g. phlogopite, quartz/basalt) are also systematically enriched in heavy Mg isotopes in plants relative to their growth media (Bolou-Bi et al., 2010; Kimmig et al., 2018). These lab-scale works indicates that root uptake of Mg is the key process answering for the enrichment of heavy Mg isotopes in bulk plants. Likewise, such plant-induced Mg fractionations are also observed in vegetation grown naturally in field-scale ecosystems, such as grass (Tipper et al., 2010, 2012; Bolou-Bi et al., 2012; Opfergelt et al. 2014), spruce (Bolou-Bi et al., 2012), pine (Mavromatis et al., 2014; Uhlig et al., 2017), and rice (Gao et al., 2018). The available plant Mg isotope compositions in up-to-date published works are summarized in Table 1.1. In general, bulk plants have higher  $\delta^{26}\text{Mg}$  values of than their Mg source, yielding an average  $\Delta^{26}\text{Mg}$  value of  $0.41 \pm 0.14\text{‰}$  (2SE,  $n = 21$ ). In addition, Mg isotopes are also fractionated during translation within plant. Typically, Mg translocation from root to shoot depletes heavy Mg isotopes, resulting in root and leaf foliage being isotopically heaviest and lightest, respectively (see literatures in Table 1.1). Internal mobilization of Mg within plant is thought to control the Mg isotope compositions in leaves of different age as well as the seasonal change (Kimmig et al., 2018). Except for vegetation, recent studies show that microorganisms' activities can also fractionate Mg isotopes towards different directions (e.g. Oelkers et al., 2015; Fahad et al., 2016). For example, Pokharel et al. (2017, 2018) found that microcolonial fungus *Knufia petricola* prefers taking up heavy Mg

isotopes, and the fractionation exhibits a dependence on both the pH of the growth media and fluxes of Mg into or from the cells.

In recent years, Mg isotope systematics is also suggested to have the potential to characterize the changes of paleoclimate. Wimpenny et al. (2011) has found a close relationship between the  $\delta^{26}\text{Mg}$  and other weathering tracers including magnetic susceptibility, grain size and Na/Ca ratios from loess-paleosol sequence in the central Chinese Loess Plateau. The record of weathering changes with Mg isotopes exerts an implication for understanding the likely behaviors of East Asian Monsoon over the last 2.6 Ma. A similar work was also done by Huang et al., (2013) who investigated the Mg isotope compositions of world-wide loess deposits. Variations of  $\delta^{26}\text{Mg}$  among these loess deposits were found to be controlled by not only source rocks but also the eolian sorting and chemical weathering, both of which are sensitive to the paleoclimatic changes. This is supported by the negative correlation between  $\text{SiO}_2/\text{TiO}_2$  molar ratios and  $\delta^{26}\text{Mg}$  of loess samples of the same loess deposit. The  $\text{SiO}_2/\text{TiO}_2$  molar ratio is generally used as a proxy for the size of eolian particles. Higher  $\text{SiO}_2$  content is observed in the coarse fraction, whereas little variation of  $\text{TiO}_2$  content among different grain-size fractions. Therefore, eolian sorting would reduce the  $\text{SiO}_2/\text{TiO}_2$  molar ratio with increasing transport distance (details see Huang et al., 2013). All in all, Mg isotope geochemistry is a promising tool not only to track the weathering processes but also reconstruct paleoclimatic conditions. However, almost all of the studies on Mg isotope composition in ecosystems are concentrated in auriferous environment. There is still lack of information about Mg isotope composition in extreme conditions, such as region undergoing million years of hyper-aridity. The footprints of Mg isotopes are expected to help understand the paleoclimatic change and earth surface evolution in this type of region.

In summary, natural biogeochemical processes can leave marked and measurable changes of Mg stable isotopes, with which cycles of Mg in a natural ecosystem or critical zone can be elucidated. In this thesis, Mg stable isotopes are applied in different systems to track both abiotic and biotic processes.

**Table 1.1** Summary on Mg isotope compositions of plants and corresponding growth mediums in laboratory and field scales.

Plant species	Growth environment	Compartment	Plant $\delta^{26}\text{Mg}$ (‰ DSM3)	Nutrient Source	Source $\delta^{26}\text{Mg}$ (‰ DSM3)	$\Delta^{26}\text{Mg}_{\text{plant-source}}$ (‰)	Reference
Wheat (Triticum aestivum L.)	Hydroponic	Root	-0.15	Nutritive solution	-0.11	-0.04	Black et al. (2008)
		Leaf	0.11	Nutritive solution	-0.11	0.22	Black et al. (2008)
		Shoot	-0.07	Nutritive solution	-0.11	0.04	Black et al. (2008)
		Seed	0.61	Nutritive solution	-0.11	0.72	Black et al. (2008)
		Bulk plant	0.13	Nutritive solution	-0.11	0.24	Black et al. (2008)
Rye-grass	Pot Experiment (Phlogopite medium)	Shoot	-0.56	Phlogopite lixiviated Solution	-1.37	0.81	Bolou-Bi et al. (2010)
		Root	0.09	Phlogopite lixiviated Solution	-1.37	1.46	Bolou-Bi et al. (2010)
		Bulk plant	-0.50	Phlogopite lixiviated Solution	-1.37	0.87	Bolou-Bi et al. (2010)
Rye-grass	Hydroponic	Shoot	-0.72	Nutritive solution	-0.97	0.25	Bolou-Bi et al. (2010)
		Root	-0.66	Nutritive solution	-0.97	0.31	Bolou-Bi et al. (2010)
		Bulk plant	-0.71	Nutritive solution	-0.97	0.26	Bolou-Bi et al. (2010)
Clover	Pot Experiment (Phlogopite medium)	Leaf	-0.31	Phlogopite lixiviated Solution	-1.39	1.08	Bolou-Bi et al. (2010)
		Stem	-0.08	Phlogopite lixiviated Solution	-1.39	1.31	Bolou-Bi et al. (2010)
		Root	0.03	Phlogopite lixiviated Solution	-1.39	1.42	Bolou-Bi et al. (2010)
		Bulk plant	-0.18	Phlogopite lixiviated Solution	-1.39	1.21	Bolou-Bi et al. (2010)
Clover	Hydroponic	Leaf	-0.61	Nutritive solution	-0.97	0.36	Bolou-Bi et al. (2010)

## Chapter 1. General introduction

		Stem	-0.55	Nutritive solution	-0.97	0.42	Bolou-Bi et al. (2010)
		Root	-0.39	Nutritive solution	-0.97	0.58	Bolou-Bi et al. (2010)
		Bulk plant	-0.56	Nutritive solution	-0.97	0.41	Bolou-Bi et al. (2010)
Grass	Field	Bulk plant	-0.58	Rain/Shallow pore-water	-0.79	0.21	Tipper et al. (2010)
<i>Rumex scutatus</i>	Field	Leaf	-0.70	Soil pore-water (mean)	-0.90	0.20	Tipper et al. (2012)
Oxyria	Field	Leaf	-0.58	Soil pore-water (mean)	-0.90	0.32	Tipper et al. (2012)
<i>Rhododendron ferrugineum</i>	Field	Leaf	-0.64	Soil pore-water (mean)	-0.90	0.26	Tipper et al. (2012)
		Root	-0.09	Soil pore-water (mean)	-0.90	0.81	Tipper et al. (2012)
Agrostis	Field	Root	-0.39	Soil pore-water (mean)	-0.90	0.51	Tipper et al. (2012)
Norway Spruce	Field	Needle (avg)	-0.66	Soil exchangeable fraction	-0.47	-0.19	Bolou-Bi et al. (2012)
		Wood (avg)	-0.23	Soil exchangeable fraction	-0.47	0.24	Bolou-Bi et al. (2012)
		Root (avg)	0.51	Soil exchangeable fraction	-0.47	0.98	Bolou-Bi et al. (2012)
		Bulk plant	-0.32	Soil exchangeable fraction	-0.47	0.15	Bolou-Bi et al. (2012)
Hair-grass	Field	Leaf	-0.49	Soil exchangeable fraction	-0.47	-0.02	Bolou-Bi et al. (2012)
		Root	-0.22	Soil exchangeable fraction	-0.47	0.25	Bolou-Bi et al. (2012)
		Bulk plant	-0.41	Soil exchangeable fraction	-0.47	0.06	Bolou-Bi et al. (2012)

## Chapter 1. General introduction

Grass - Histic Andosol	Field	Bulk plant	-0.18	Soil exchangeable fraction in A1	-0.70	0.52	Opfergelt et al. (2014)
Grass - Histosol	Field	Bulk plant	-0.28	Soil exchangeable fraction in O1	-0.82	0.54	Opfergelt et al. (2014)
Grass - Brown Andosol	Field	Bulk plant	-0.18	Soil exchangeable fraction in A1	-0.68	0.50	Opfergelt et al. (2014)
Grass - Gleyic Andosol	Field	Bulk plant	-0.25	Soil exchangeable fraction in A1	-0.83	0.58	Opfergelt et al. (2014)
Grass - Vitrisol	Field	Bulk plant	-0.50	Soil exchangeable fraction in A	-0.84	0.34	Opfergelt et al. (2014)
<hr/>							
Sphagnum (north-slope)	Field	Bulk plant (live)	-0.57	N-slope Soil Solution (avg)	-0.39	-0.18	Mavromatis et al. (2014)
		Bulk plant (dead)	-0.57	N-slope Soil Solution (avg)	-0.39	-0.18	Mavromatis et al. (2014)
Sphagnum (south-slope)	Field	Bulk plant (live)	-0.49	S-slope Soil Solution (avg)	-0.60	0.11	Mavromatis et al. (2014)
		Bulk plant (dead)	-0.56	S-slope Soil Solution (avg)	-0.60	0.04	Mavromatis et al. (2014)
Larix gmelinii (north-slope)	Field	Needle (trough)	-0.51	N-slope Soil Solution (avg)	-0.39	-0.12	Mavromatis et al. (2014)
		Needle (mound)	-0.45	N-slope Soil Solution (avg)	-0.39	-0.06	Mavromatis et al. (2014)
Larix gmelinii (south-slope)	Field	Needle (trough)	-0.28	S-slope Soil Solution (avg)	-0.60	0.32	Mavromatis et al. (2014)
		Needle (mound)	-0.35	S-slope Soil Solution (avg)	-0.60	0.25	Mavromatis et al. (2014)
		Root	-0.31	S-slope Soil Solution (avg)	-0.60	0.29	Mavromatis et al. (2014)
		Stemwood	-0.45	S-slope Soil Solution (avg)	-0.60	0.15	Mavromatis et al. (2014)
		Branch	-0.30	S-slope Soil Solution (avg)	-0.60	0.30	Mavromatis et al. (2014)
		Seed	-0.37	S-slope Soil Solution (avg)	-0.60	0.23	Mavromatis et al. (2014)
Dwarf shrub ( <i>V. uliginosum</i> )	Field	Stem	-0.43	N-slope Soil Solution (avg)	-0.39	-0.04	Mavromatis et al. (2014)

## Chapter 1. General introduction

		Leaf	-0.57	N-slope Soil Solution (avg)	-0.39	-0.18	Mavromatis et al. (2014)
Dwarf shrub ( <i>V. vitis-idaea</i> )	Field	Stem	-0.68	N-slope Soil Solution (avg)	-0.39	-0.29	Mavromatis et al. (2014)
Lichen ( <i>Cladonia islandica</i> )	Field	Bulk plant	0.16	N-slope Soil Solution (avg)	-0.39	0.55	Mavromatis et al. (2014)
Lichen ( <i>Cladonia stellaris</i> )	Field	Bulk plant	-0.48	N-slope Soil Solution (avg)	-0.39	-0.09	Mavromatis et al. (2014)
Ponderosa Pine	Field	Needle	-0.72	Soil exchangeable fraction	-0.68	-0.04	Uhlig et al. (2017)
		Wood	-0.16	Soil exchangeable fraction	-0.68	0.52	Uhlig et al. (2017)
Jeffrey Pine	Field	Needle	-0.43	Soil exchangeable fraction	-0.68	0.25	Uhlig et al. (2017)
		Wood	-0.15	Soil exchangeable fraction	-0.68	0.53	Uhlig et al. (2017)
Manzanita	Field	Leaf	-0.33	Soil exchangeable fraction	-0.68	0.35	Uhlig et al. (2017)
		Wood	0.01	Soil exchangeable fraction	-0.68	0.69	Uhlig et al. (2017)
Whitethorn	Field	Leaf	-0.10	Soil exchangeable fraction	-0.68	0.58	Uhlig et al. (2017)
		Wood	0.16	Soil exchangeable fraction	-0.68	0.84	Uhlig et al. (2017)
Pine (mean)	Field	Bulk plant	-0.07	Soil exchangeable fraction	-0.68	0.61	Uhlig et al. (2017)
Tabonuco	Field	bark	-0.72	Soil pore-water	-0.77	0.05	Lara et al. (2017)



## Chapter 1. General introduction

Sugar Maple (seedling)	Pot Experiment (Quartz/Basalt medium)	Leaf	0.01	Quartz/Basalt exchangeable	-1.08	1.09	Kimming et al. (2018)
		Stem	-0.52	Quartz/Basalt exchangeable	-1.08	0.56	Kimming et al. (2018)
		Root	-0.02	Quartz/Basalt exchangeable	-1.08	1.06	Kimming et al. (2018)
		Bulk plant	-0.35	Quartz/Basalt exchangeable	-1.08	0.73	Kimming et al. (2018)
Sugar Maple	Field	Leaf (autumn)	-1.02	Soil solution	-0.65	-0.37	Kimming et al. (2018)
		Leaf (litter)	-1.09	Soil solution	-0.65	-0.44	Kimming et al. (2018)
		Leaf (spring)	-0.27	Soil solution	-0.65	0.38	Kimming et al. (2018)
		Stemwood	-0.70	Soil solution	-0.65	-0.05	Kimming et al. (2018)
		Root (fine)	-0.60	Soil solution	-0.65	0.05	Kimming et al. (2018)
		Seedling	-0.66	Soil solution	-0.65	-0.01	Kimming et al. (2018)
Rice	Field	Root	-0.67	Soil water (A horizon)	-1.65	0.98	Gao et al. (2018)
		Stem	-0.98	Soil water (A horizon)	-1.65	0.67	Gao et al. (2018)
		Leaf	-1.17	Soil water (A horizon)	-1.65	0.48	Gao et al. (2018)
		Grain	-0.67	Soil water (A horizon)	-1.65	0.98	Gao et al. (2018)
		Bulk plant	-0.92	Soil water (A horizon)	-1.65	0.73	Gao et al. (2018)

## 1.6 Objectives and scopes of the thesis

The overall aim of this doctorate study is to use the Mg stable isotopes as a new tool to provide a better understanding on the Mg-related biogeochemical processes in the terrestrial environment.

**The first objective** is to improve our understanding of plant response to Mg-deficient environment reflected by varied Mg isotope compositions of plants grown with low-Mg supply. This work was done in order to provide a further insight into the regulation of plant when living in the low-Mg environment, which may help guide the soil practices in the agricultural sustainable development as Mg deficiency has been an increasingly concerned problem in Europe. To achieve this aim, a pot experiment in greenhouse was performed to grow wheat plants along with the whole growth cycle under both Mg-sufficient (control, 1 mM  $\text{MgSO}_4$ ) and deficient (low-Mg, 0.05 mM  $\text{MgSO}_4$ ) conditions. The Mg concentrations and isotope compositions of individual plant organ (root, stem, leaf, and spike) at different growth stage were analyzed systematically.

**The second objective** is to evaluate the effect of anthropogenic practice on crop uptake of Mg in field-scale agricultural system with Mg isotope signatures. Natural Mg isotope signatures have been used to elucidate the Mg cycle in field-scale ecosystems (e.g. Bolou-Bi et al., 2012; Uhlig et al., 2017; Kimmig et al., 2018). However, to our knowledge most of these studies were performed in forest system or riverine catchment, and only Gao et al. (2018) investigated Mg isotope compositions in a paddy soil. The goals of this study are to investigate the Mg isotope compositions of soil-plant profile in an agricultural system with liming practice nearly 100 years and to evaluate how the liming practice

impact the uptake of Mg by crops. For this, soil samples were collected down to 1 m depth with six horizons in both limed and non-limed fields located in Berlin-Dahlem, Germany in the frame work of project “Sustainable Subsoil Management- Soil<sup>3</sup>” funded by the German Federal Ministry of Education and Research (BMBF). Magnesium isotope compositions in bulk soil and exchangeable pool in each horizon were analyzed. In addition, Mg isotope compositions in the grown winter rye in two field trials were also studied.

**The third objective** is to provide an insight of Mg isotope signatures in a field of hyper-aridity, the Atacama Desert in the frame work of project “Earth-Evolution at the dry limit (CRC 1211)” funded by German Research Foundation (DFG). Silicate weathering is confirmed to fractionate Mg isotopes in nature (Schmitt et al., 2012; Teng, 2017). However, how Mg isotopes are fractionated under extreme climate is still not reported. In this work, Mg isotope compositions of surface soil samples with altitudinal gradient (from 1300 to 2700 m a.s.l.), as well the pit soil samples collected from the Aroma transect were analyzed. The source of Mg in the soil and the weathering degree in such hyper-arid area was investigated with Mg stable isotopes as a tool. Results of this work improved our understanding on the weathering process in hyper-arid environment and provided supplementary insights into the Mg isotope signatures in the desert system on Earth which can help evaluate the  $\delta^{26}\text{Mg}$  of upper earth crust.

# Chapter 2

## Materials and methods<sup>1</sup>

### 2.1 Plant culture experiment in greenhouse

Summer wheat was selected as the model crop in this experiment. The seeds of summer wheat (*Triticum aestivum*) were germinated on a moistened filter paper in the dark for 48 h. Afterwards, well developed seedlings were selected and transferred into small pots filled with sterile quartz sand ( $\text{SiO}_2 > 98\%$ ,  $\text{MgO} < 0.1\%$ , w.) which had been pre-cleaned thoroughly with deionized water. In the first three days after transfer, the seedlings were watered without nutrient supply to allow them to adapt to the sand growing environment. Afterwards, the seedlings were placed into larger plastic pots containing sterile quartz sand (2 plants per pot) and cultivated in controlled climatic environments until harvest (day/night rhythm 16/8 h, temperature 24/18 °C, relative humidity 50-60%, and light intensity  $250 \mu\text{mol m}^{-2} \text{s}^{-1}$  supplied by fluorescent tubes). A modified  $\frac{1}{2}$  Hoagland nutrient solution (Table 2.1) was used to supply nutrients for plant.

---

<sup>1</sup> Contains parts from “*Magnesium isotope fractionation reflects plant response to magnesium deficiency: a greenhouse study with wheat*”, by Yi Wang\*, Bei Wu, Anne E. Berns, Ying Xing, Arnd J. Kuhn, and Wulf Amelung. Submitted to Plant and Soil, 2019” and “*Magnesium isotope signatures trace liming effects on crop nutrient uptake in long-term agricultural field trial*”, by Yi Wang\*, Bei Wu, Anne E. Bern, Roland Bol, Frank Wombacher, Frank Ellmer, and Wulf Amelung. Submitted to Geoderma, 2019”

Compared with sufficient Mg supply (1 mM  $\text{MgSO}_4$ ), 0.05 mM  $\text{MgSO}_4$  was supplied as the low-Mg condition. The nutrient solutions were supplied three times a day with 8 ml per pot each time via a pump controlled by a timer. To study Mg isotope fractionation along the growing stages, wheat plants were sampled when they were in boot, flowering, post-flowering and in maturity (39, 46, 67 and 82 days after seedling, respectively). Four pot replicates were set for both full-nutrient-supply (control) and low-Mg-supply at each sampling time. Upon sampling, wheat plants were carefully taken out of the pot together with the sand which was then washed off with running deionized water. The wheat plants were then separated into roots, stems, leaves, and spikes. At the stage of maturity, grains were isolated from their bran instead of full spikes as previous stages. All plant materials were lyophilized and milled to powder in a custom-designed ball mill (Collomix Viba 330, Collomix GmbH, Germany) using metal-free plastic bottles and tungsten carbide milling balls.

**Table 2.1** Chemical compositions of nutrient solution.

Chemicals	Concentration in control (mM)
$\text{KNO}_3$	2.5
$\text{Ca}(\text{NO}_3)_2 \cdot 4\text{H}_2\text{O}$	2.5
$\text{MgSO}_4 \cdot 7\text{H}_2\text{O}$	1
$\text{KH}_2\text{PO}_4$	0.5
Fe-EDTA	0.0896
$\text{MnCl}_2 \cdot 4\text{H}_2\text{O}$	0.01
$\text{CuSO}_4 \cdot 5\text{H}_2\text{O}$	0.001
$\text{ZnSO}_4 \cdot 7\text{H}_2\text{O}$	0.001
$\text{H}_3\text{BO}_3$	0.05
$\text{Na}_2\text{MoO}_4 \cdot 2\text{H}_2\text{O}$	0.0005

## 2.2 Field sites description and sampling

### 2.2.1 Berlin-Dahlem site

The studied long-term experimental field is located in Berlin-Dahlem, Germany (52° 28' N, 13° 18' E). Varieties of agricultural managements have been practiced since the year 1923 to investigate the effects of phosphorus fertilization, liming practice, and tillage depth on crop growth and yields. Vegetation practices in this field are performed as annual rotation with cereals and non-cereals crops planted alternately each year since 1967. The climate is semi-continental with the mean annual temperature of 9.9 °C and the average annual precipitation of 562 mm. According to the FAO (IUSS Working Group WRB, 2014), the soil at this experimental site is classified as Albic Luvisol being developed from glacial till. The soil texture here is sandy to loamy sand dominated by sand over 50%. More detailed information (soil pH, organic carbon, etc.) about the soil physicochemical properties in each layer to a depth of 100 cm was given in Table 2.2. Field map was shown in Figure 2.1 (Sümer, 2012).

The soil cores in this work were sampled down to 100 cm deep in six plots with phosphorus fertilizer (20 kg ha<sup>-1</sup> a<sup>-1</sup>) and farm yard manure (15 t ha<sup>-1</sup> a<sup>-1</sup>) fertilized and deeply ploughed (28 cm depth) before crop sowing. Among these six field plots, three were treated by lime addition biennially (Figure 2.1). In the year of 2014, lime product Dolokorn (contains 30% MgCO<sub>3</sub>) was applied with 920 kg ha<sup>-1</sup> in the limed plots, which corresponds to 79.3 kg ha<sup>-1</sup> Mg added into the limed plots. Field sampling were performed in the year of 2016 before liming practice in this year. Two soil cores were collected at random places in each plot. Each soil core was then separated into six layers (with depth 0-15 cm for Ap1 horizon, 15-30 cm for Ap2, 30-40 cm for Bw1 horizon, 40-50 cm for Bw2, 50-70 cm for Ael/Bt, 70-100

cm for Bt). Soil layers at same depth from these two soil cores were well mixed in the field. A soil sample collected below the soil development layer in the plot without any treatment was considered as the representative of parent material in this study. All of the soil samples were lyophilized to totally dry, ground in an agar mortar and passed through a 2 mm sieve before chemical and physical analyses.

Whole plants of winter rye (*Secale cereale*) grown in these plots were taken out when they were at the flowering stage. Afterwards, roots and shoots were separated and stored in the dry-ice box immediately in the field. In the lab, the shoots then the shoots were divided into stems, leaves and spikes and, together with the roots, were rinsed with Milli-Q water thoroughly to remove fine soil particles and ash. The cleaned plant samples were then immediately frozen at -20 °C and freeze-dried. The dried plant tissues were milled to powder using a custom-made ball mill equipped with metal-free plastic bottles and tungsten carbide milling balls (Collomix Viba 330, Collomix GmbH, Germany). Both soil and plant samples were well stored for further analysis.

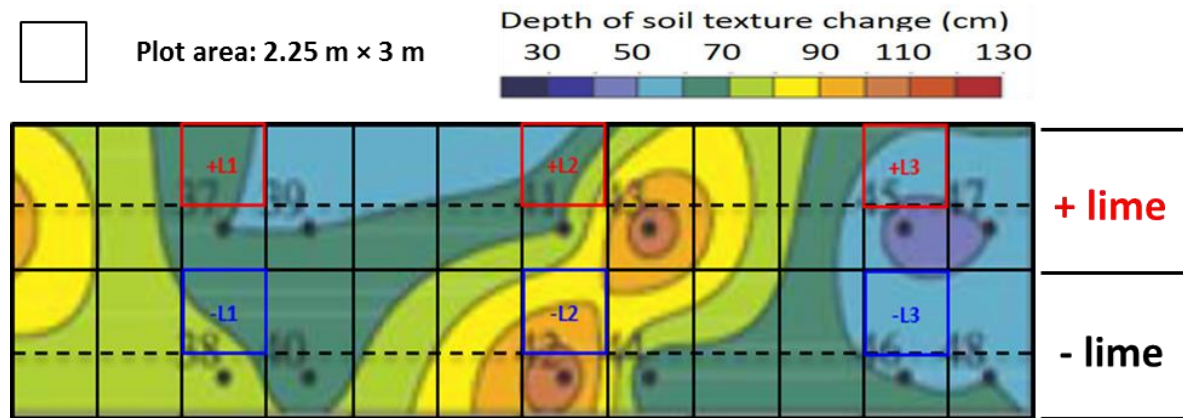


**Figure 2.1** Field map and sampling plots with soil texture change profile (Sümer 2012). The red and blue squares represent the studied plots with or without liming practice, respectively. Subsoil displayed great heterogeneity in this investigated field.



**Table 2.2** Physicochemical properties of soil samples along with depth in two investigated fields. Data are given as mean value  $\pm$  SE of three field replicates.<sup>a</sup>The mass ratio of soil:water = 1:2.5

soil management	layer depth (cm)	bulk density (g cm <sup>-3</sup> )	pH <sup>a</sup> (CaCl <sub>2</sub> )	SOC (%)	Total N (%)	C/N	SiO <sub>2</sub> (%)	Al <sub>2</sub> O <sub>3</sub> (%)	Fe <sub>2</sub> O <sub>3</sub> (%)	particle-size distribution		
										sand (%)	silt (%)	clay (%)
non-limed	0-15	1.42 $\pm$ 0.06	4.76 $\pm$ 0.40	0.64 $\pm$ 0.06	0.06 $\pm$ 0.00	11.6 $\pm$ 0.1	83.9 $\pm$ 2.4	3.52 $\pm$ 0.09	0.86 $\pm$ 0.02	71.9 $\pm$ 1.3	18.4 $\pm$ 0.8	8.9 $\pm$ 0.3
	15-30	1.62 $\pm$ 0.08	4.59 $\pm$ 0.19	0.59 $\pm$ 0.03	0.05 $\pm$ 0.00	11.4 $\pm$ 0.3	86.0 $\pm$ 1.9	3.42 $\pm$ 0.07	0.80 $\pm$ 0.05	72.3 $\pm$ 1.3	19.9 $\pm$ 2.2	8.2 $\pm$ 0.5
	30-40	1.64 $\pm$ 0.11	4.57 $\pm$ 0.11	0.27 $\pm$ 0.06	0.03 $\pm$ 0.00	9.6 $\pm$ 1.6	77.2 $\pm$ 8.0	4.65 $\pm$ 1.42	1.35 $\pm$ 0.85	66.6 $\pm$ 4.8	19.8 $\pm$ 2.3	12.9 $\pm$ 5.3
	40-50	1.64 $\pm$ 0.09	4.85 $\pm$ 0.14	0.13 $\pm$ 0.02	0.02 $\pm$ 0.01	7.7 $\pm$ 1.4	80.9 $\pm$ 6.1	5.01 $\pm$ 1.82	1.63 $\pm$ 1.08	62.9 $\pm$ 6.7	23.0 $\pm$ 9.8	15.4 $\pm$ 5.5
	50-70	1.69 $\pm$ 0.09	5.21 $\pm$ 0.48	0.12 $\pm$ 0.05	0.01 $\pm$ 0.00	9.3 $\pm$ 2.4	78.4 $\pm$ 0.6	4.81 $\pm$ 1.35	1.41 $\pm$ 0.60	64.9 $\pm$ 5.7	19.2 $\pm$ 2.5	14.9 $\pm$ 6.8
	70-100	1.81 $\pm$ 0.03	5.78 $\pm$ 0.33	0.09 $\pm$ 0.01	0.01 $\pm$ 0.00	6.8 $\pm$ 0.8	77.0 $\pm$ 6.3	5.50 $\pm$ 1.05	1.97 $\pm$ 0.69	51.2 $\pm$ 3.5	25.2 $\pm$ 7.8	22.4 $\pm$ 2.5
limed	0-15	1.38 $\pm$ 0.05	5.44 $\pm$ 0.44	0.50 $\pm$ 0.03	0.04 $\pm$ 0.00	11.6 $\pm$ 0.4	84.7 $\pm$ 3.2	3.53 $\pm$ 0.23	0.85 $\pm$ 0.03	68.8 $\pm$ 3.5	21.6 $\pm$ 2.5	10.2 $\pm$ 1.5
	15-30	1.59 $\pm$ 0.13	5.58 $\pm$ 0.45	0.50 $\pm$ 0.10	0.04 $\pm$ 0.01	11.4 $\pm$ 0.4	84.8 $\pm$ 2.8	3.59 $\pm$ 0.25	0.86 $\pm$ 0.08	68.2 $\pm$ 1.0	22.9 $\pm$ 1.6	10.4 $\pm$ 0.8
	30-40	1.82 $\pm$ 0.10	5.94 $\pm$ 0.42	0.18 $\pm$ 0.07	0.02 $\pm$ 0.01	9.2 $\pm$ 1.1	84.0 $\pm$ 4.5	4.17 $\pm$ 1.23	0.99 $\pm$ 0.43	70.7 $\pm$ 4.1	19.8 $\pm$ 5.7	10.6 $\pm$ 2.3
	40-50	1.85 $\pm$ 0.15	6.06 $\pm$ 0.34	0.10 $\pm$ 0.04	0.01 $\pm$ 0.01	6.8 $\pm$ 0.6	81.5 $\pm$ 2.3	4.84 $\pm$ 1.79	1.43 $\pm$ 1.01	66.9 $\pm$ 7.1	18.0 $\pm$ 1.1	13.6 $\pm$ 7.7
	50-70	1.77 $\pm$ 0.15	6.29 $\pm$ 0.24	0.09 $\pm$ 0.03	0.02 $\pm$ 0.00	5.8 $\pm$ 0.1	79.6 $\pm$ 7.2	5.56 $\pm$ 0.83	1.99 $\pm$ 0.46	63.0 $\pm$ 4.2	17.0 $\pm$ 0.2	19.9 $\pm$ 3.1
	70-100	1.79 $\pm$ 0.19	6.64 $\pm$ 0.78	0.08 $\pm$ 0.02	0.01 $\pm$ 0.00	5.4 $\pm$ 0.1	81.5 $\pm$ 2.2	5.87 $\pm$ 0.29	2.05 $\pm$ 0.27	49.9 $\pm$ 8.9	22.5 $\pm$ 3.1	24.1 $\pm$ 3.2

### 2.2.2 The Atacama Desert sites

The Atacama Desert located in the Northern Chile bordering Peru, along the western border of South America continent between the central Andes to Pacific Ocean is one of the driest region on Earth (Tapia et al., 2018). One of the study areas is the Aroma transect, located in the north part of Quebrada Aroma, northern Chile between the Central Depression of the Atacama Desert and the western side of the Andean Precordillera (from 1300 m a.s.l. 19°46'51.7"S, 69°40'13.8"W to 2700 m a.s.l. 19°31'37.9"S, 69°22'48.8"W; Figure 2.2). This is a flat lying planation surface developed on alluvial gravels of the Upper El Diablo Formation. The gravel deposits of the El Diablo Formation consists of ignimbritic (pumice, quartz, ash), andesitic and basaltic–andesitic fragments which forms the surface of the Aroma transect (Pinto et al., 2004; Evenstar et al., 2009). An increasing gradient of aridity is observed from arid sites at the high elevation down to hyper-arid sites at low elevation with the decrease in precipitation (Houston and Hartley, 2003). Typically, the annual amount of precipitation in Aroma transect is less than 2 mm/yr, resulting in an absence of any vegetation, although annual plants can be observed briefly at higher elevations near Pre-Cordillera when the water availability is sufficient.

Soil samples were taken in 2016 along with an altitudinal gradient (from high to low: 2700, 2600, 2400, 2000, 1600, and 1300 m a.s.l.) in the Aroma transect from the Pre-Cordillera towards the Central Depression (Figure 2.2). In each site the surface samples (0-10 cm,  $n = 3$ ) were collected by horizons with three depths (0-1, 1-5, 5-10 cm). In addition, pit soils with profile were also sampled in the site at the elevation of 2540, 2350, 2000, and 1320 m, respectively ( $n = 1$ ). Also, pit samples down to 3 m depth were also taken in the other studied site Yungay region (1000 m a.s.l.; 24°03'48.9"S, 69°52'50.7"W;  $n = 1$ ; Figure

2.2) which is located in the southeast of Antogagasta city and considered as the typical core of the Atacama Desert with extreme hyper-aridity and devoid of any vegetation (Bull et al., 2016). All of the samples were homogenized by sieving (< 2 mm) and well-stored in sealed tubes, and delivered to Germany for the labwork.

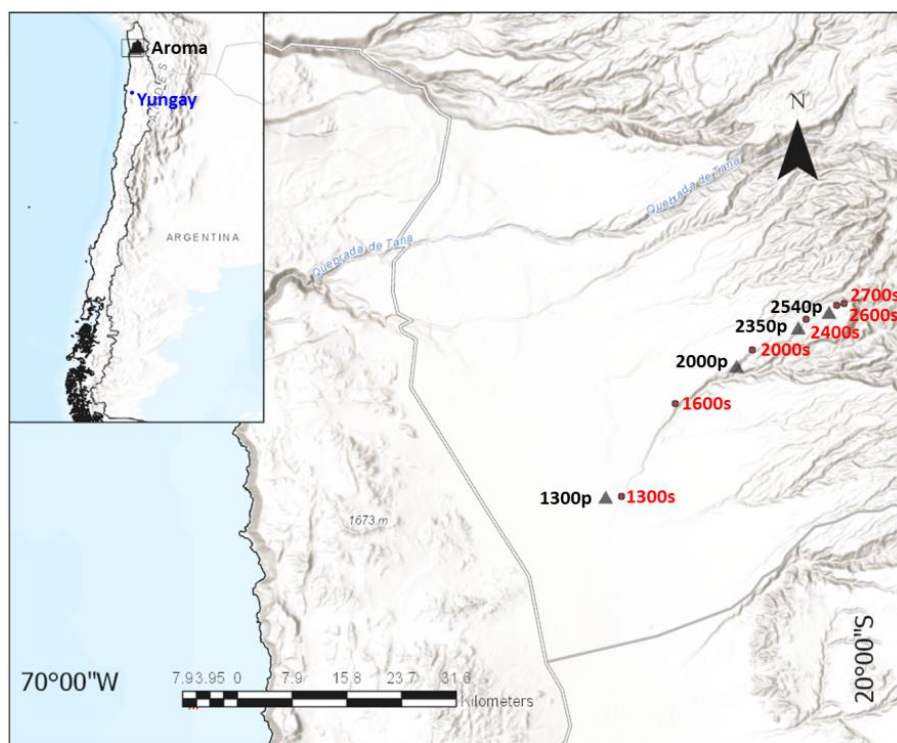


**Figure 2.2** Location of the investigated sites in the Atacama Desert. The exact sampling sites are marked in the map with labels. The red labels indicate the sites where surface samples (end with s) were collected and black ones represent the pit samples (end with p). The Yungay site is marked with blue color.

### 2.3 Bulk soil digestion

Two methods of soil digestion were applied in this doctorate work. The first one is pressurized microwave-assisted acid digestion system (turboWAVE 1500, MILESTONE, Italy) by adding samples with distilled concentrated  $\text{HNO}_3$  (68%) and  $\text{H}_2\text{O}_2$  (30%) into PFA

vessels and reacting in a closed cylinder under 225 °C. The obtained Mg from soil sample was regarded as bulk soil Mg ( $Mg_{\text{bulk}}$  soil) in this work. A certified in-house soil standard was used to validate the analytical procedure with respect to Mg concentration.

The second one is the HF-H<sub>2</sub>SO<sub>4</sub> method used for the total digestion of all the soil samples from the Atacama Desert. This type of total digestion was performed at the Institute for Biodiversity and Ecosystem Dynamics, in the University of Amsterdam with a HF-H<sub>2</sub>SO<sub>4</sub> method. In brief, approximate 100 mg soil samples were weighed accurately into a platinum crucible. The crucible was heated at 800 °C for about half an hour to destroy the soil organic matter. Afterwards, 2 ml of 2 M H<sub>2</sub>SO<sub>4</sub> acid and 5 ml of 48% HF acid were mixed in the soil and heated at 400 °C until the SO<sub>3</sub> fume stopped escaping. After the crucible cooled down, 10 ml of 2 M HCl acid were added to dissolve the content by heating to about 120 °C until no more residues were observed. Then the solution was transferred into a volumetric flask of 50 ml by rinsing the crucible and cover three times furthermore. The solution in the flask was adjusted to 50 ml volume with Milli Q water finally and well stored for elemental analysis with ICP-MS and Mg purification.

### 2.4 Extraction of exchangeable Mg in soil

The exchangeable pool of Mg in soil is usually defined as the Mg pool that is available for plant uptake (Metson, 1974). For extraction of the exchangeable Mg pool in soil ( $Mg_{\text{exch}}$ ), the method of NH<sub>4</sub>-Acetate extraction was applied from the procedure reported before (Bolou-Bi et al., 2012; Gao et al., 2018). Thirty milliliter 1 M NH<sub>4</sub>-Acetate (pH=7) solution was added to 3 g soil and the mixture was shaken at a speed of 220 oscillation per minute for 2 h. The sample suspension was then centrifuged at 6000 g for 15 min. The

supernatant was collected and filtered through 0.45  $\mu\text{m}$  using a PTFE filter. The filtrate was then transferred into a Savillex PFA vial and drying down. Ultrapure  $\text{HNO}_3$  and  $\text{H}_2\text{O}_2$  were used to remove organic matters after repeated dry-down and re-dissolve process. The residue was finally dissolved into 1M  $\text{HNO}_3$  solution for Mg purification.

### 2.5 Digestion of plant material

About 50 mg plant materials were weighed in Teflon tubes and digested in a mixture of 3 ml ultrapure  $\text{HNO}_3$  (68%) and 1 ml  $\text{H}_2\text{O}_2$  (30%, p.a.) in a pressurized microwave-assisted acid digestion system (turboWAVE, Milestone Srl, Italy). Elemental concentrations were analyzed by inductively coupled plasma mass spectrometry (ICP-MS, Agilent 7900, Germany).

### 2.6 Magnesium purification

Purified Mg solution is required before the sample introduction into the MC-ICP-MS for isotope analysis. Separation of Mg from matrix elements can be accomplished through cation exchange chromatography column. The cation exchange resin Bio-Rad AG50W-X8 (200-400 mesh) was used for column chemistry following the modified procedures of Teng et al. (2007) and Wombacher et al. (2009) as shown in table 2.3. The  $\text{HNO}_3$  column and HCl column repeated several times according to the concentration of matrix elements, especially K, Ca, Ti, Zn, and Mn as their eluted peak is close to or partially overlapped with Mg peak. After column chemistry Mg elutes were dried down and re-dissolved into 2 ml 1 M distilled  $\text{HNO}_3$  solution for check of Mg recovery and purity. Full recovery of Mg (over 95% given the analytical uncertainty) and the absence of matrix elements (ratio of

matrix concentration to Mg concentration less than 5% according to Teng et al., 2010) were validated by analyzing their concentrations in the eluted Mg solution with Inductively Coupled Plasma Mass Spectrometry (ICP-MS).

**Table 2.3** Procedure for Mg purification.

	Eluent	Volume (ml)
<b>Step 1: HNO<sub>3</sub> column</b>		
Resin conditioning	1M HNO <sub>3</sub>	20
Sample loading	1M HNO <sub>3</sub>	0.5-1.5
Matrix eluate	1M HNO <sub>3</sub>	18
Mg-cut_HNO <sub>3</sub> eluate <sup>a</sup>	1M HNO <sub>3</sub>	18
<b>Step 2: HCl column</b>		
Resin conditioning	0.4M HCl	20
Sample loading	0.4M HCl	0.5-1.5
Matrix eluate	0.4M HCl	2
	95%acetone-0.5M HCl	10
	0.4M HCl	2
	0.4M HCl	2
<b>Step 3: HCl column Collection of Mg ("Mg-cut")</b>		
Mg-cut_HCl eluate <sup>b</sup>	2M HCl	12
<sup>a</sup> Dried down and re-dissolved in 0.4 M HCl for Step 2.		
<sup>b</sup> Dried down, re-dissolved in 1 M HNO <sub>3</sub> for MC-ICP-MS analysis.		

## 2.7 Magnesium isotope measurement

Measurement of Mg isotope ratios in samples throughout the doctorate work was performed using a Multi Collector-Inductively Coupled Plasma Mass Spectrometry (MC-ICP-MS, Nu Plasma II, Nu Instruments Ltd., UK). For isotope ratio measurement the purified Mg samples were diluted to a concentration of  $800 \mu\text{g L}^{-1}$  with 0.3 M distilled  $\text{HNO}_3$  solution, and then introduced into the source region through a twister quartz spray chamber with helix (Glass Expansion, West Melbourne, Australia) equipped with a glass nebulizer (MicroMist, Glass Expansion) at an uptake rate of ca.  $100 \mu\text{L min}^{-1}$ . A wet plasma at low-resolution mode was used to well separate the three Mg isotopes simultaneously with a typical signal intensity of  $^{24}\text{Mg}$  around 6.0-7.0 V. A strategy of standard-sample-standard bracketing was applied to correct instrumental mass bias by ensuring the difference of Mg concentrations between the standard and the samples within 5%. In the doctorate work, Mg isotope standard NIST SRM 980 was used as the bracketing standard. Therefore, the measured Mg isotope ratios of a sample were calculated using  $\delta$  notation with equation 2.1:

$$\delta^x\text{Mg}_{\text{sample } i} (\text{‰}) = \left\{ \frac{(\text{}^x\text{Mg}/^{24}\text{Mg})_{\text{sample } i}}{\frac{(\text{}^x\text{Mg}/^{24}\text{Mg})_{\text{NIST980 } i} + (\text{}^x\text{Mg}/^{24}\text{Mg})_{\text{NIST980 } i+1}}{2}} - 1 \right\} \times 1000 \quad (2.1)$$

where x represents 25 or 26. The analytical uncertainty of the MC-ICP-MS was determined based on repeated measurement of NIST SRM 980 over 48 h, giving 0.07‰ for  $^{25}\text{Mg}/^{24}\text{Mg}$  and 0.09‰ for  $^{26}\text{Mg}/^{24}\text{Mg}$  (2SD), respectively. The three-isotope-plot was used to assess any possible interference that induces mass-independent fractionation

and showed that the analyzed isotope ratios were mass-dependent fractionation following the exponential law (e.g. Figure 2.3). The accuracy of isotope analysis was validated by repeated measurements of the in-house soil standard and the certified NIST1575a Pine Needles standard for soil and plant samples, respectively (Table 2.4).

**Table 2.4** Magnesium concentrations and isotope compositions of the in-house soil standard and the NIST SRM 1575a Pine needles for the sample validation.

Standard	[Mg] <sup>a</sup> (mg kg <sup>-1</sup> )		N <sup>b</sup>	δ <sup>26</sup> Mg <sup>a</sup> (‰)		N <sup>b</sup>
	mean	SE		mean	SE	
in-house soil standard	4588	20	4	-0.15	0.03	4
NIST SRM 1575a Pine Needles	1046	37	4	-0.76	0.04	4

<sup>a</sup> extracted by pressurized microwave-assisted acid digestion (see Section 2.2). <sup>b</sup> the number of measured samples.

In order to avoid the reported heterogeneity of Mg isotope composition in NIST SRM 980 (Galy et al., 2003) and better compare our results with others, the measured δ<sup>26</sup>Mg values relative to NIST SRM 980 were converted to that relative to the world widely used standard material DSM3 (Dead Sea Magnesium, Galy et al., 2003) using the equation outlined in Young and Galy (2004):

$$\delta^{26}\text{Mg}^{\text{DSM3}} = \delta^{26}\text{Mg}_{\text{NIST980}}^{\text{sample}} + \delta^{26}\text{Mg}_{\text{DSM3}}^{\text{NIST980}} + 0.001\delta^{26}\text{Mg}_{\text{NIST980}}^{\text{sample}} \delta^{26}\text{Mg}_{\text{DSM3}}^{\text{NIST980}} \quad (2.2)$$

The Mg isotope composition of our NIST SRM 980 relative to DSM3 ( $\delta^{26}\text{Mg}_{\text{DSM3}}^{\text{NIST980}}$ ) was measured at Institute of Geology and Mineralogy at University of Cologne, Germany. Here we greatly appreciate Dr. Frank Wombacher for his help in measuring δ<sup>26</sup>Mg of our NIST SRM 980 relative to the DSM3 ( $\delta^{26}\text{Mg}_{\text{DSM3}}^{\text{NIST980}} = 3.91 \pm 0.09\text{‰}$ , 2SD, n = 12). Therefore,



the  $\delta^{26}\text{Mg}$  values of our samples throughout the doctorate work are reported relative to the DSM3.

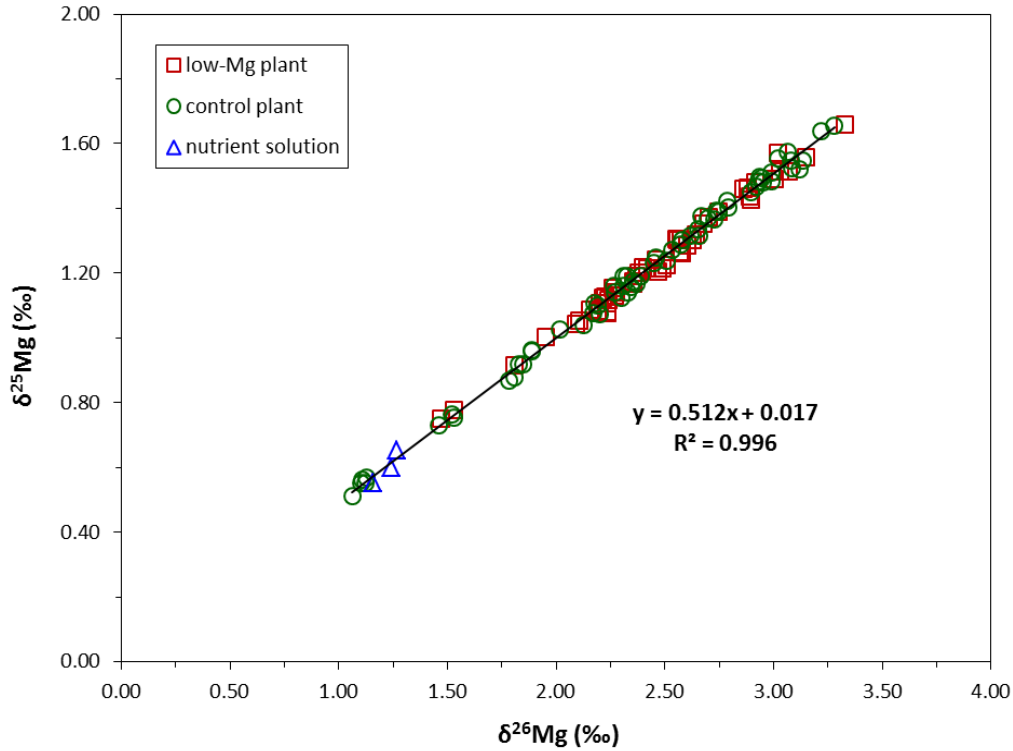


**Figure 2.3** Three-isotope plot for measured values of  $\delta^{26}\text{Mg}$  and  $\delta^{25}\text{Mg}$  (relative to NIST SRM980) of plant samples in the control group (green circles) and low-Mg supply pots (red squares), as well as those of nutrient solution relicates (blue diamonds). The fitting equation with a slope of 0.512 ( $R^2 = 0.996$ ) indicates the absence of mass-independent isotope fractionation during analytical sessions (Data from section 3.1).

## 2.8 Data calculation

The Mg isotope composition in shoot ( $\delta^{26}\text{Mg}_{\text{shoot}}$ ) and/or of the bulk plant ( $\delta^{26}\text{Mg}_{\text{plant}}$ ) was calculated using the following mass balance equation:

$$\delta^{26}\text{Mg}_{\text{shoot or plant}} (\text{‰}) = \sum (\delta^{26}\text{Mg}_i \times \frac{m_i c_i}{\sum m_i c_i}) \quad (2.3)$$

where  $m_i$  (in gram) was the dry biomass of the respective plant organ  $i$  (root, stem, leaf, and spike/seed),  $C_i$  (in  $\mu\text{g g}^{-1}$ ) the corresponding concentration of Mg, and  $\delta^{26}\text{Mg}_i$  (‰) the isotope ratio of plant organ  $i$ .

The apparent difference of Mg isotope composition between different Mg pools was calculated using:

$$\Delta^{26}\text{Mg}_{\text{A-B}} = \delta^{26}\text{Mg}_{\text{A}} - \delta^{26}\text{Mg}_{\text{B}} \quad (2.4)$$

The statistical analyses were carried by OriginPro 2015 (Version b9.2.272). Here, we used pair-sample t-test to evaluate the significant difference ( $P < 0.05$ ), within each soil block, among six soil layers, plant organs, and between exchangeable Mg pool in soil and plants. The effect of liming practice on Mg concentration and isotope composition of both soil and plant samples was tested with two-sample t-test between limed and non-limed fields, following an F-test used for the equal variance checking ( $P < 0.05$ ).

# Chapter 3

## Results and discussion

### 3.1 Wheat plants response to Mg deficiency reflected by Mg isotope fractionation<sup>1</sup>

#### 3.1.1 Plant biomass and Mg concentration in wheat under different Mg conditions

An insufficient Mg supply did not significantly reduce dry biomass of the wheat plants (Figure 3.1). Similarly, the root to shoot ratios in biomass did not show significant differences between low-Mg supply and the control group either (Figure 3.1). However, Mg concentrations were much lower in all wheat organs under low-Mg conditions compared with the control group (Figure 3.2). Specifically in leaves, where Mg was concentrated most, low-Mg supply drastically hindered Mg accumulation, particularly on the stage of maturity with a decrease in Mg concentration by 14 folds (Figure 3.2, Table 3.1). Mg was increasingly consumed during the growth in control. In contrast, the low-Mg variant considerably limited Mg accumulation in its leaves through the entire growth period (Figure 3.1, Table 3.1).

---

<sup>1</sup> Contains parts from “*Magnesium isotope fractionation reflects plant response to magnesium deficiency: a greenhouse study with wheat*”, by Yi Wang\*, Bei Wu, Anne E. Berns, Ying Xing, Arnd J. Kuhn, and Wulf Amelung. Submitted to Plant and Soil, 2019,

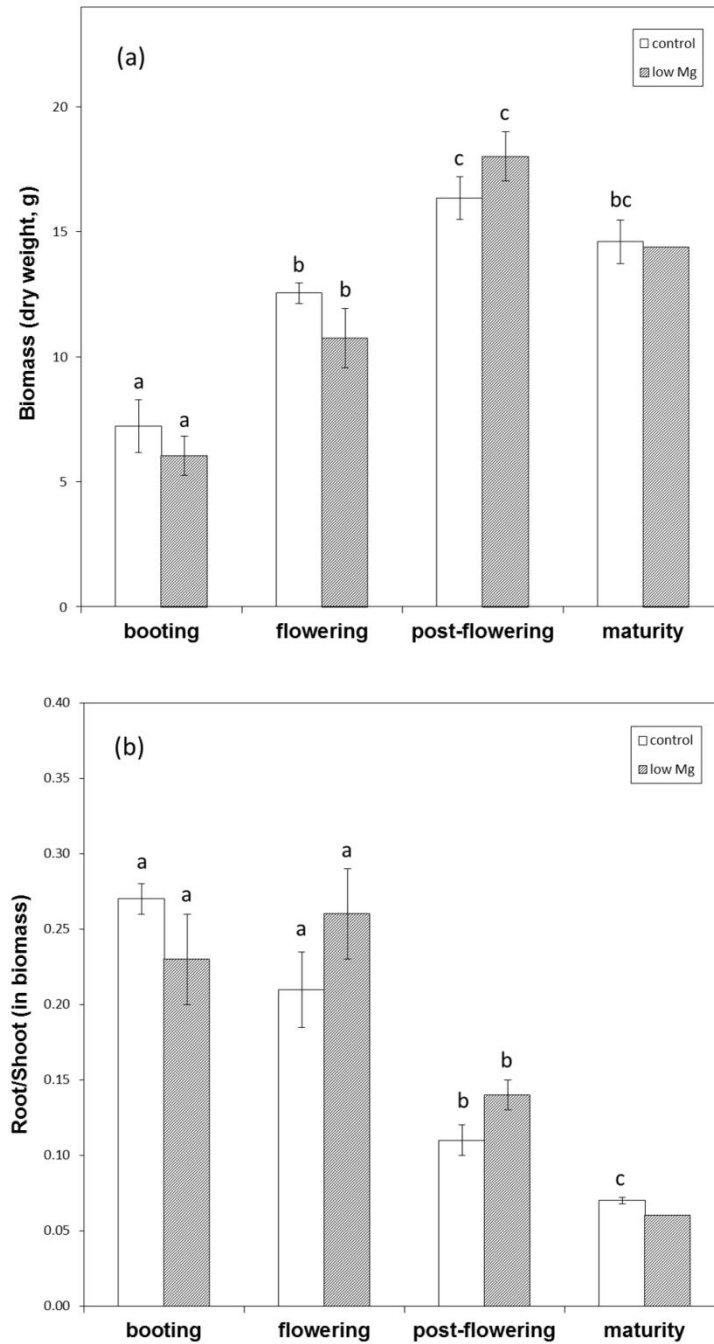


**Figure 3.1** Plant biomass in dry weight (a) and root/shoot ratio of biomass (b) at different growth stages with different Mg supply: control, 1 mM Mg; low Mg, 0.05 mM Mg. Data are given as the mean  $\pm$  SE of four pot replicates. Different letters denote statically significant differences between two groups at the same growth phase using ANOVA with OriginPro 2015 ( $p < 0.05$ ).

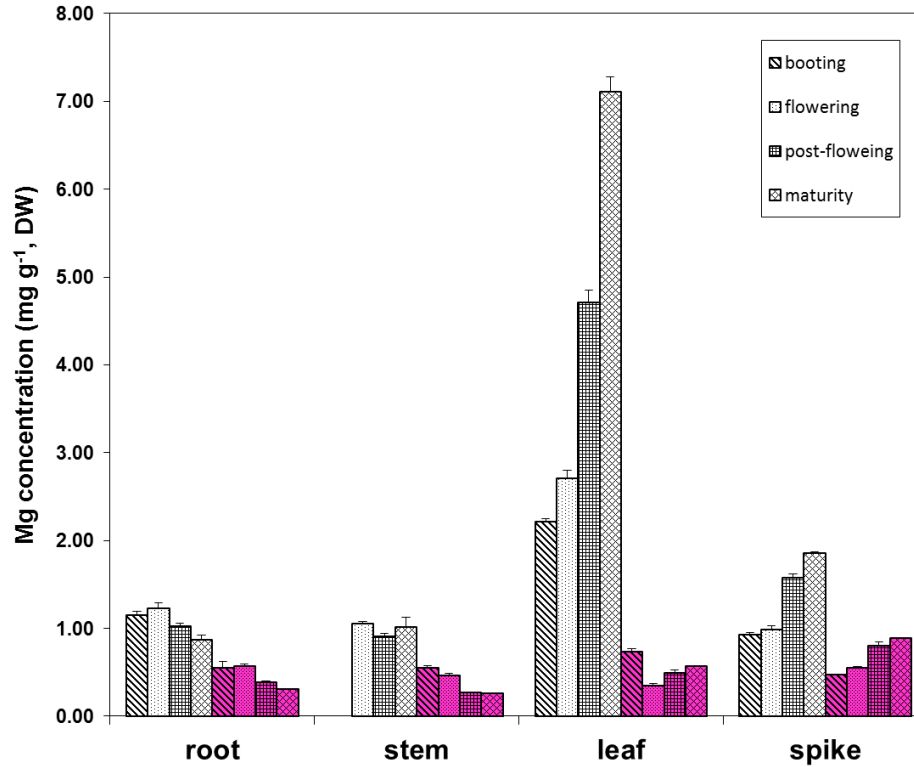


**Figure 3.2** Mg concentration in each plant tissue along the growth stage at different Mg supply: control, 1 mM Mg (white); low-Mg supply, 0.05 mM Mg (purple). Patterns represent different growth stage (from left to right: booting, flowering, post-flowering, maturity). Data are given as the mean  $\pm$  SE of four pot replicates.

### 3.1.2 Magnesium isotope composition in plants

Compared with the nutrient solution ( $\delta^{26}\text{Mg} = -2.70 \pm 0.03\text{‰}$ ), wheat plants exhibited heavier Mg isotope compositions in both control ( $\delta^{26}\text{Mg}$  ranges from -2.08 to -1.28‰) and low-supply ( $\delta^{26}\text{Mg}$  ranges from -1.73 to -1.54‰), showing preferential uptake of heavy Mg isotopes, regardless of the amounts of Mg supplies. However, the apparent difference in Mg isotope compositions between the plant and the nutrient solution varied under the two Mg-supply conditions. With sufficient Mg supply, Mg isotope compositions of the wheat plant became increasingly heavier during the growth, indicating that the degree of Mg

isotope fractionation was pronounced by the rising consumption of Mg from the unlimited Mg pool in the nutrient solution (Figure 3.3). The enrichment of heavy Mg isotopes in plants during growth was observed to go along with the increases in  $\delta^{26}\text{Mg}$  of each individual plant organ (Figure 3.4). However, when Mg in the nutrient solution was limited for plant growth, Mg isotope composition of the wheat plant did not change during the growth, with a relatively constant  $\delta^{26}\text{Mg}_{\text{plant}}$  value about -1.60‰ which was always 1.10‰ heavier than the nutrient solution (Figure 3.3). The constant  $\delta^{26}\text{Mg}_{\text{plant}}$  values were not reflected by  $\delta^{26}\text{Mg}$  of each individual plant organ, the variation of which were rather organ-specific during growth (Figure 3.4). Nevertheless, regardless of Mg conditions in the nutrient solution, the leaves exhibited the lightest Mg isotope compositions among all plant organs (Figure 3.4). In addition, the aboveground shoot always showed lower  $\delta^{26}\text{Mg}$  values compared with the roots on all growing stages, indicating that the processes of in-plant translocation from the roots to aboveground parts were in favor of lighter Mg isotopes.

### **3.1.3 Magnesium isotope fractionation during root uptake**

Discrepancies of Mg isotope compositions were found not only between plants and nutrient solution, but also between bulk plants as well as plant organs of the two groups with different Mg supply. These discrepancies can be explained with the uptake process of Mg into plant by roots which is mainly controlled by i) adsorption of Mg on the root cell wall and ii) cross-membrane transport of Mg into cytoplasm. Previous studies have shown that Mg is firstly adsorbed on root surface before entering root epidermal cells (Komaï, 1962; Kuhn et al., 2000), a process which leads to adsorbed Mg being isotopically heavier than that in soil because of Mg binding into organic functional groups (Bolou-Bi et al., 2010;

Pokharel et al., 2018) and which ultimately results in plants exhibiting heavier Mg isotope compositions than the soil where they grow. Our results demonstrated that preferential adsorption and uptake of heavier Mg isotopes did not depend on Mg availability in the growth media. However, the extent of this fractionation may vary depending on both Mg availability and growing stages (Figure 3.3). The adsorbed Mg can further be loaded to cross the plasma membrane of root epidermal cells either actively by Mg-specific transporters (Li et al., 2001; Gebert et al., 2009) or passively via non-selective cation channels or the K/Ca-channels in the plasma membrane (Hermans et al., 2013; Tang and Luan, 2017). The two cross-membrane transport systems, active and passive transport, however have different preferences for Mg isotopes, because they transport Mg either associated to organic compounds or as free Mg ions, respectively (Marschner, 2011). As a result, the degree Mg isotope fractionation between cytoplasm Mg and adsorbed Mg is dependent on the participation of the two cell membrane-located functional transport systems, which can vary based on both the vegetal demand and Mg availability in the growth media, as observed in rice (Cai et al., 2012; Tanoi et al., 2014). In the present study, the isotope composition of the bulk plant thus reflected a combination of the two above-mentioned transport systems: When Mg was supplied in sufficient amounts in the control group, the  $\delta^{26}\text{Mg}$  values of the bulk plants increased during growth, supporting previous studies on plant-induced Mg fractionation, apparently due to increasing involvement of active transporter systems with advanced plant development (Black et al., 2008; Bolou-Bi et al., 2010; 2012). Conversely, under low-Mg supply, the bulk plants displayed a limited variation in their Mg isotope composition along their life cycle (Figure 3.3). Active transporter systems are dominating from the beginning for low Mg supply of the plant, which can be ascribed to the competition between Mg and other nutrient cations,

in particular for K and Ca, for binding sites onto the root surface (Ding et al., 2006; Gransee and Führs, 2013; Li et al., 2018). The antagonistic effects appear to suppress the passive transport systems, thus reducing the extent of overall isotope fractionation in the plant during growth. In addition, the higher  $\delta^{26}\text{Mg}$  values in the roots under low-Mg conditions than in those of the control (Figure 3.4), also present with earlier suggestions that Mg deficiency may trigger the high-affinity uptake strategy for Mg, because it is required to actively transport Mg across the cell membrane against the chemical gradient (Marschner, 2011; Hermans et al., 2013). In contrast, with sufficient Mg in the growth medium, particularly during the earlier stages of plant growth, both transport systems contribute to Mg uptake (Marschner, 2011; Deng et al., 2014), as reflected here by lower  $\delta^{26}\text{Mg}$  values in the roots (Figure 3.4). The exact threshold at which Mg supply may induce switches between the two transport systems remains still uncertain, but at least we can use the  $\delta^{26}\text{Mg}$  signature of bulk plants as a qualitative indicator for different Mg uptake mechanism during trans-membrane loading. The degree of heavy Mg isotope enrichment in the bulk plants can thus serve as an indicator on the degree at which the cross-membrane transport is dominated by active, carrier-mediated transport mechanisms relative to that by Mg-permeable channels. Directly correlating the degree of isotope fractionation to the monitoring of the different transport systems might now warrant further attention.



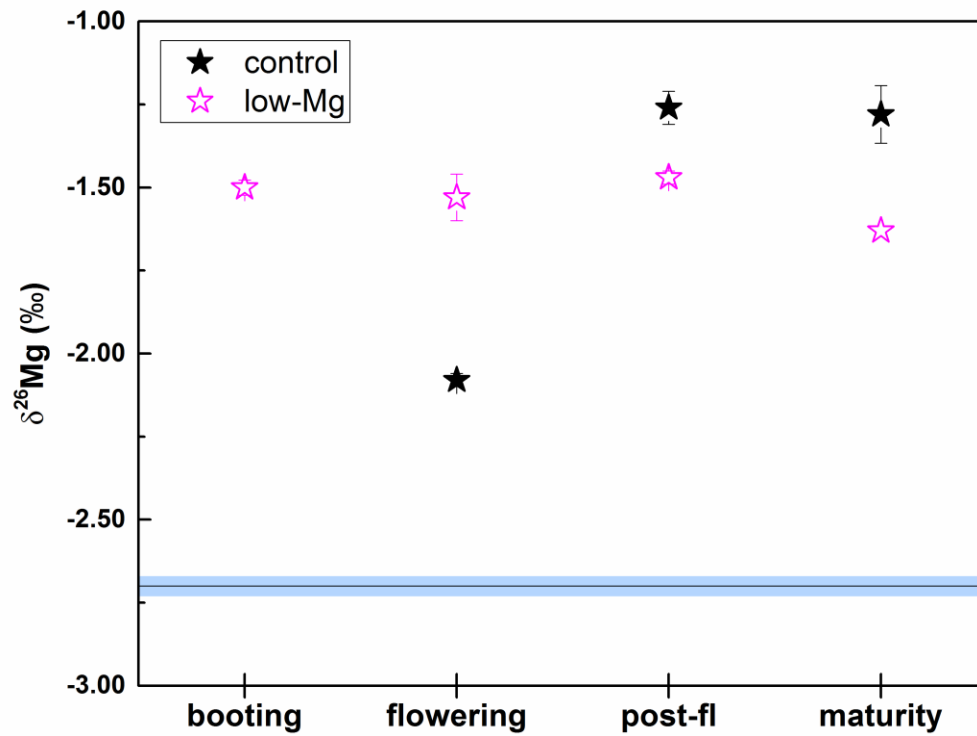


**Figure 3.3** Changes of Mg isotope composition of the bulk plant along with growth stages at different Mg supply. The black solid line and blue area represent the  $\delta^{26}\text{Mg}$  values of the nutrient solution ( $-2.70 \pm 0.03\text{‰}$ , 2SD,  $n=3$ ). Plants grown under both control and low-Mg conditions showed enrichment of heavy Mg isotopes relative to the nutrient solution. Data are calculated based on mass-balance equation and given as the mean  $\pm$  SE of four pot replicates. In the horizontal axis post-fl is short for post-flowering.

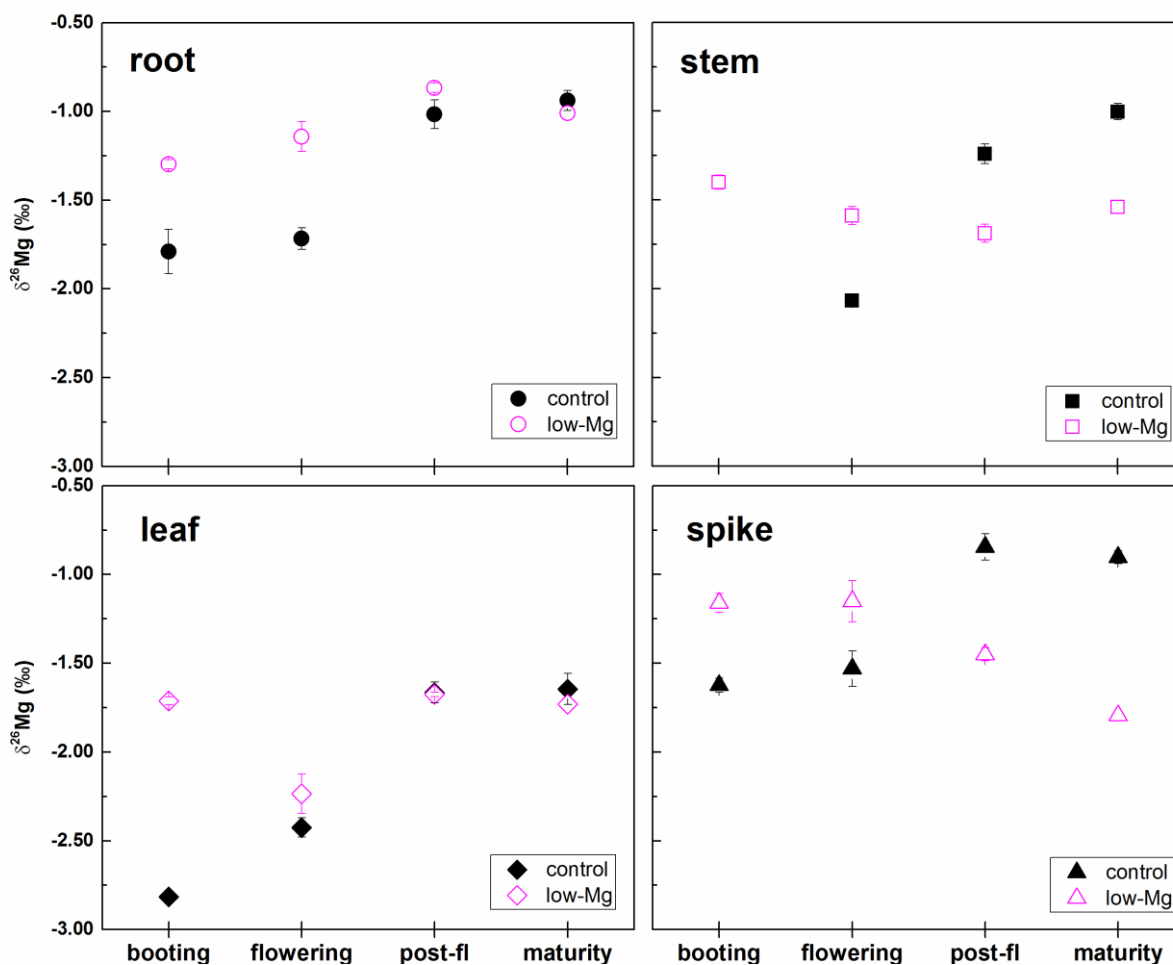


**Figure 3.4** Evolution of Mg isotope composition in each organ of wheat plants (root, stem, leaf, spike) having grown under control (1 mM Mg) and low-Mg (0.05 mM Mg) conditions during the growth period from the booting to the full maturity. Data are given as the mean  $\pm$  SE of four pot replicates. In the horizontal axis post-fl is short for post-flowering.

**Table 3.1** Mg concentrations and isotope compositions ( $\delta^{26}\text{Mg}$ ) of all plant organs with wheat plant growth.

Plant organ	Replicate	Plant biomass (g, dry weight)		Mg concentration (mg kg <sup>-1</sup> )		<i>P</i> <sup>a</sup>		δ <sup>26</sup> Mg (‰) <sup>b</sup>		
		control	Low Mg	control	Low Mg	control	Low Mg	control	Low Mg	
Booting	Root	1	2.10	1.70	1090	616	–	0.18	-1.55	-1.23
		2	0.90	0.40	1218	722	–	0.16	-2.14	-1.29
		3	1.70	1.20	1166	433	–	0.14	-1.72	-1.32
		4	1.40	1.40	1078	418	–	0.13	-1.75	-1.35
		Mean	1.53	1.18	1138	547	–	0.16	-1.79	-1.30
		SE	0.25	0.28	33	74	–	0.02	0.12	0.03
	stem	1	4.00	2.50	–	577	–	0.35	–	-1.52
		2	1.20	1.50	–	493	–	0.40	–	-1.36
		3	3.50	2.40	–	590	–	0.38	–	-1.37
		4	2.90	3.50	–	563	–	0.43	–	-1.35
		Mean	2.90	2.48	–	556	–	0.38	–	-1.40
		SE	0.61	0.41	–	22	–	0.03	–	0.04
	leaf	1	2.80	2.40	2203	824	–	0.42	-2.85	-1.65
		2	1.70	1.00	2249	669	–	0.37	-2.79	-1.72
		3	3.00	2.50	2136	728	–	0.48	-2.81	-1.76
		4	2.60	2.50	2281	717	–	0.39	-2.81	-1.72
		Mean	2.53	2.10	2217	735	–	0.42	-2.82	-1.71
		SE	0.29	0.37	31	32	–	0.03	0.01	0.02
	spike	1	0.70	0.40	969	477	–	0.04	-1.66	-1.18
		2	–	0.30	–	448	–	0.07	–	-1.06
		3	0.20	–	893	–	–	–	-1.61	–
		4	0.20	0.50	939	489	–	0.05	-1.60	-1.24
		Mean	0.37	0.40	934	471	–	0.06	-1.62	-1.16
		SE	0.17	0.06	22	12	–	0.01	0.02	0.05
shoot	Mean	5.70	4.88	–	627	–	0.84	–	-1.54	
	SE	1.00	0.77	–	29	–	0.02	–	0.02	
whole plant	Mean	7.23	6.05	–	609	–	1.00	–	-1.50	
	SE	1.25	1.02	–	21	–	0.00	–	0.02	
Flowering										
Flowering	Root	1	2.20	1.40	1378	511	0.16	0.24	-1.62	-0.97
		2	2.10	2.10	1156	461	0.14	0.19	-1.70	-1.34
		3	2.80	1.70	1172	393	0.17	0.23	-1.73	-1.22
		4	1.50	3.80	1143	479	0.11	0.28	-1.83	-1.04
		Mean	2.15	2.25	1226	461	0.15	0.23	-1.72	-1.14
		SE	0.27	0.54	76	25	0.01	0.03	0.04	0.08
	stem	1	4.70	3.70	1055	411	0.27	0.52	-2.04	-1.46
		2	5.20	4.40	1096	320	0.33	0.29	-2.03	-1.55
		3	5.40	5.00	957	353	0.27	0.29	-2.11	-1.66
		4	5.70	5.30	1093	321	0.39	0.26	-2.09	-1.68
		Mean	5.25	4.60	1050	351	0.31	0.36	-2.07	-1.59
		SE	0.21	0.35	32	21	0.03	0.06	0.02	0.05
	leaf	1	2.40	0.50	2956	526	0.38	0.09	-2.58	-1.99
		2	2.90	2.40	2582	591	0.43	0.30	-2.39	-2.11
		3	3.00	2.80	2721	548	0.43	0.30	-2.33	-2.39
		4	2.20	2.90	2566	541	0.35	0.24	-2.40	-2.45
		Mean	2.63	2.15	2706	552	0.40	0.23	-2.43	-2.24
		SE	0.19	0.56	90	14	0.02	0.05	0.05	0.11
	spike	1	3.20	0.70	1058	631	0.18	0.15	-1.30	-0.89
		2	2.00	1.80	864	547	0.10	0.21	-1.46	-1.03

### Chapter 3. Results and discussion

shoot	3	2.50	2.00	973	544	0.13	0.22	-1.77	-1.40
	4	2.40	2.50	1039	575	0.16	0.22	-1.59	-1.28
	Mean	2.53	1.75	984	574	0.14	0.20	-1.53	-1.15
	SE	0.25	0.38	44	20	0.02	0.02	0.10	0.12
	Mean	10.40	8.50	1454	446	0.85	0.79	-2.14	-1.67
	SE	0.17	1.27	22	3	0.01	0.03	0.01	0.10
	Mean	12.55	10.75	1413	451	1.00	1.00	-2.08	-1.56
	SE	0.41	1.69	25	6	0.00	0.00	0.01	0.10
<b>Post-flowering</b>									
Root	1	1.50	2.30	1111	408	0.07	0.09	-0.80	-0.80
	2	2.10	3.00	995	410	0.06	0.12	-0.99	-0.90
	3	1.70	2.50	990	389	0.05	0.10	-1.15	-0.85
	4	1.40	1.70	1026	357	0.05	0.08	-1.13	-0.92
	Mean	1.68	2.38	1031	391	0.06	0.10	-1.02	-0.87
	SE	0.15	0.27	28	12	0.00	0.01	0.08	0.03
	1	4.80	6.00	924	247	0.18	0.14	-1.18	-1.68
	2	5.90	6.50	978	275	0.18	0.18	-1.13	-1.56
stem	3	5.20	5.40	810	283	0.13	0.16	-1.27	-1.70
	4	5.10	5.20	911	265	0.16	0.18	-1.38	-1.81
	Mean	5.25	5.78	906	268	0.16	0.17	-1.24	-1.69
	SE	0.23	0.30	35	8	0.01	0.01	0.05	0.05
	1	2.20	3.30	4327	480	0.39	0.15	-1.57	-1.68
	2	2.60	3.10	5010	529	0.40	0.17	-1.56	-1.69
	3	2.90	3.10	4850	548	0.43	0.17	-1.74	-1.69
	4	2.60	2.60	4643	418	0.43	0.15	-1.79	-1.64
leaf	Mean	2.58	3.03	4708	494	0.41	0.16	-1.67	-1.68
	SE	0.14	0.15	147	29	0.01	0.01	0.06	0.01
	1	5.60	8.40	1557	794	0.36	0.62	-0.64	-1.56
	2	7.50	6.70	1571	780	0.36	0.53	-0.97	-1.40
	3	7.40	6.00	1696	918	0.39	0.57	-0.93	-1.41
	4	6.90	6.30	1476	701	0.36	0.59	-0.84	-1.43
	Mean	6.85	6.85	1575	798	0.37	0.58	-0.85	-1.45
	SE	0.44	0.54	45	45	0.01	0.02	0.07	0.04
spike	Mean	14.68	15.65	1886	543	0.94	0.90	-1.27	-1.54
	SE	0.75	0.83	41	24	0.00	0.01	0.05	0.02
	Mean	16.35	18.03	1798	523	1.00	1.00	-1.26	-1.47
	SE	0.86	0.98	35	20	0.00	0.00	0.05	0.02
<b>Maturity</b>									
Root	1	1.10	0.80	811	309	0.03	0.03	-0.93	-1.01
	2	1.00	–	822	–	0.03	–	-0.98	–
	3	1.00	–	992	–	0.03	–	-1.06	–
	4	0.90	–	565	–	0.02	–	-0.79	–
	Mean	1.00	0.80	798	309	0.02	0.03	-0.94	-1.01
	SE	0.04	–	88	–	0.00	–	0.06	–
	1	4.10	4.60	655	259	0.08	0.12	-0.99	-1.54
	2	4.20	–	774	–	0.10	–	-1.00	–
stem	3	3.80	–	1078	–	0.12	–	-0.90	–
	4	3.70	–	1192	–	0.15	–	-1.12	–
	Mean	3.95	4.60	925	259	0.11	0.12	-1.00	-1.54
	SE	0.12	–	126	–	0.01	–	0.05	–
	1	2.30	1.60	6666	573	0.43	0.19	-1.53	-1.73
	2	2.00	–	7129	–	0.44	–	-1.61	–
	3	2.00	–	7488	–	0.44	–	-1.54	–
	4	2.00	–	7167	–	0.47	–	-1.90	–
leaf	Mean	2.08	3.20	7113	573	0.44	0.19	-1.65	-1.73
	SE	0.08	–	169	–	0.01	–	0.09	–

### Chapter 3. Results and discussion

<b>spelt</b>	1	3.00	2.40	1630	551	0.14	0.13	-1.19	-1.65
	2	2.40	–	1455	–	0.11	–	-1.20	–
	3	2.50	–	1666	–	0.12	–	-1.22	–
	4	1.70	–	1827	–	0.10	–	-1.41	–
	Mean	2.40	2.40	1645	551	0.12	0.13	-1.26	-1.65
	SE	0.27	–	76	–	0.01	–	0.05	–
<b>grain</b>	1	6.00	5.00	1956	1056	0.33	0.53	-0.84	-1.83
	2	5.30	–	2057	–	0.33	–	-0.86	–
	3	5.40	–	1855	–	0.29	–	-0.80	–
	4	4.00	–	1960	–	0.26	–	-0.95	–
	Mean	5.18	5.00	1957	1056	0.30	0.53	-0.86	-1.83
	SE	0.42	–	41	–	0.02	–	0.03	–
<b>shoot</b>	Mean	13.60	13.60	2394	633	0.98	0.97	-1.28	-1.75
	SE	0.83	–	80	–	0.00	0.00	0.07	–
<b>whole plant</b>	Mean	15.60	14.40	2284	617	1.00	1.00	-1.28	-1.73
	SE	0.87	–	68	–	0.00	0.00	0.07	–
<b>Nutrient solution<sup>c</sup></b>								<b>-2.70 ± 0.03</b>	

<sup>a</sup>*F* means the Mg fraction of different plant tissues, given as the ratio of Mg mass in each plant part to that in whole plant. <sup>b</sup>Isotopic measurement of each sample was conducted at least three times from the same solution with  $2\sigma$  less than 0.09‰. <sup>c</sup>Data was given as mean ± 2SD of three sample replicates.

### 3.1.4 Magnesium isotope fractionation during translocation

After entering into the root cells, Mg is promoted to move for storage into the cell vacuoles or it is loaded into the xylem for upwards transport besides metabolic activities (Marschner, 2011). The Mg distribution and isotope fractionation between roots and shoots is thus affected by both root sequestration and xylem loading processes. To evaluate the effect of low-Mg supply on these processes, we calculated the translocation factors ( $TF_{Mg} = \text{Mg concentration in shoot} / \text{Mg concentration in root}$ , Baker and Brooks, 1989) in the two variants. In the control group, the  $TF_{Mg}$  values increased from 1.20 to 3.16 with plant growth, indicating an enhancement of the Mg translocation process from roots to shoots over time (Table 3.1). Under low-Mg supply, the wheat plants displayed smaller  $TF_{Mg}$  values, ranging from 0.98 to 2.05 along the growth cycle (Table 3.1). The data thus reflected an increased Mg transfer from roots to the shoots as the plants grew. However, this transfer was increasingly hindered with time under low Mg supply suggested by the increased difference in  $TF_{Mg}$  values to the control with time.

We now used a Rayleigh mass-balance calculation to illustrate Mg isotope fractionation between roots and shoots by plotting  $\Delta^{26}\text{Mg}_{\text{root-plant}}$  as a function of the mass fraction of Mg in the root ( $F_{\text{root}}$ ) as suggested by Aucour et al. (2011) and Tang et al. (2012):

$$\Delta^{26}\text{Mg}_{\text{root-plant}} = \delta^{26}\text{Mg}_{\text{root}} - \delta^{26}\text{Mg}_{\text{plant}} = \Delta^{26}\text{Mg}_{\text{trans}} \cdot \ln(F_{\text{root}}). \quad (3.1)$$

At sufficient Mg supply, the positive relationship between  $\Delta^{26}\text{Mg}_{\text{root-plant}}$  and  $F_{\text{root}}$  (Figure 3.5; black line) thus confirmed that the enrichment of heavy Mg isotopes in the roots was attributed to uptake process during the whole growth cycle (Figure 3.5). For the low-Mg treatments, this relationship was evident for the first two growth cycles, only; at post-flowering state the data even grouped along an individual curve. In addition, the plants

grown under low-Mg supply exhibited larger root mass fractions and a steeper fitting curve (Figure 3.5). The findings suggested that Mg was transiently retarded in the roots instead of being transferred immediately upwards under Mg deficient conditions. Likely, elevated competition between Mg and Ca and particularly K was responsible for the retarded Mg transfer into the shoots. Potassium is the most abundant cation in the cytosol and mainly utilized for pH and/or osmosis regulation in living cells (Marschner, 2011). Previous studies showed that under low-Mg supply, the K/Mg ratio in cellular surroundings was much elevated, and Mg was used as storage ion in the cell vacuoles to control ion balance, which is mediated by an  $\text{Mg}^{2+}/\text{H}^{+}$  exchanger in the tonoplast and considered to enrich heavy Mg isotopes in vacuoles (Shaul et al., 1999; Pokharel et al., 2017). The further movement of Mg to the xylem is thus confined. As a result, a transient reduction of Mg concentration as well as a negative shift of  $\delta^{26}\text{Mg}$  values in the shoot was observed (Figure 3.2, 3.4). We thus infer from our data that low-Mg supply likely restricts the translocation of heavy Mg from roots to shoots, thus additionally preventing the further enrichment of heavy Mg in the shoots. The mechanism answering for this restriction is not totally understood yet. Specific measurements of Mg isotope signatures in e.g. the xylem sap and the cytosol of xylem parenchyma cells could help to clarify which processes are involved.

When Mg is supplied sufficiently, there was a continuous enrichment of heavy Mg isotopes in all plant organs during growth. Particularly, the increasing values of  $\delta^{26}\text{Mg}$  in spikes indicated an isotopically heavy Mg pool in the phloem as proposed by Bolou-Bi et al. (2010). In contrast, this effect was lacking under low-Mg supply. In Mg deficiency, the spikes showed lower  $\delta^{26}\text{Mg}$  values and became isotopically lighter continuously with growth cycle, suggesting that the import of Mg into spikes derived at least partially from

xylem and/or phloem loaded with light Mg isotopes (Figure 3.4), because of both initial heavier  $\delta^{26}\text{Mg}$  signatures in the roots from active Mg uptake as well as due to retarded Mg translocation in the mesophyll cells of Mg-deficient plants (see also Verbruggen and Hermans, 2013). In a similar manner, adequate amounts of cytosolic Mg are required for loading photosynthates as well as organic-bond Mg (isotopically heavy) into the phloem, which is limited under low-Mg supply conditions (Cakmak et al., 1994; Marschner, 2011). Intriguingly, these effects became clearly evident despite other processes such as the xylem-to-phloem transfer of Mg in the plants that were not studied yet. Also Mg remobilization processes during the reproductive stage may affect the isotope composition of the spikes (Martin, 1982; Billard et al., 2016). The remobilized Mg in leaves tends to be isotopically light since it is suggested to come mainly from free Mg ions depleted in heavy Mg isotopes (Billard et al., 2016; Pokharel et al., 2018). In this regard our result agrees with a study of Kimmig et al., (2018) who showed that yellow leaves presented higher  $\delta^{26}\text{Mg}$  values than green ones due to Mg remobilization. In general, the discrepancy in Mg isotope composition of plant organs grown under different Mg supply indicates different strategies involved in the xylem and phloem transport processes. In this regard, the  $\delta^{26}\text{Mg}$  isotope composition provides a novel, integrative tracer of different Mg utilization patterns of the plants, which may be used also to study Mg acquisition strategies under field conditions without sophisticated transporter analyses.



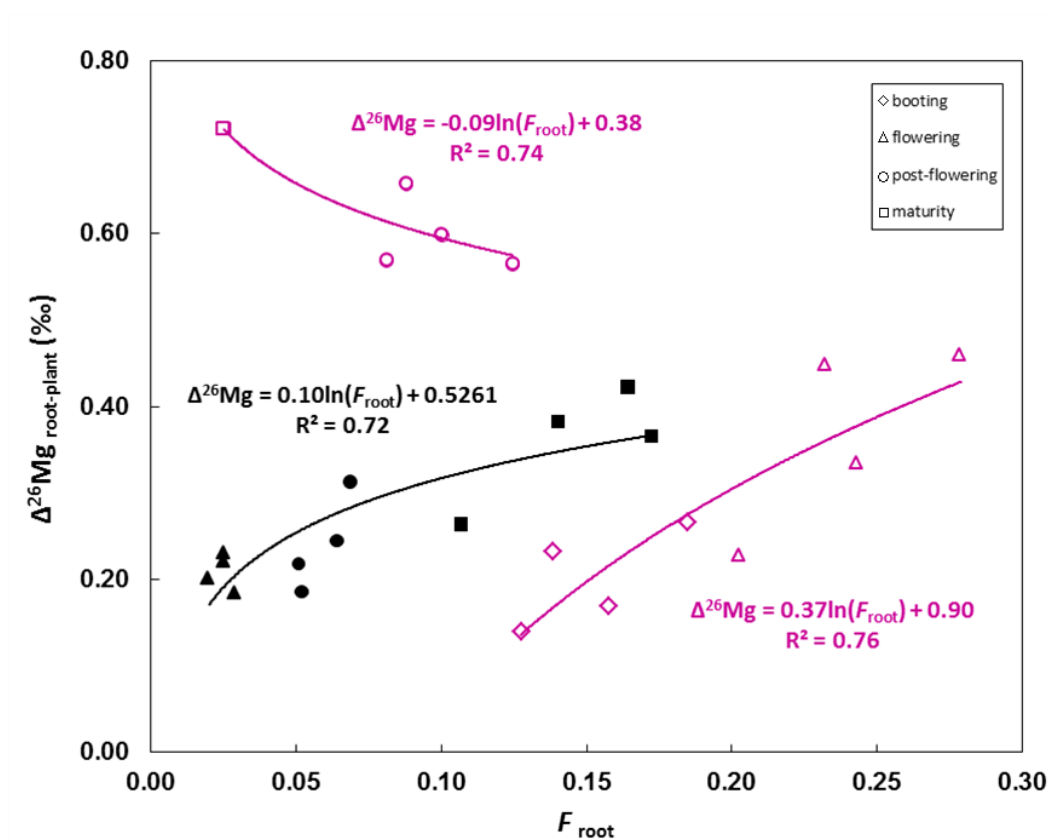


**Figure 3.5** Rayleigh-type mass balance model to illustrate Mg isotope fractionation between root and whole plant ( $\Delta^{26}\text{Mg}_{\text{Root-Plant}}$ ) during Mg translocation, based on the mass ratio of Mg between root and plant ( $F_{\text{root}}$ , see Table 3.1). Different symbols represent different growth stages under control (filled symbols) and low-Mg supply (open symbols): booting (diamond), flowering (triangle), post-flowering (circle) and maturity (square).

**3.1.5 Implications for Mg homeostasis in plant**

Nowadays, Mg deficiency in plants occurs increasingly both in agriculture and forestry at a worldwide scale (Marschner, 2011). However, plants can develop various strategies to deal with frequently encountered environmental stress like nutrient deficiencies (Cai et al., 2012). Our work traced the isotope compositions of widely grown agronomic crop wheat across its life cycle under low-Mg supply. Variations of the Mg isotope signatures in different plant organs demonstrated that different mechanisms are potentially involved in the plant's response to nutrient deficiency. The uptake of Mg was controlled by both cross-membrane transport systems in the wheat root, with the Mg-carrier transporters dominating under Mg deficient conditions and resulting in larger enrichment of heavy Mg isotopes in roots and whole plants. Besides, Mg deficiency retarded the upwards transport of Mg from root to shoot so that seasonal variations in the  $\delta^{26}\text{Mg}$  isotope composition of the plant organs were hardly evident. To date, though a number of plant MRS2/MGT transporters have been identified, our knowledge about the contribution of different Mg transporters to the Mg acquisition strategy of whole plants is still limited. Also the overexpression of known Mg transporters in response to Mg supply by plants has hardly, if at all, been clarified. The same applies to transporters taking part in xylem and phloem loading or unloading process as well as in the long-distance transport of Mg within the plant. Stable isotopes could thereby be a useful tool to assist the study on the molecular biology of phytophysiological activities, e.g., on how plants survive through the strategic adjustment at different growth stage under limited nutrient supply, and to which extent different biological processes contribute to the plant growth.

## 3.2 Mg isotope signatures in an agricultural field with long-term liming practice<sup>1</sup>

### 3.2.1 Magnesium concentrations, stocks and isotope compositions in bulk soil

The Mg concentration in bulk soil displayed increasing trend from the surface soil to the deeper soil layers in both field trials with and without liming practice, varying from 871 to 3005 mg kg<sup>-1</sup> (Figure 3.6a). In the topsoil (0-30 cm), Mg concentrations in these two trials were found to be uniform and showed good homogeneity (Figure 3.6a). By contrast, Mg concentration in the subsoil below ploughing depth (down to 28 cm) varied a lot among plots due to the different processes of soil movement in the last ice age (Chmielewski and Kohn, 1999). Magnesium stock in each soil layer was calculated as the accumulation of Mg in bulk soils down to this layer from the surface (Figure 3.6b). These two fields presented identical Mg stocks within the 100 cm depth with the accumulated Mg stocks of  $37.5 \pm 7.3$  and  $29.4 \pm 5.0$  (SE, n=3) ton ha<sup>-1</sup> for limed field and non-limed field, respectively. The mean value of  $\delta^{26}\text{Mg}_{\text{bulk soil}}$  in the limed and non-limed field was  $0.11 \pm 0.06$  and  $0.09 \pm 0.01$  (SE, n=3) respectively, and consistent along with the soil profile (Figure 3.6c). By comparing  $\delta^{26}\text{Mg}_{\text{bulk soil}}$  between treatments, liming practice displayed no variation in the Mg isotope composition of the bulk soil (Albic Luvisol) when taking the analytical uncertainty into consideration (Figure 3.6c). Negative shift of  $\delta^{26}\text{Mg}_{\text{bulk soil}}$  values was observed by extent of more than 0.17 in limed field and 0.24 in non-limed fields relative to the parent material.

---

<sup>1</sup> Contains parts from “*Magnesium isotope signatures trace liming effects on crop nutrient uptake in long-term agricultural field trial*”, by Yi Wang\*, Bei Wu, Anne E. Bern, Roland Bol, Frank Wombacher, Frank Ellmer, and Wulf Amelung. Submitted to *Geoderma*, 2019”

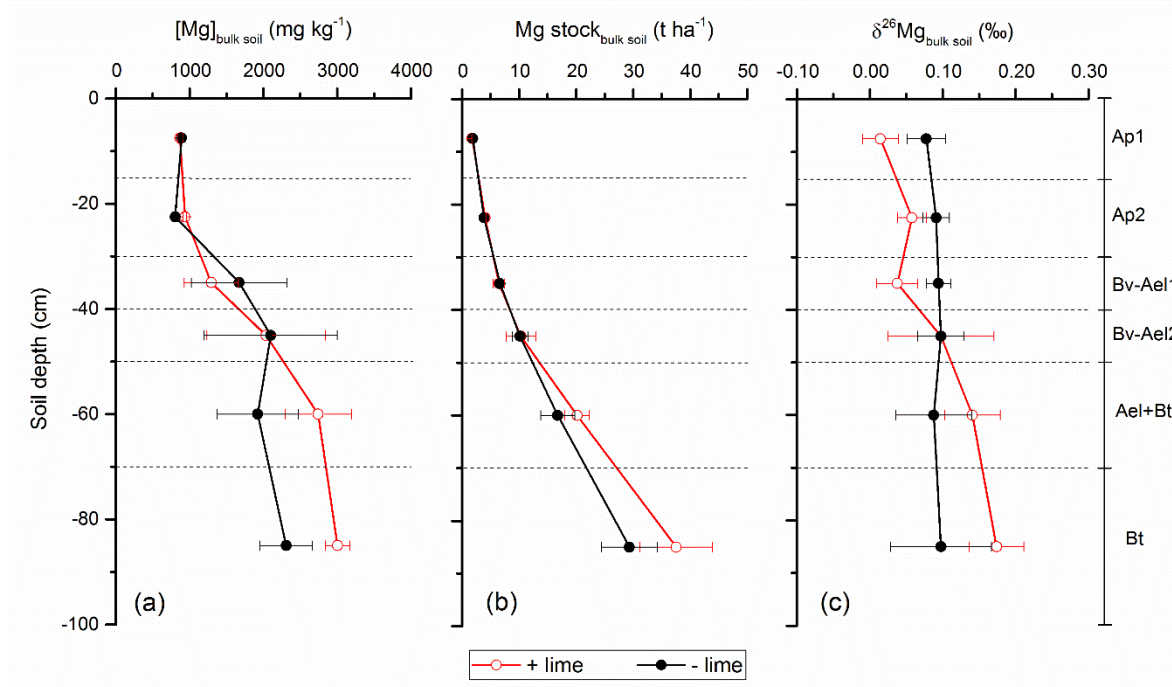


**Figure 3.6** Depth profiles of Mg concentrations (a), stocks (b), and isotope compositions (c) in bulk soil samples collected from experimental fields with (open red) or without (solid black) liming management. Horizon designations given according to German classification are German descriptions of a representative key soil profile at the experimental site, where Ap is the ploughed topsoil, Bv-Ael and Ael correspond to an eluvial horizon, and Ael+Bt and Bt to an argic horizon according to World Reference Base (IUSS Working Group WRB, 2015). Data are shown as mean  $\pm$  SE of three field replicates. Larger error bars in figure (a) indicate heterogeneity of Mg concentration in the upper subsoil.

### 3.2.2 Magnesium concentrations, stocks and isotope compositions in the exchangeable Mg pool

Increasing trend of Mg concentration with soil depth was also observed in soil exchangeable pool with good homogeneity in topsoil (0-30 cm) and great heterogeneity in subsoil in both limed and non-limed fields, which is similar to that of bulk soil Mg (Figure 3.7). However, the proportions of  $Mg_{\text{exch}}$  relative to  $Mg_{\text{bulk soil}}$  displayed much smaller

variation than  $[Mg]_{\text{exch}}$  among plots (Figure 3.8). In the soil depth down to 40cm, limed field contained significant higher proportions of  $Mg_{\text{exch}}$  (3.65 to 3.74%) than that in non-limed field (2.71 to 3.18%), while tended to be indential in deeper layers (Figure 3.8a). Additionally, liming management seemed to induce no increase of Mg stock in soil exchangeable pool (Figure 3.8b).

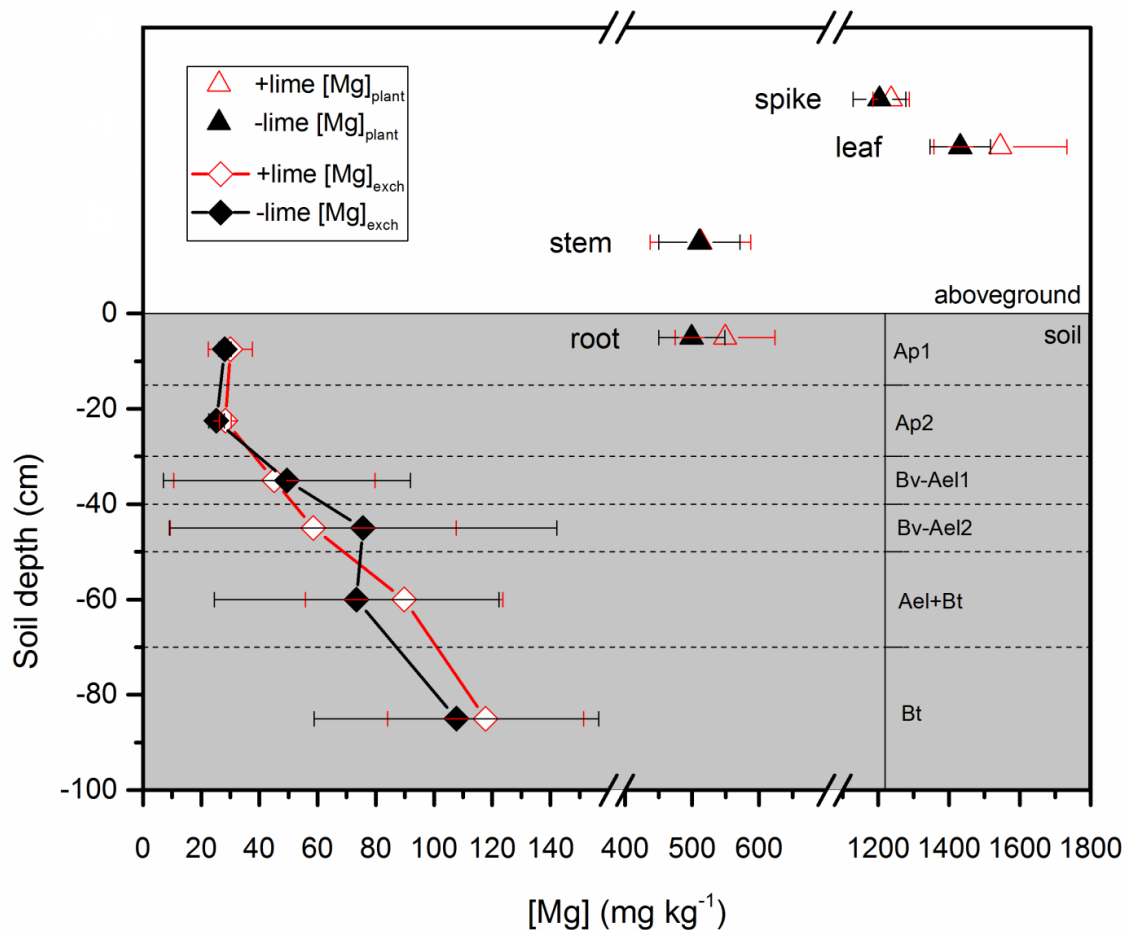


**Figure 3.7** Concentration of exchangeable Mg in soil ( $[Mg]_{\text{exch}}$ ) along soil depth (diamond) and in each plant organ of winter rye (triangle) in limed (open red) and non-limed (solid black) plots. Horizon designations and descriptions are shown in Figure 3.6. Data are given as mean value  $\pm$  SE of three field replicates.

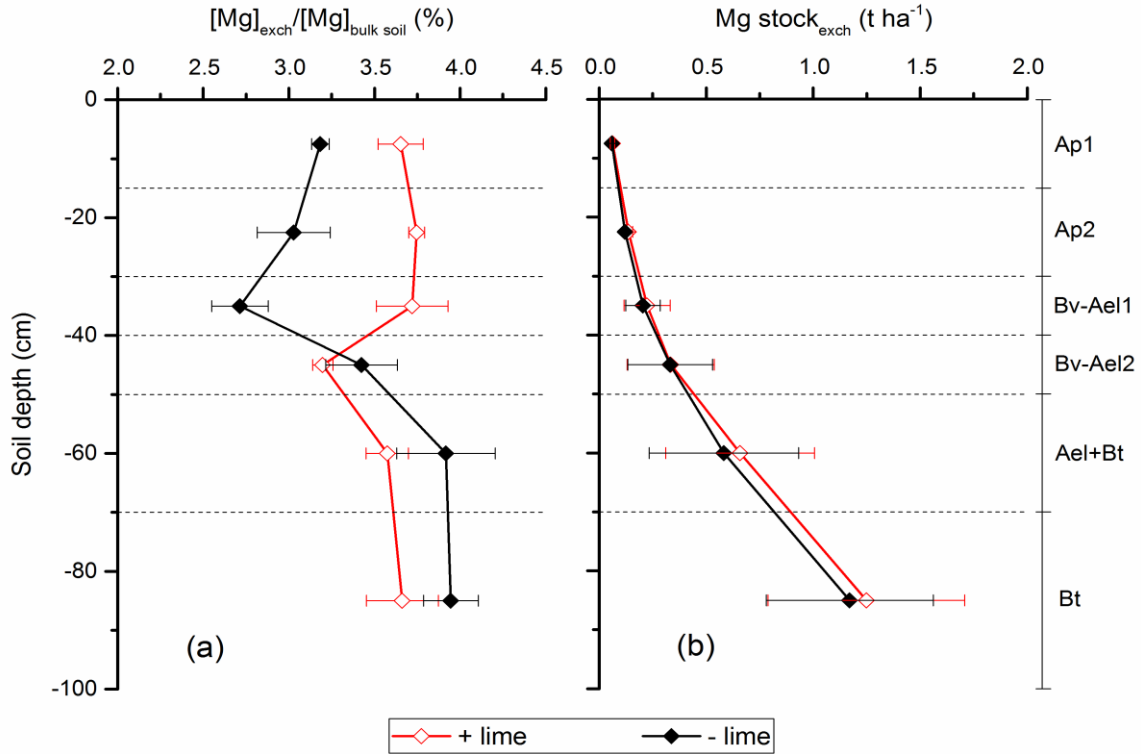


**Figure 3.8** Ratio of Mg concentration in soil exchangeable pool to bulk soil with (a) and Mg stock in soil exchangeable pool (b) with depths in study fields receiving different soil management. Data are shown as mean value  $\pm$  SE of three field replicates.

Compared with the bulk soil, exchangeable Mg pool of the soil was enriched in light Mg isotopes with the Mg isotope signatures down to  $-1.54\text{‰}$  in the very surface layer in limed field (Figure 3.9). Different from the limited Mg fractionation in bulk soil profile, Mg in exchangeable pool became isotopically heavier from the topsoil down to 100 cm depth. In the soil layer of 0-50 cm depth, liming field exhibited more negative  $\delta^{26}\text{Mg}$  value than non-limed field with the apparent difference in  $\delta^{26}\text{Mg}$  between two fields ( $\Delta^{26}\text{Mg}_{\text{limed-non}} = \delta^{26}\text{Mg}_{\text{limed}} - \delta^{26}\text{Mg}_{\text{non}}$ ) of  $-0.20\text{‰}$ , possibly due to the lime applied on the soil in the past few years (Figure 3.9).

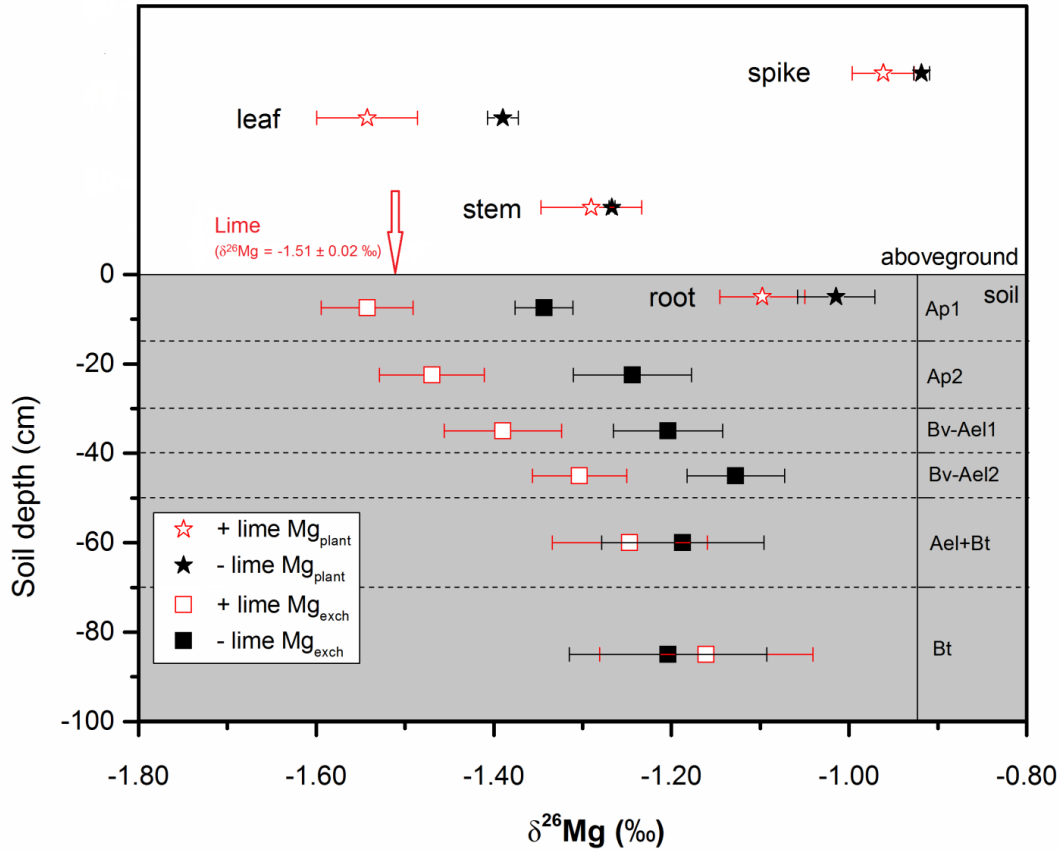


**Figure 3.9** Isotope compositions of the exchangeable Mg pool in soil (square) along soil depth and in each plant organ (star) in limed (open red) and non-limed (solid black) plots. The red arrow represents the addition of lime in limed plots with a  $\delta^{26}\text{Mg}$  of  $-1.51 \pm 0.02$  ‰ (2SD,  $n=3$ ). For horizon designations and descriptions see caption of Figure 3.6. Data are presented as mean value  $\pm$  SE of three field replicates.

### 3.2.3 Magnesium concentration and isotope composition in plants

Plants displayed much higher Mg concentration than  $\text{Mg}_{\text{exch}}$  pool with a large variation among plant organs, ranging from  $497 \pm 49$  to  $1541 \pm 88 \text{ mg kg}^{-1}$  (SE,  $n=3$ , Figure 3.7). Compared with roots, aboveground organs contained quite higher Mg concentration, particularly in leaves (Figure 3.7). No significant differences of plant individual biomass on

average and Mg concentration were observed between fields with or without liming practice, while liming practice tended to increase the biomass of roots and spikes (Figure 3.7, Figure 3.10).

The root of winter rye showed heavier Mg isotope composition relative to the exchangeable Mg pool in the soil layer of 0-15 cm depth where roots exist most (Figure 3.9). The stems and leaves were enriched in light Mg isotopes compared with the root, while the spike exhibited the heaviest Mg isotope composition among the plant organs. This trend was observed for plants growing both limed and non-limed fields. However, the plants in the limed field generally displayed more negative  $\delta^{26}\text{Mg}$  values compared with those in non-limed field (Figure 3.9).

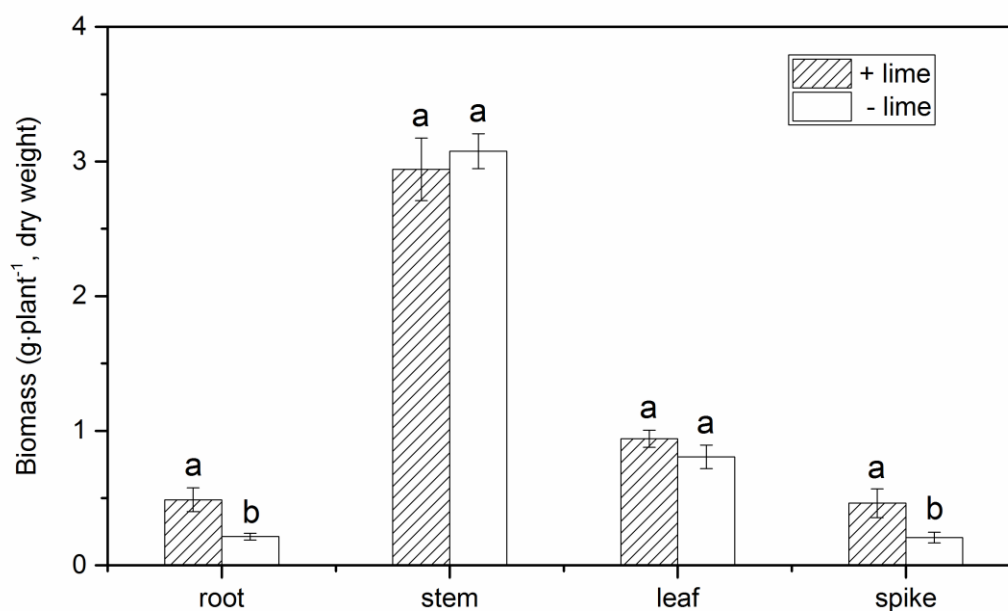


**Figure 3.10** Biomass in dry weight of each plant organ of winter rye. Data are given as mean  $\pm$  SD ( $n > 10$ ). No significant difference of crop biomass was shown due to liming.



### **3.2.4 Magnesium isotope fractionation in the soil profile**

Environmental behaviors of Mg isotopes potentially provide a powerful approach to trace the Mg cycle because Mg isotope signatures could be fractionated significantly by its transport among various phases during both abiotic and biotic processes (Schmitt et al., 2012; Teng, 2017). Figure 3.11 presents a comprehensive overview of the natural processes of Mg in an agricultural soil-plant system. Mineral weathering, associated with pedogenic processes, has been demonstrated to fractionate Mg isotopes significantly (Teng, 2017). Dissolution of primary silicate minerals induces preferential loss of light Mg isotopes into soil solutions and so that retention of heavy Mg isotopes in the unweathered residues (amorphous phases, etc), leaving the soils isotopically heavier than their parent silicate rocks (e.g. Brenot et al., 2008; Tipper et al., 2006, 2008). Additionally, secondary mineral formation during weathering is reported to be another process resulting in depletion of heavy Mg isotopes in fluid phases by favorably incorporating heavy Mg isotopes into the crystal structure of minerals (e.g. Opfergelt et al., 2012, 2014; Teng et al., 2010). However, natural soils showed various Mg isotope compositions ranging from -1.0 to 1.8‰ and are also reported to be isotopically lighter than their parent rock (Gao et al., 2018). Other processes are thought to be involved to impact Mg isotope composition of soils apart from chemical weathering, such as adsorption processes on clay minerals (Huang et al., 2012), clay mineral transformation (Ma et al., 2015), presence of carbonates or Mg-depleted clay mineral (Gao et al., 2018; Wimpenny et al., 2014b), and environmental depositions (Opfergelt et al., 2014). Therefore, shift direction of Mg isotope signatures in soil system is determined not only by an individual process but rather by a mixture of multi-processes. Moreover, the released Mg in soil solutions could be taken up

by vegetation with registering biotic-induced Mg isotope fractionations. Previous studies showed that plants preferentially take heavier Mg isotopes and thus exhibited more positive  $\delta^{26}\text{Mg}$  values compared with the Mg source (e.g. Black et al., 2008; Bolou-Bi et al., 2010, 2012). The so-far reported apparent uptake-induced fractionation factor between plant and soil  $\Delta^{26}\text{Mg}_{\text{plant-source}}$  is present up to 1.21‰ as summarized by (Kimmig et al., 2018) and (Pokharel et al., 2018).

Values of Mg isotope composition in bulk soil displayed no increase as Mg concentration along with depths (Figure 3.6), which indicates that the Mg isotope compositions in the investigated field are not under Mg-content control. This is presumably caused by the high extent of lessivation that physically mobilizes soil particles, especially in clay size, from surface to deeper layers by such as precipitation without apparent isotope fractionation. In addition, because of the considerably small pool size of soil exchangeable Mg (Figure 3.8) and plant uptake Mg relative to bulk soil (less than 0.4%), the present bulk soil Mg isotope compositions are mainly related to the parent material here. While compared with the bulk soil, the soil exchangeable pool displayed an enrichment of much isotopically light Mg in the fields with or without liming practices (Figure 3.6, 3.9). This is in good line with the studies reported before and could be partially ascribed to the mineral weathering processes mentioned above (e.g. Gao et al., 2018; Opfergelt et al., 2014). Since Albic luvisol is dominated by vermiculite and kaolinite minerals that have high capacity to contain isotopically light Mg ions in their interlayers, the Mg isotope composition of soil exchangeable pool is likely dependent on the amounts of Mg ions absorbed into these minerals as exchangeable form (Gao et al., 2018; Ma et al., 2015; Mile and Mitkova, 2013). However, the variation of the  $\delta^{26}\text{Mg}_{\text{exch}}$  values along with the vertical profiles indicated a depletion of heavy Mg isotopes in upper soil layer (0-50 cm depth) compared with deeper

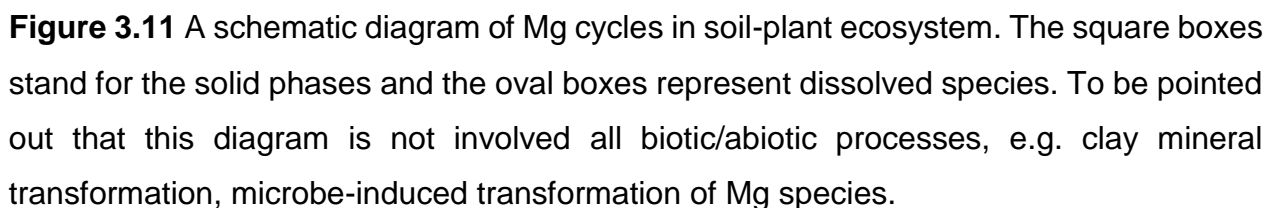


**Table 3.2** Magnesium concentrations, stocks, and isotope compositions in both soil total pool and exchangeable pool in the studied non-limed and limed plots.

Soil manage-ment	Field ID	Layer depth (cm)	Soil horizon <sup>a</sup>	Dry bulk density <sup>b</sup> (g cm <sup>-3</sup> )	[Mg] <sup>bulk</sup> soil <sup>c</sup> (mg kg <sup>-1</sup> )	[Mg] <sup>exch</sup> <sup>c</sup> (mg kg <sup>-1</sup> )	[Mg] <sup>exch</sup> / [Mg] <sup>bulk</sup> soil (%)	Mg <sup>bulk</sup> soil Stock <sup>d</sup> (t ha <sup>-1</sup> )	Mg <sup>exch</sup> Stock <sup>d</sup> (t ha <sup>-1</sup> )	$\delta^{26}\text{Mg}^{\text{bulk}}$ soil <sup>e</sup> (‰)	$\delta^{26}\text{Mg}^{\text{bulk}}$ soil 2SD <sup>f</sup> (‰)	$\delta^{26}\text{Mg}^{\text{exch}}$ (‰)	$\delta^{26}\text{Mg}^{\text{exch}}$ 2SD <sup>f</sup> (‰)
- Lime	-L1	0-15	Ap1	1.36	889	28	3.17	1.8	0.06	-0.01	0.08	-1.37	0.07
		15-30	Ap2	1.60	842	27	3.21	2.0	0.07	0.03	0.06	-1.07	0.01
		30-40	Bv-Ael1	1.60	1372	31	2.26	2.2	0.05	0.09	0.01	-1.24	0.04
		40-50	Bv-Ael2	1.57	1937	62	3.18	3.0	0.10	0.12	0.04	-1.17	0.06
		50-70	Ael+Bt	1.63	2248	99	4.42	7.3	0.32	0.17	0.04	-1.27	0.05
		70-100	Bt	1.84	2739	142	5.19	15.1	0.79	0.22	0.02	-1.41	0.02
	-L2	0-15	Ap1	1.41	869	26	2.98	1.8	0.05	0.08	0.08	-1.44	0.05
		15-30	Ap2	1.54	739	26	3.58	1.7	0.06	0.02	0.01	-1.54	0.03
		30-40	Bv-Ael1	1.55	730	19	2.64	1.1	0.03	0.04	0.05	-1.53	0.04
		40-50	Bv-Ael2	1.60	625	17	2.74	1.0	0.03	0.01	0.07	-1.38	0.05
		50-70	Ael+Bt	1.64	842	17	2.01	2.8	0.06	-0.01	0.09	-1.33	0.05
		70-100	Bt	1.77	1603	52	3.23	8.5	0.28	-0.02	0.02	-1.38	0.05
	-L3	0-15	Ap1	1.48	917	30	3.30	2.0	0.07	0.15	0.08	-1.22	0.03
		15-30	Ap2	1.71	839	22	2.64	2.1	0.06	0.21	0.06	-1.12	0.06
		30-40	Bv-Ael1	1.76	2919	98	3.36	5.1	0.17	0.14	0.01	-0.93	0.04
		40-50	Bv-Ael2	1.74	3735	148	3.96	6.5	0.26	0.15	0.04	-0.83	0.06
		50-70	Ael+Bt	1.80	2680	104	3.87	9.6	0.37	0.09	0.04	-0.96	0.08
		70-100	Bt	1.81	2589	129	4.99	14.1	0.70	0.08	0.02	-0.82	0.02
+ Lime	+L1	0-15	Ap1	1.43	935	38	4.10	2.0	0.08	0.10	0.08	-1.45	0.07
		15-30	Ap2	1.62	967	38	3.93	2.4	0.09	0.16	0.01	-1.47	0.05
		30-40	Bv-Ael1	2.05	2028	85	4.19	4.1	0.17	0.16	0.05	-1.29	0.01

### Chapter 3. Results and discussion

	40-50	Bv-Ael2	1.92	3636	115	3.17	7.0	0.22	0.26	0.07	-1.25	0.04
	50-70	Ael+Bt	1.93	3467	126	3.65	13.4	0.49	0.17	0.06	-1.22	0.04
	70-100	Bt	2.00	3338	147	4.39	20.1	0.88	0.17	0.02	-1.06	0.02
+L2	0-15	Ap1	1.34	867	26	2.94	1.7	0.05	-0.04	0.07	-1.63	0.07
	15-30	Ap2	1.45	891	30	3.34	1.9	0.06	0.00	0.02	-1.59	0.01
	30-40	Bv-Ael1	1.74	915	27	2.93	1.6	0.05	-0.01	0.03	-1.54	0.02
	40-50	Bv-Ael2	1.68	1149	29	2.54	1.9	0.05	0.00	0.06	-1.41	0.05
	50-70	Ael+Bt	1.72	2839	83	2.94	9.8	0.29	0.15	0.05	-1.41	0.05
	70-100	Bt	1.73	2815	86	3.07	14.6	0.45	0.19	0.01	-1.40	0.02
+L3	0-15	Ap1	1.36	812	26	3.23	1.7	0.05	-0.03	0.06	-1.55	0.06
	15-30	Ap2	1.71	956	27	2.82	2.4	0.07	0.00	0.03	-1.35	0.02
	30-40	Bv-Ael1	1.68	943	24	2.49	1.6	0.04	-0.05	0.04	-1.34	0.03
	40-50	Bv-Ael2	1.96	1327	31	2.35	2.6	0.06	0.02	0.06	-1.25	0.05
	50-70	Ael+Bt	1.65	1920	60	3.10	6.3	0.20	0.09	0.06	-1.11	0.04
	70-100	Bt	1.63	2865	90	3.15	14.0	0.44	0.15	0.06	-1.02	0.01

<sup>a</sup> Horizon designations are given according to German classification of a representative key soil profile at the studied field. Descriptions of the soil horizons are shown in the caption of Figure 3.6. <sup>b</sup> Methods for Mg concentrations in different soil pools were detailed in Section 2.3. <sup>c</sup> Dry bulk density of soil samples were obtained according to the method given by Bauke et al. (2018). <sup>d</sup> Magnesium stock in different pool was calculated with the  $[Mg]_{\text{bulk soil}}$  (or  $[Mg]_{\text{exch}}$ ) multiplied by the soil dry bulk density and thickness of each soil layer. <sup>e</sup> Here  $\delta^{26}\text{Mg}$  values were represent relative to the referred Mg isotope standard DSM3. <sup>f</sup> The SD means the standard deviation of repeated measurements for each sample ( $n > 4$ ).

**Table 3.3** Plant dry biomass, Mg concentration, and isotope composition of plant organs in each plot.

Soil Management	Field ID	Plant organ	Dry biomass <sup>a</sup> (g plant <sup>-1</sup> )	[Mg] <sup>b</sup> (mg kg <sup>-1</sup> )	$\delta^{26}\text{Mg}^c$ (‰)	$\delta^{26}\text{Mg}$ 2SD <sup>d</sup> (‰)	$\Delta^{26}\text{Mg}_{\text{leaf-spike}}^e$ (‰)	$\Delta^{26}\text{Mg}_{\text{root-shoot}}^e$ (‰)	$\Delta^{26}\text{Mg}_{\text{plant-source}}^{e,f}$ (‰)
- Lime	-L1	Root	0.17	490	-0.98	0.08		0.31	
		Stem	2.99	612	-1.27	0.01			
		Leaf	0.63	1273	-1.39	0.05	-0.47		
		Spike	0.13	1078	-0.92	0.07			
		Shoot <sup>g</sup>		740	-1.29				
		Bulk plant <sup>g</sup>		729	-1.28				0.07
	-L2	Root	0.22	586	-0.96	0.07		0.31	
		Stem	2.91	512	-1.26	0.02			
		Leaf	0.91	1441	-1.36	0.03	-0.46		
		Spike	0.26	1182	-0.90	0.06			
		Shoot <sup>g</sup>		763	-1.27				
		Bulk plant <sup>g</sup>		754	-1.25				0.10
	-L3	Root	0.25	417	-1.10	0.06		0.20	
		Stem	3.33	403	-1.27	0.03			
		Leaf	0.87	1569	-1.42	0.04	-0.49		
		Spike	0.23	1335	-0.93	0.06			
		Shoot <sup>g</sup>		680	-1.30				
		Bulk plant <sup>g</sup>		666	-1.29				0.05
+ Lime	+L1	Root	0.31	520	-1.07	0.08		0.29	
		Stem	2.95	368	-1.40	0.06			
		Leaf	0.98	1206	-1.48	0.01	-0.49		
		Spike	0.39	1178	-0.99	0.04			
		Shoot <sup>g</sup>		632	-1.37				
		Bulk plant <sup>g</sup>		624	-1.35				0.19
	+L2	Root	0.57	686	-1.03			0.20	
		Stem	2.54	621	-1.21	0.01			
		Leaf	0.94	1561	-1.34	0.05	-0.45		

### Chapter 3. Results and discussion

	Spike	0.32	1182	-0.89	0.07		
	Shoot <sup>g</sup>		900	-1.23			
	Bulk plant <sup>g</sup>		872	-1.21			0.33
+L3	Root	0.58	435	-1.19		0.23	
	Stem	3.34	543	-1.26	0.06		
	Leaf	0.90	1857	-1.81	0.01	-0.81	
	Spike	0.67	1335	-1.00	0.04		
	Shoot <sup>g</sup>		893	-1.42			
	Bulk plant <sup>g</sup>		845	-1.40			0.14

<sup>a</sup> Data are given as averaged dry weight per plant in each plot <sup>b</sup> Methods for Mg concentration determination were detailed in Section 2.3. <sup>c</sup> Here  $\delta^{26}\text{Mg}$  values were represent relative to the referred Mg isotope standard DSM3. <sup>d</sup> The SD means the standard deviation of repeated measurements for each sample ( $n > 4$ ). <sup>e</sup> Apparent difference in  $\delta^{26}\text{Mg}$  between Mg pool A and B. <sup>f</sup> The Mg source here represents the  $\text{Mg}_{\text{exch}}$  pool in the surface soil (0-15 cm depth) <sup>g</sup> The  $\delta^{26}\text{Mg}$  of shoot and bulk plant is obtained with the mass-balance calculation, see Section 2.8.

### **3.2.5 Estimating Mg isotope composition in exchangeable Mg pool**

The isotope composition of the exchangeable Mg pool can be influenced by several processes: i) adsorption onto secondary mineral surfaces (e.g. Mg clays), ii) carbonate precipitation, iii) atmospheric inputs (e.g. sea spray) and iv) vegetation uptake (Huang et al., 2012; Ma et al., 2015; Opfergelt et al., 2014; Uhlig et al., 2017). Adsorption of Mg on clay fractions from soil solution favors heavy Mg isotopes (Huang et al., 2012; Opfergelt et al., 2014), while carbonate minerals are reported to enrich light Mg isotopes (Galy et al., 2002; Li et al., 2012; Wang et al., 2015). In our soils, the exchangeable Mg pool was, on average, significantly lighter than that of the bulk Mg pool in soil, both in the plots with and without liming practices (Figure 3.6, Figure 3.9). This finding is in good agreement with earlier studies and can be partially ascribed to mineral weathering as mentioned above (Gao et al., 2018; Opfergelt et al., 2014). As Albic Luvisols are usually dominated by three-layered clay minerals that have a high capacity to store isotopically light Mg ions in their interlayers, the released Mg ions from the dissolution process can be adsorbed in an exchangeable form onto these clay minerals. In this regard the Mg isotope composition of exchangeable Mg pool in soil should depend on the amounts of Mg absorbed into these minerals as exchangeable form (Gao et al., 2018; Ma et al., 2015; Mile and Mitkova, 2013).

The concentrations of exchangeable Mg increased from the A to the Bt horizon. However, particularly in the upper part of the soil profile (0-50 cm depth) the  $\delta^{26}\text{Mg}_{\text{exch}}$  values were depleted in heavy Mg isotopes, specifically in the limed plots (Figure 3.9). The lighter Mg isotope composition of the exchangeable pool did thus not follow the depth profile of increasing clay contents (Hobley and Prater, 2019), suggesting that apart from mineral weathering combined with subsequent adsorption onto clay minerals further processes



determined its composition. One process was certainly the lime addition, another one most likely plant uptake. The low  $\delta^{26}\text{Mg}$  value of the lime is in line with the general observation that carbonate minerals are enriched in light Mg isotopes (Galy et al., 2002; Li et al., 2012; Wang et al., 2015). Lime products used in this long-term field trial over past 90 years was composed of  $\text{CaCO}_3$ . However, in the year of 2014, application of dolomite lime “Dolokorn 90” (containing 30%  $\text{MgCO}_3$ ) introduced  $79.3 \text{ kg ha}^{-1}$  Mg into the limed plots which accounted for 24% of the  $\text{Mg}_{\text{exch}}$  stock in the soil layers down to 50 cm soil depth of the limed plots (Figure 3.8). As the dolomite lime was enriched in light Mg isotopes ( $-1.51 \pm 0.02\text{‰}$ , 2SD,  $n=3$ , Figure 3.9), the addition of this fertilizer could still be traced using Mg isotope analyses. Noteworthy, the  $\delta^{26}\text{Mg}_{\text{exch}}$  values in the soil layers below 50 cm depth approached another in the limed and non-limed plots (Figure 3.9). Hence, the effect of liming on Mg isotope composition was restricted to the soil layers < 50 cm depth.

To clarify the respective contributions of the lime addition and the plant uptake to the negative shift of  $\delta^{26}\text{Mg}_{\text{exch}}$  in limed plots, we developed an isotope-mixing model for mass balance calculation (Figure 3.12). Because of the limited effect of liming on  $\delta^{26}\text{Mg}_{\text{exch}}$  of the soil layers below 50 cm depth, we assumed an extreme case that all the added lime was retained in the top 50cm of soil and the plant and soil block of 0-50 cm depth was considered as a whole, to check the maximum of lime-induced decrease of  $\delta^{26}\text{Mg}_{\text{exch}}$  in limed field. The average Mg stock<sub>exch</sub> in the top 50 cm of soil was consistent between these two field trials ( $334 \pm 193 \text{ kg ha}^{-1}$  for limed and  $332 \pm 187 \text{ kg ha}^{-1}$  for non-limed plots, SE,  $n=3$ ; Table 3.2) and the calculated average  $\delta^{26}\text{Mg}_{\text{exch}}$  values of the soil blocks (0 – 50 cm) in limed and non-limed plots were  $-1.41 \pm 0.07\text{‰}$  and  $-1.21 \pm 0.18\text{‰}$ , respectively (SE,  $n=3$ ). Using the non-limed plots as reference, the calculated value of  $\delta^{26}\text{Mg}_{\text{exch}}$  in the limed

plots due to the lime addition should be  $-1.26 \pm 0.16\text{‰}$  according to the mass balance. The accrual of  $\delta^{26}\text{Mg}_{\text{exch}}$  by  $0.05\text{‰}$  induced by the lime addition only accounted for 25% of the difference in  $\delta^{26}\text{Mg}_{\text{exch}}$  values between limed and non-limed plots ( $\Delta^{26}\text{Mg}_{\text{limed-non}} = -0.20\text{‰}$ , section 3.2), which means that the negative shift of  $\delta^{26}\text{Mg}_{\text{exch}}$  in limed plots could not be fulfilled simply by the addition of lime product even in such extreme case. If considering the leaching of lime, the contribution of added lime on  $\delta^{26}\text{Mg}_{\text{exch}}$  shift should be even less than 25%. Instead, it could be considered that the removal of Mg by plant uptake in limed plots might be more than that in non-limed plots, which could partially answer for the Mg isotope discrepancy, even though the presently sampled winter rye plants in limed plots displayed no significantly increased removal of Mg relative to that of non-limed plots with regards to the Mg content (Table 3.3). This also indicates that in such field study, only several plants may not be able to represent the plants in the whole plots. Because according to our documentation the rotation crop maize (for silage since 2014) in limed plots has taken about  $5 \text{ kg ha}^{-1}$  Mg more than that in non-limed plots on a whole plot scale. As plant are reported to preferentially take up heavy Mg isotopes (Bolou-Bi et al., 2012; Gao et al., 2018), decades of more removal of heavy Mg isotopes compared with non-limed plots thus could have additionally contributed to the isotopically lighter Mg composition of  $\text{Mg}_{\text{exch}}$  in limed plots relative to non-limed plots, i.e. the long-term liming practice is, to a certain extent, expected to enhance the uptake of Mg by the agricultural field crops.

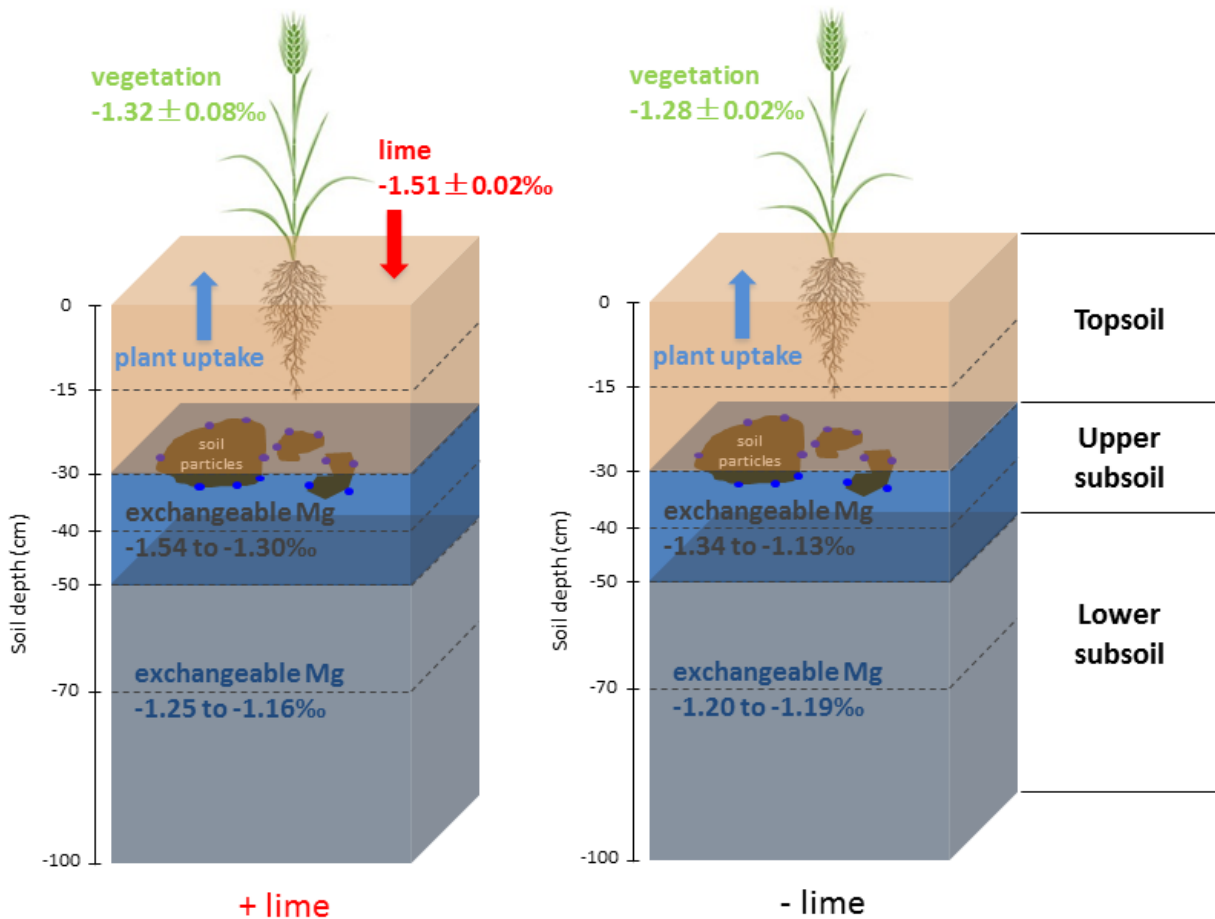


**Figure 3.12** Conceptual diagram of the isotope-mixing model to calculate the Mg isotope mass balance between plant and exchangeable Mg pool in the present agricultural system with (left) and without (right) liming practice. Soil profiles were divided into three horizons topsoil, upper subsoil and lower subsoil with soil depth of 0-30, 30-50, 50-100 cm, respectively (blocks marked in different colors). We considered the topsoil (brown) and upper subsoil (blue) as a combined block according to the hypothesis. The Mg isotope compositions in the exchangeable Mg pools are given as range of the  $\delta^{26}\text{Mg}$  values in the combined blocks of topsoil-upper subsoil (brown and blue) and the blocks of lower subsoil (grey), respectively (Table 3.2). The  $\delta^{26}\text{Mg}$  values of the crop (green) are given as calculated mean of the whole plant  $\pm$  SE of three field replicates (Table 3.3) and the  $\delta^{26}\text{Mg}$  value of the lime product (red) is given as mean  $\pm$  2SD of sample replicates ( $n=3$ ).

### 3.2.6 Magnesium isotope fractionation in plants

In cropped fields, any released Mg in soil solutions can be taken up by the vegetation, subjecting it to biotic-induced Mg isotope fractionations. Previous studies showed that plants preferentially take up heavier Mg isotopes and thus exhibited more positive  $\delta^{26}\text{Mg}$  values than the Mg source (Black et al., 2008; Bolou-Bi et al., 2010, 2012). The range of so-far reported apparent uptake-induced fractionation factors  $\Delta^{26}\text{Mg}_{\text{plant-source}}$ , in both lab and field scales, has presently been estimated to be  $-0.10 \sim 1.21\text{‰}$  (Kimmig et al., 2018; Pokharel et al., 2018). In the site under study, the  $\delta^{26}\text{Mg}$  values of bulk plants were calculated to be  $-1.32 \pm 0.06\text{‰}$  and  $-1.25 \pm 0.01\text{‰}$  for the limed and non-limed plots, respectively (SE,  $n=3$ ). These values were lower than previously reported for field-grown rice ( $-0.92\text{‰}$ , Gao et al., 2018), grass ( $-0.28\text{‰}$ , Opfergelt et al., 2014) and spruce ( $-0.32\text{‰}$ , Bolou-Bi et al., 2012), which may be attributed to the plant species and reservoir effects of Mg sources (Gao et al., 2018). However, the apparent difference in isotope composition between the whole rye plants and the  $\text{Mg}_{\text{exch}}$  pool in the surface soil (0-15 cm depth) averaged  $\Delta^{26}\text{Mg}_{\text{plant-source}} = 0.18 \pm 0.04\text{‰}$  (SE,  $n=6$ ; Table 3.3) resembled reported  $\Delta^{26}\text{Mg}_{\text{plant-source}}$  ranges of specifically field studies ( $-0.10$  to  $0.64\text{‰}$ ), and was close to the yielded average value of  $0.14 \pm 0.16\text{‰}$  (2SE) (Kimmig et al., 2018). The positive shift of  $\delta^{26}\text{Mg}_{\text{plant}}$  relative to the  $\text{Mg}_{\text{exch}}$  reflected the preferential uptake of heavy Mg isotopes occurring in the soil-root interface (Bolou-Bi et al., 2010). Magnesium in soil solution (here exchangeable pool) is first absorbed on negative charge sites at the root surface before entering the plant through the soil-root interface (Kelly and Barber, 1991; Stok et al., 1981; van der Heijden et al., 2013). The exchange sites contain mostly organic functional groups, such as  $-\text{COOH}$  (Marschner, 2011) and the quantity of Mg absorbed on the root depends

on the number of available functional groups, which in turn is regulated by pH (Bolou-Bi et al., 2010). At lower pH values, carboxylic groups provide the dominant exchange site, whereas other functional groups (-NH<sub>2</sub>, -SH, -OH) are rather ionized at higher pH level (Taylor et al., 1990). With light Mg remaining in solution, it is mainly heavy Mg that is adsorbed on the different root functional groups, resulting in an enrichment of isotopically heavy Mg during Mg uptake and leaving behind an exchangeable Mg pool in soil that is isotopically lighter (Bolou-Bi et al., 2010; Pokharel et al., 2017, 2018).

The apparent difference of Mg isotope composition between root and aboveground organs  $\Delta^{26}\text{Mg}_{\text{root-shoot}}$  was calculated to range from 0.20 to 0.31‰, indicating Mg fractionation during the root-shoot translocation with an enrichment of light Mg isotopes in shoots, particularly in leaves (Figure 3.9). Previous studies indicated similar results by explaining that free Mg cations are translocated upwards in the xylem sap, which goes along with a preferential transport of <sup>24</sup>Mg, because of the relatively higher diffusion rates for the light Mg isotopes (Bolou-Bi et al., 2010, 2012). Isotopically light Mg ions then reach and accumulate in leaf cells for plant physiological activities (e.g. photosynthesis), leading to a negative shift of  $\delta^{26}\text{Mg}$  values in the leaves. Additionally, the transport of Mg from leaf to spike in the phloem contributes to the depletion of heavy Mg isotopes in leaves as Mg is associated with organic compounds (e.g. polyphosphate) in leaves and transported by the phloem sap from leaf to storage organs, a process, which preferentially transports heavy Mg isotopes (Bolou-Bi et al., 2010). The extent of fractionation either by root-shoot translocation ( $\Delta^{26}\text{Mg}_{\text{root-shoot}} = 0.24 \pm 0.03\text{‰}$  in limed plots vs.  $0.27 \pm 0.03\text{‰}$  in non-limed plots, SE, n=3) or by leaf-spike translocation ( $\Delta^{26}\text{Mg}_{\text{leaf-spike}} = -0.58 \pm 0.10\text{‰}$  in limed plots vs.  $-0.47 \pm 0.01\text{‰}$  in non-limed plots, SE, n=3) in the investigated winter rye was similar for the limed and non-limed trials. The liming practice did not change Mg internal

translocation processes within the plants. A main reason for this observation was likely that the crops under consideration did not suffer from adverse environmental growth stress that could have been related to Mg deficient soil conditions.

### **3.3 Weathering degree in hyper-arid area of the Atacama Desert, Chile as revealed by magnesium isotope signatures**

#### **3.3.1 Magnesium isotope compositions of surface soil in the Aroma transect**

Generally, soil  $\delta^{26}\text{Mg}$  of the surface layer (0-10 cm) ranged from -0.38 to -0.03‰ in the Aroma transect with the maximum and minimum  $\delta^{26}\text{Mg}$  value observed in the highest elevation of 2700 and elevation of 1600, respectively (Figure 3.13; Table 3.4). At all sites, the very surface soil samples (0-1 cm depth) displayed identically the lowest  $\delta^{26}\text{Mg}$  values, though limited variation of soil  $\delta^{26}\text{Mg}$  among three soil horizons (0-1, 1-5, 5-10 cm with depth) was found in each individual site (Figure 3.13). Soil  $\delta^{26}\text{Mg}$  showed a negative shift with the decreasing elevation, as well as increasing aridity, from the Andes to the Central Depression. However, in the elevation of 2000 m, an enrichment of heavy Mg isotopes was observed again, with soil  $\delta^{26}\text{Mg}$  higher than that of 2400 and 2600 m. And at the site Ar1300, close to the bottom of the alluvial fan, soil displayed a clearly higher  $\delta^{26}\text{Mg}$  value relative to the site Ar1600 (Figure 3.13). The atmospheric deposition is considered as the major materials forming the surface soil layer in the Atacama (Ewing et al., 2006). In the case of Mg, Wang et al. (2014) reported that Mg at the Atacama Desert was of oceanic origin, mainly from the seawater, as the Mg deposition rate declined with the distance from coast. However, this seems not be supported by the present results, at least another Mg source may exist except for the seawater because the Mg isotope composition of seawater ( $\delta^{26}\text{Mg} = -0.83 \pm 0.09\text{‰}$ ) is much lower than the soil  $\delta^{26}\text{Mg}$ . As suggested by Rech et al. (2003), the Andean input is a significant source

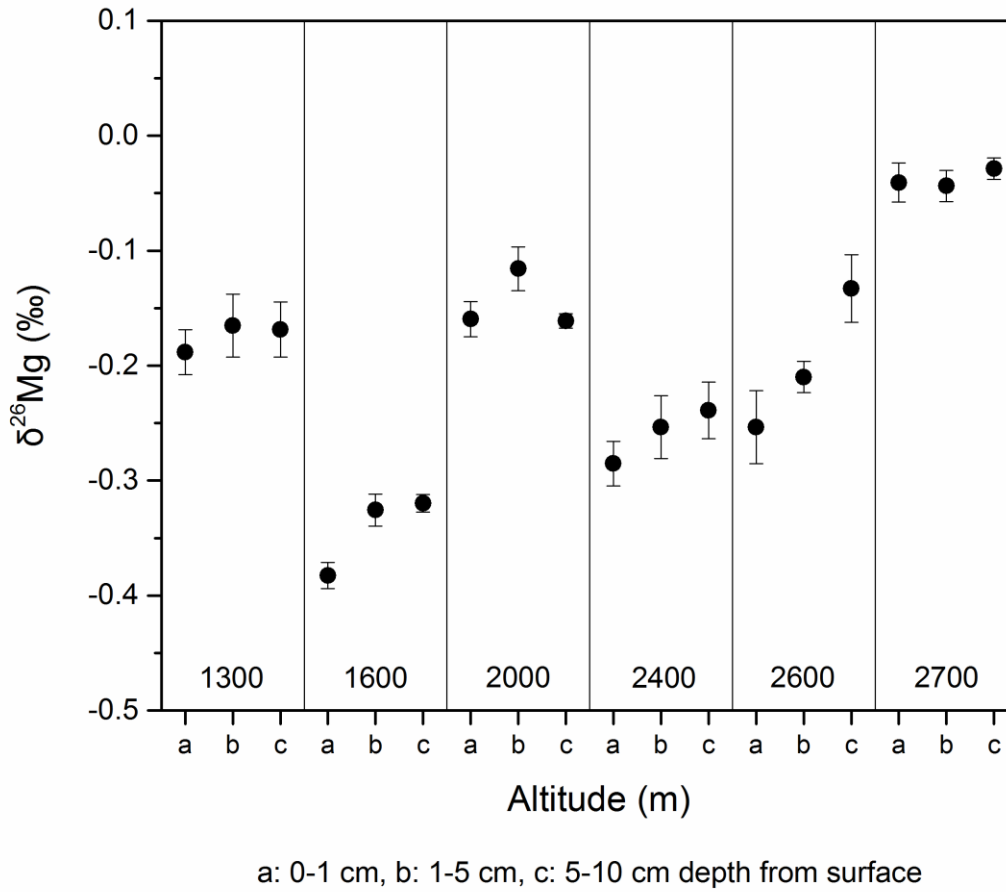


**Figure 3.13** Magnesium isotope compositions with altitudinal gradient in Aroma region. Symbol in each block from left to right represents the sampling soil horizon of 0-1, 1-5, 5-10 cm depth, respectively. Error bar in the figure means the standard error of three field replicates.

of materials in the Central Depression. A recent study by Xie et al. (2018) showed isotopically heavier Mg composition of the continental arc andesites ( $\delta^{26}\text{Mg} = -0.26$  to  $0.15\text{‰}$ ). Thus we considered the Mg source in surface soil layer as a mixture of deposition from both oceanic aerosols and the Andean inputs. Another process influencing the soil  $\delta^{26}\text{Mg}$  is the eolian transport of soil particles as the dust deposition may be eroded away by the westerly wind in the Atacama (Wang et al., 2015). In the study of Huang et al.



(2013), eolian transport can result in sorting of loess materials with coarse fraction of relatively higher SiO<sub>2</sub> content ultimately, which induced an enrichment of light Mg isotopes. However this is likely to be a minor role because no obvious dependence of soil  $\delta^{26}\text{Mg}$  on the SiO<sub>2</sub>/TiO<sub>2</sub> ratio was observed (Figure 3.14).

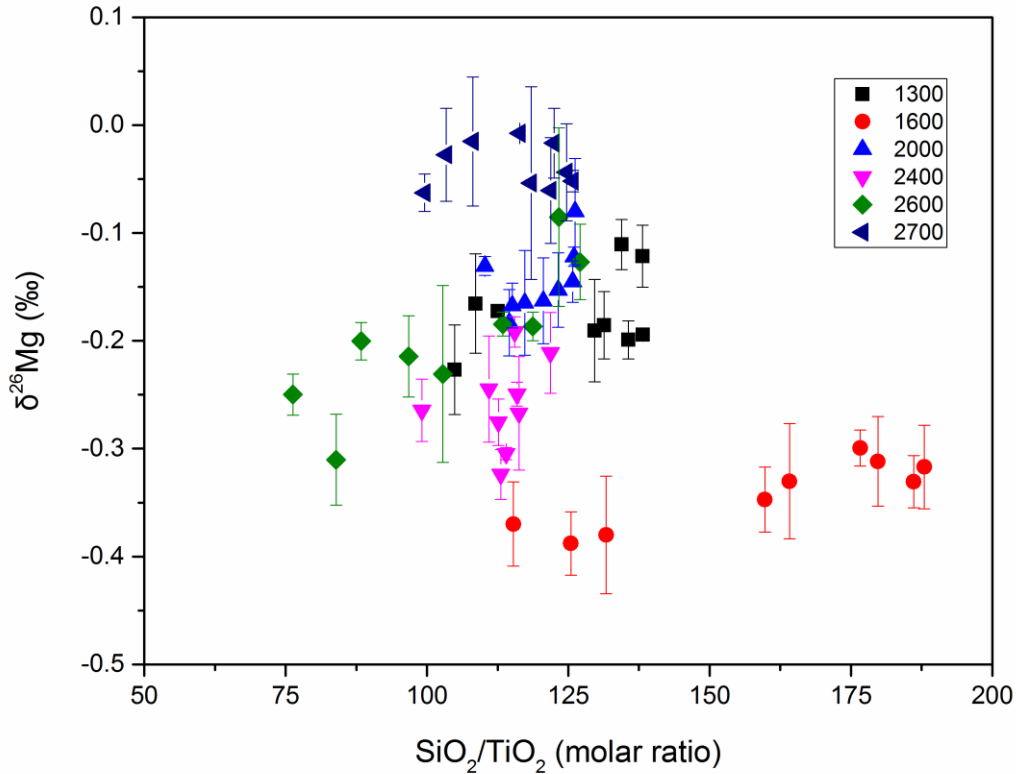


**Figure 3.14** The relationship between  $\delta^{26}\text{Mg}$  and SiO<sub>2</sub>/TiO<sub>2</sub> molar ratio of the surface soil at each site in the Aroma transect. The  $\delta^{26}\text{Mg}$  are present as the mean  $\pm$  SE of three field replicates. No significant effect of the SiO<sub>2</sub>/TiO<sub>2</sub> molar ratio on surface soil Mg isotope compositions was observed.

Higher soil  $\delta^{26}\text{Mg}$  at the site Ar2000 may indicate another Mg source here. This is supported by the distribution of Mg concentration in the Aroma transect (Figure 3.15). Notably, the surface soil at the site of Ar2000 displayed much higher Mg concentration

compared with sites in other elevation, particularly in the soil layer 1-5 and 5-10 cm. However, despite the accrual of MgO content in each layer with the depth, the Mg isotope composition in the site Ar2000 seemed to show independence on the MgO content (Figure 3.16). This may arise from the downwards movement of mineral particles and soluble salts during the formation of desert pavement (Cooke, 1970). However, as only physical movements do not fractionate Mg isotopes in soils, such isotopically heavier Mg accumulation in this elevation may indicate another Mg source. Distinct Mg isotope compositions in the surface soil layer at the site with different elevation reflect various input and the Mg isotope systematics is potentially to be used to trace the source of the surface soil layer in the Aroma transect.

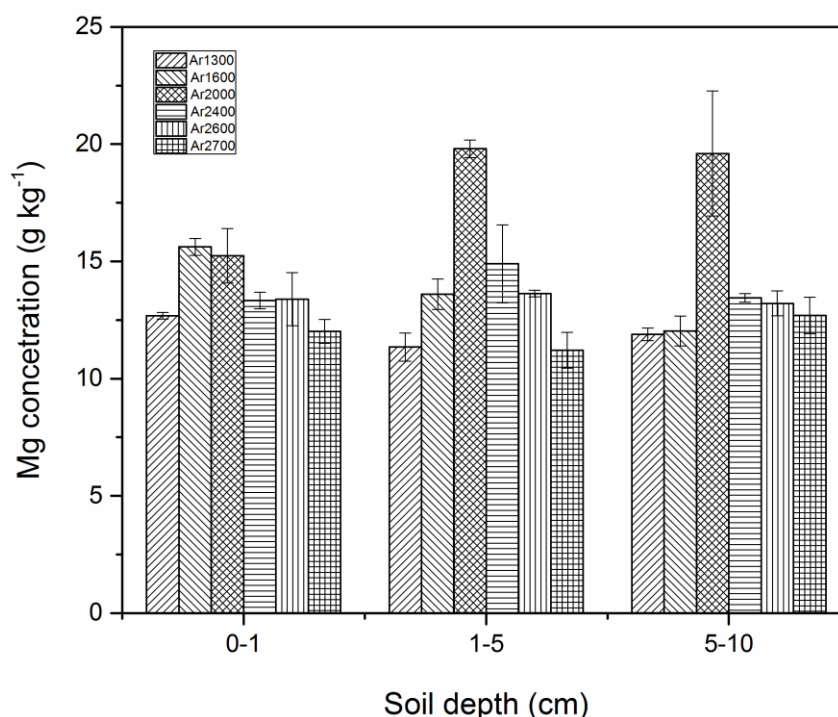


**Figure 3.15** Variation of Mg concentrations in different soil layer at each site in the Aroma transect. Data are present as the mean  $\pm$  SE of three field replicates.

**Table 3.4** Major element concentrations (wt %) expressed as oxides and Mg isotope compositions of surface soil samples in the Aroma transect.

Sample name		SiO <sub>2</sub>	Al <sub>2</sub> O <sub>3</sub>	CaO	MgO	TiO <sub>2</sub>	Na <sub>2</sub> O	MnO	Fe <sub>2</sub> O <sub>3</sub>	K <sub>2</sub> O	P <sub>2</sub> O <sub>5</sub>	LOI <sup>a</sup>	total	δ <sup>26</sup> Mg <sub>DSM33</sub>	SD <sup>b</sup>
Aroma1300-1	0-1cm	64.8	15.26	5.36	2.03	0.77	3.26	0.10	7.01	2.31	0.14	0.07	101.1	-0.17	0.00
	1-5cm	62.4	11.82	13.44	1.75	0.62	2.52	0.07	5.46	1.81	0.11	1.05	101.1	-0.11	0.02
	5-10cm	62.6	11.33	11.62	1.90	0.60	2.49	0.07	5.86	1.89	0.12	0.66	99.1	-0.12	0.03
Aroma1300-2	0-1cm	65.8	14.96	4.49	2.15	0.81	3.18	0.10	7.07	2.33	0.16	0.07	101.1	-0.17	0.05
	1-5cm	63.8	13.98	6.86	2.00	0.66	2.92	0.10	6.34	2.25	0.15	1.01	100.1	-0.19	0.05
	5-10cm	64.4	13.22	7.62	1.92	0.65	2.88	0.10	6.14	2.13	0.14	0.75	99.9	-0.19	0.03
Aroma1300-3	0-1cm	65.4	15.04	4.96	2.13	0.83	3.18	0.10	7.03	2.35	0.16	0.29	101.4	-0.23	0.04
	1-5cm	63.6	13.41	8.72	1.78	0.61	3.01	0.08	5.36	2.28	0.13	0.72	99.7	-0.19	0.00
	5-10cm	62.7	13.41	10.04	2.02	0.62	3.17	0.08	5.68	2.22	0.12	0.42	100.5	-0.20	0.02
Aroma1600-1	0-1cm	62.3	16.96	4.28	2.62	0.66	3.01	0.11	6.69	2.47	0.19	0.19	99.5	-0.39	0.03
	1-5cm	62.7	16.74	5.31	2.72	0.51	2.86	0.09	6.11	2.47	0.19	0.66	100.3	-0.33	0.05
	5-10cm	64.1	13.11	10.42	2.02	0.48	2.52	0.08	4.51	1.92	0.13	0.95	100.2	-0.31	0.04
Aroma1600-2	0-1cm	63.6	16.23	4.10	2.62	0.74	2.91	0.12	6.89	2.43	0.20	0.30	100.2	-0.37	0.04
	1-5cm	63.7	14.71	7.63	2.43	0.53	2.68	0.09	5.30	2.22	0.15	0.76	100.2	-0.35	0.03
	5-10cm	61.8	13.20	11.68	1.80	0.44	2.67	0.07	4.01	1.96	0.12	1.38	99.1	-0.32	0.04
Aroma1600-3	0-1cm	62.4	16.51	4.42	2.65	0.63	2.82	0.11	6.34	2.42	0.19	0.38	98.8	-0.38	0.05
	1-5cm	64.1	15.19	7.18	2.23	0.48	2.86	0.09	5.10	2.25	0.14	0.55	100.2	-0.30	0.02
	5-10cm	64.0	13.77	9.35	1.97	0.46	2.80	0.08	4.54	2.01	0.13	1.27	100.4	-0.33	0.02
Aroma2000-1	0-1cm	61.9	16.24	4.14	2.57	0.75	2.99	0.11	7.93	2.27	0.18	0.31	99.5	-0.13	0.01
	1-5cm	63.4	15.49	3.85	3.37	0.67	2.33	0.10	6.83	2.45	0.17	0.31	99.0	-0.12	0.01
	5-10cm	64.9	14.92	3.07	3.97	0.75	1.91	0.11	6.21	2.86	0.14	0.51	99.4	-0.17	0.02
Aroma2000-2	0-1cm	63.9	16.06	4.16	2.47	0.74	3.03	0.10	7.31	2.22	0.17	0.04	100.2	-0.18	0.03
	1-5cm	62.3	15.92	3.81	3.25	0.66	2.37	0.11	6.66	2.49	0.18	0.30	98.0	-0.15	0.02
	5-10cm	65.0	14.34	3.07	4.08	0.72	1.52	0.07	5.83	2.81	0.19	0.53	98.2	-0.16	0.04
Aroma2000-3	0-1cm	64.6	16.06	3.68	2.70	0.73	2.60	0.11	6.91	2.42	0.19	0.26	100.3	-0.16	0.05
	1-5cm	62.6	16.17	3.04	3.47	0.66	1.86	0.10	6.30	2.90	0.22	0.64	98.0	-0.08	0.05
	5-10cm	67.3	14.03	2.43	4.07	0.73	1.23	0.08	5.27	3.41	0.17	1.02	99.7	-0.15	0.03
Aroma2400-1	0-1cm	63.2	16.45	4.03	2.25	0.74	3.03	0.11	6.63	2.30	0.18	0.02	98.9	-0.32	0.02
	1-5cm	63.8	16.85	4.10	2.32	0.75	2.98	0.07	6.63	2.25	0.15	0.06	99.9	-0.30	0.01
	5-10cm	61.5	17.53	4.25	2.28	0.73	3.13	0.11	6.73	2.17	0.09	0.11	98.6	-0.28	0.02

### Chapter 3. Results and discussion

Aroma2400-2	0-1cm	62.8	16.55	4.20	2.13	0.72	3.15	0.11	6.51	2.28	0.19	0.41	99.0	-0.27	0.05
	1-5cm	63.4	17.38	4.15	2.32	0.76	3.09	0.11	6.94	2.36	0.19	0.12	100.8	-0.24	0.05
	5-10cm	62.4	17.57	4.14	2.30	0.72	3.07	0.11	7.07	2.24	0.13	0.64	100.4	-0.25	0.01
Aroma2400-3	0-1cm	61.1	16.49	4.02	2.33	0.82	2.95	0.12	7.70	2.28	0.19	0.15	98.1	-0.26	0.03
	1-5cm	61.7	17.38	4.14	2.43	0.68	2.95	0.10	7.03	2.28	0.15	0.15	99.0	-0.21	0.04
	5-10cm	62.4	17.38	4.14	2.30	0.72	2.99	0.11	6.67	2.19	0.11	0.29	99.3	-0.19	0.01
Aroma2600-1	0-1cm	60.4	15.89	4.12	2.52	1.06	2.90	0.13	8.91	2.13	0.16	0.09	98.3	-0.25	0.02
	1-5cm	63.5	16.58	3.98	2.50	0.87	2.74	0.12	8.34	2.13	0.19	0.03	100.9	-0.21	0.04
	5-10cm	62.6	16.87	3.89	2.33	0.70	2.78	0.09	6.96	2.07	0.10	0.91	99.3	-0.19	0.01
Aroma2600-2	0-1cm	60.6	15.49	3.93	2.35	0.92	2.90	0.09	7.67	2.21	0.15	0.52	96.9	-0.20	0.02
	1-5cm	61.5	15.90	3.82	2.38	0.72	2.86	0.10	6.84	2.39	0.10	0.57	97.2	-0.18	0.01
	5-10cm	62.9	16.47	3.53	2.57	0.66	2.71	0.09	6.43	2.47	0.06	0.92	98.8	-0.13	0.04
Aroma2600-3	0-1cm	60.9	15.68	4.27	2.62	0.97	3.02	0.11	9.54	2.22	0.15	0.45	99.9	-0.31	0.04
	1-5cm	61.5	16.62	4.10	2.38	0.80	2.95	0.11	7.60	2.21	0.11	0.61	99.0	-0.23	0.08
	5-10cm	63.1	17.00	3.74	2.25	0.68	2.74	0.09	6.63	2.19	0.08	0.97	99.5	-0.09	0.08
Aroma2700-1	0-1cm	62.3	16.11	4.05	2.23	0.83	3.01	0.10	7.56	2.20	0.15	0.51	99.0	-0.06	0.02
	1-5cm	61.3	17.00	3.74	2.27	0.67	2.74	0.11	7.23	2.39	0.25	0.63	98.3	-0.02	0.03
	5-10cm	62.9	17.55	3.60	2.13	0.78	2.75	0.12	7.07	2.18	0.13	0.85	100.1	-0.02	0.06
Aroma2700-2	0-1cm	62.6	17.02	3.69	2.03	0.72	2.82	0.11	6.50	2.32	0.19	0.44	98.4	-0.01	0.00
	1-5cm	62.9	16.24	3.68	2.20	0.71	2.74	0.11	6.59	2.31	0.17	0.46	98.1	-0.05	0.09
	5-10cm	63.8	16.96	3.59	2.07	0.68	2.80	0.11	6.62	2.24	0.10	0.52	99.5	-0.04	0.04
Aroma2700-3	0-1cm	63.3	15.93	4.12	2.15	0.67	2.86	0.10	6.34	2.28	0.39	0.31	98.4	-0.05	0.01
	1-5cm	62.4	16.60	3.81	2.07	0.68	2.72	0.09	5.94	2.28	0.33	0.46	97.3	-0.06	0.05
	5-10cm	62.9	16.06	3.82	2.13	0.81	2.88	0.13	6.63	2.29	0.17	0.44	98.2	-0.03	0.04

<sup>a</sup> LOI = loss on ignition. <sup>b</sup> SD = the analytical uncertainty based on repeated measurements of each sample (n > 3).

**Table 3.5** Major element concentrations (wt %) expressed as oxides and Mg isotope compositions of soil samples with profile from the Aroma and Yungay regions.

Sample name	Depth (cm)	SiO <sub>2</sub>	Al <sub>2</sub> O <sub>3</sub>	CaO	MgO	TiO <sub>2</sub>	Na <sub>2</sub> O	MnO	Fe <sub>2</sub> O <sub>3</sub>	K <sub>2</sub> O	P <sub>2</sub> O <sub>5</sub>	LOI <sup>a</sup>	total	δ <sup>26</sup> Mg <sub>DSM3</sub>	SD <sup>b</sup>
<b>Aroma</b>															
A1300 pit 1	0-7	66.5	15.69	4.84	1.65	0.59	3.71	0.07	4.94	2.63	0.18	0.06	100.9	0.03	0.02
A1300 pit 2	7-25	66.9	8.48	14.14	1.37	0.51	1.89	0.07	3.84	1.49	0.14	0.94	99.7	-0.01	0.08
A1300 pit 3	25-30	61.4	14.03	6.44	2.13	0.82	3.55	0.10	6.65	2.48	0.17	0.59	98.4	-0.08	0.04
A1300 pit 4	30-48	60.4	4.39	28.42	1.44	0.33	2.75	0.04	3.06	0.96	0.06	0.06	101.9	-0.42	0.04
A1300 pit 5	48-88	64.0	4.29	16.38	2.03	0.28	9.34	0.03	2.50	3.69	0.12	0.90	103.6	-0.40	0.05
A1300 pit 6	88-100	64.5	11.15	6.10	3.42	0.66	4.27	0.09	5.83	4.49	0.22	0.67	101.4	-0.26	0.04
A1300 pit 7	100-140	62.2	10.82	6.85	3.59	0.65	4.64	0.09	6.46	4.42	0.20	0.26	100.2	-0.17	0.06
A2000 pit 1	0-10	61.7	17.76	3.50	3.92	0.51	2.25	0.09	7.71	3.89	0.19	1.31	102.8	-0.12	0.03
A2000 pit 2	20-30	64.4	13.60	3.36	5.17	0.38	2.21	0.06	5.69	3.75	0.22	0.32	99.1	-0.41	0.03
A2000 pit 3	60-70	64.6	9.80	10.64	5.83	0.37	2.92	0.05	4.50	1.87	0.24	0.32	101.1	-0.52	0.04
A2000 pit 4	80-90	63.5	8.84	17.22	2.93	0.38	2.26	0.05	4.60	1.57	0.14	0.53	102.0	-0.39	0.05
A2000 pit 5	100-110	62.3	10.92	8.68	4.22	0.50	2.45	0.07	6.77	2.10	0.15	0.04	98.2	-0.44	0.05
A2000 pit 6	200-240	67.5	6.80	15.26	3.87	0.16	1.79	0.03	1.71	2.43	0.17	0.28	100.0	-0.83	0.04
A2000 pit 7	240-280	62.0	3.89	26.04	1.67	0.08	1.23	0.01	0.93	1.47	0.04	0.51	97.9	-0.83	0.03
A2000 pit 8	280-350	64.1	5.89	22.96	0.95	0.11	1.55	0.02	1.20	2.22	0.09	0.25	99.3	-0.30	0.06
A2350 pit 1	0-5	60.2	17.46	4.86	2.92	0.65	3.48	0.09	7.93	2.81	0.15	0.98	101.5	-0.24	0.04
A2350 pit 2	10-20	65.1	17.76	2.95	3.57	0.39	1.60	0.05	7.13	3.39	0.07	0.02	102.0	-0.16	0.04
A2350 pit 3	60-70	69.9	12.69	3.44	3.77	0.34	1.83	0.04	5.16	2.07	0.18	0.06	99.4	-0.34	0.02
A2350 pit 4	110-120	71.5	11.13	3.43	4.93	0.37	2.04	0.04	5.14	1.61	0.18	0.10	100.5	-0.40	0.06
A2350 pit 5	150-160	73.6	8.97	3.71	6.28	0.47	1.86	0.05	5.43	1.23	0.25	0.40	102.3	-0.48	0.07

### Chapter 3. Results and discussion

A2350 pit 6	180-200	64.1	13.84	5.14	4.58	0.59	2.91	0.07	7.10	1.75	0.29	0.12	100.5	-0.51	0.03
A2540 pit 1	0-5	62.1	16.32	4.10	2.48	0.81	2.92	0.11	8.61	2.12	0.30	0.62	100.5	-0.27	0.06
A2540 pit 2	10-20	63.2	18.70	3.77	2.18	0.65	2.84	0.09	7.37	2.28	0.11	0.15	101.3	-0.24	0.05
A2540 pit 3	40-50	66.7	17.06	2.67	2.38	0.49	1.73	0.06	6.61	2.11	0.21	0.15	100.2	0.00	0.06
A2540 pit 4	80-90	75.6	11.91	2.16	2.04	0.33	0.99	0.03	4.72	1.54	0.37	0.28	99.9	-0.09	0.02
A2540 pit 5	130-140	75.9	11.62	2.80	2.35	0.31	1.32	0.03	4.59	1.40	0.25	0.11	100.6	-0.14	0.04
A2540 pit 6	140-150	70.3	14.07	4.24	2.45	0.35	3.28	0.06	4.27	1.87	0.39	0.03	101.3	-0.04	0.04
<b>Yungay</b>															
yungay pit 1	0-10	66.7	12.98	7.88	1.22	0.51	4.08	0.06	4.61	2.29	0.06	0.65	101.1	-0.26	0.05
yungay pit 2	30-40	85.3	5.72	1.59	0.83	0.31	2.67	0.04	2.59	0.88	0.04	1.04	101.0	-0.61	0.07
yungay pit 3	60-70	65.5	12.92	2.84	1.82	0.60	8.40	0.07	6.43	2.12	0.07	0.51	101.3	-0.53	0.07
yungay pit 4	90-100	66.0	14.81	3.05	1.55	0.50	4.87	0.08	5.33	2.65	0.07	0.69	99.6	-0.41	0.05
yungay pit 5	120-130	64.3	13.90	3.12	1.48	1.02	4.06	0.11	8.70	2.53	0.07	1.09	100.4	-0.33	0.07
yungay pit 6	150-160	66.6	15.30	2.95	1.98	0.77	4.72	0.10	6.86	2.92	0.12	0.57	102.9	-0.35	0.06
yungay pit 7	180-190	66.4	16.21	3.57	1.85	0.52	4.76	0.08	5.43	2.76	0.10	0.72	102.4	-0.37	0.05
yungay pit 8	210-220	63.0	15.24	2.45	2.32	0.44	4.77	0.08	5.16	3.06	0.15	0.96	97.6	-0.41	0.03
yungay pit 9	240-250	64.4	14.45	1.86	2.75	0.36	4.77	0.06	4.49	2.21	0.15	0.50	96.0	-0.52	0.05
yungay pit 10	270-280	64.1	16.34	2.11	2.62	0.38	5.69	0.08	5.21	3.35	0.20	0.51	100.6	-0.31	0.08
yungay pit 11	300-310	67.9	14.28	2.67	2.53	0.39	5.32	0.07	5.04	3.13	0.18	0.56	102.1	-0.35	0.04
yungay pit 12	330-340	65.5	16.07	1.34	3.13	0.43	4.46	0.10	5.37	3.55	0.17	0.34	100.4	-0.37	0.08

<sup>a</sup> LOI = loss on ignition. <sup>b</sup> SD = the analytical uncertainty based on repeated measurements of each sample (n > 3).

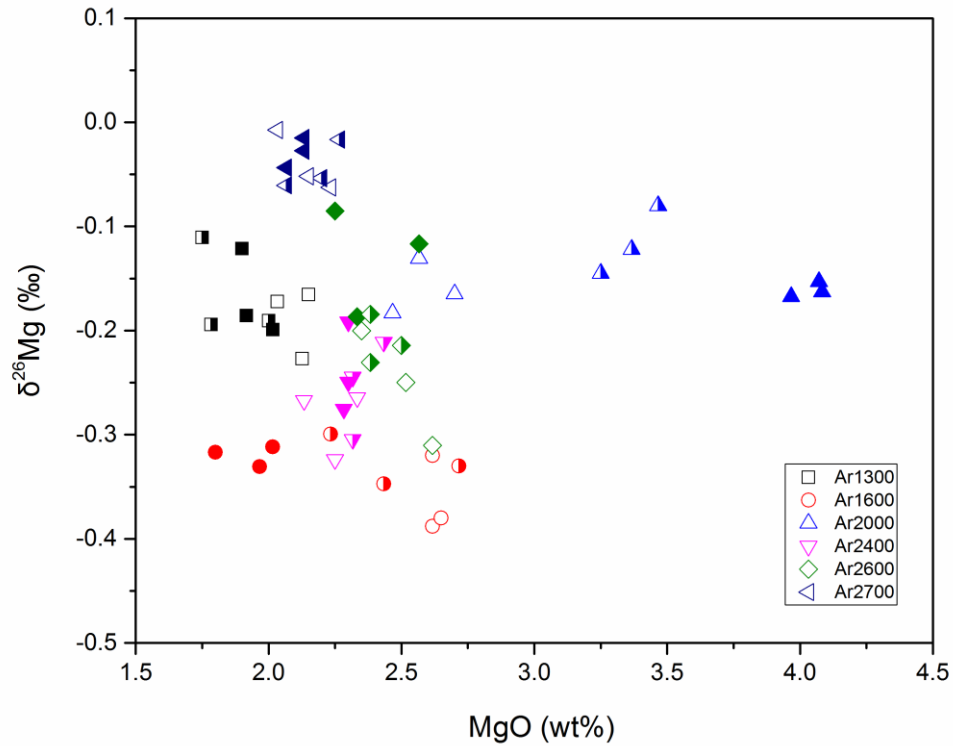


**Figure 3.16**  $\delta^{26}\text{Mg}$  as a function of Mg content (expressed as calculated MgO content wt %) in surface soil samples from the Aroma transect. Open symbols represent the soil depth of 0-1 cm, while half-solid and solid symbols correspond to the soil depth of 1-5 and 5-10 cm, respectively.

### 3.3.2 Soil Mg isotope compositions along with profile at different elevation

The overall pit samples of soil from the Aroma transect exhibited a range of Mg isotope composition over 0.8‰, from -0.83 to -0.03‰ with an average  $\delta^{26}\text{Mg}$  of  $-0.35 \pm 0.18$  (SD,  $n = 38$ , Figure 3.17, Table 3.5), which is a little isotopically lighter to the estimated average Mg isotope composition of the upper continental crust ( $\delta^{26}\text{Mg}_{\text{UCC}} = -0.22$ , Li et al., 2010). However, in each site the variation of  $\delta^{26}\text{Mg}$  was quite limited (less than 0.35‰) except for the site Aroma 2000 which included two outlier samples (Figure 3.17). In the upper

layer of the pit profile (0-40 cm depth) at the site Aroma 1300, Aroma 2000, Aroma 2350, and Yungay, soils displayed an enrichment of heavier Mg isotopes compared with deeper layers. Contrary case was only observed in the site Aroma 2540 whose Mg isotope compositions of upper soil were isotopically heavier than its sediments (Figure 3.17).

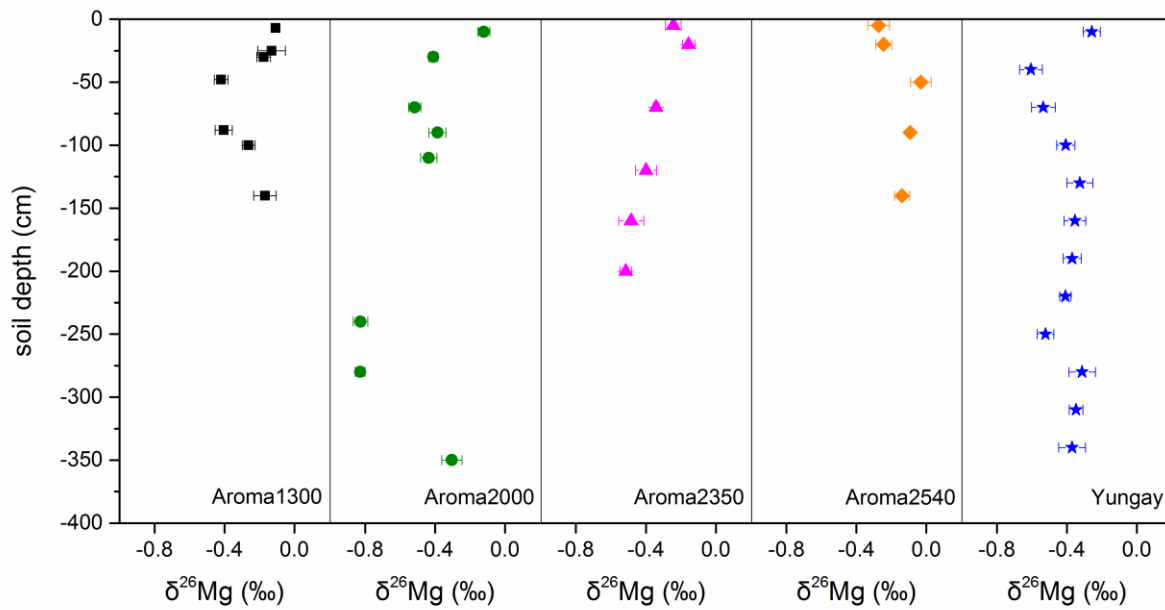


**Figure 3.17** Evolution of Mg isotope compositions with soil profiles at different altitudinal level in the Aroma and Yungay regions. Error bar represents the analytical uncertainty based on repeated measurements (2SD,  $n > 3$ ).

The distinct Mg isotope fractionation along with the whole profile in each site is hypothesized to be weathering-dependent. To verify the hypothesis, the Chemical Proxy of Alteration (CPA), i.e. the molar ratio  $\text{Al}_2\text{O}_3/(\text{Al}_2\text{O}_3 + \text{Na}_2\text{O}) \times 100$ , is introduced as it is proposed to be the most appropriate index for silicate weathering (Buggle et al., 2011).



Soil sample with higher CPA values indicates stronger degree of weathering process. By calculating the CPA of each soil sample, the larger value of  $\delta^{26}\text{Mg}$  was found to correspond to the larger CPA in the upper layer of the pit profile (0-40 cm depth) at the site Aroma 1300, Aroma 2000, Aroma 2350, and Yungay (Table 3.5), vice versa at the site Aroma 2540, indicating a weathering-dependent Mg isotope fractionation. This is in good agreement with previous studies that silicate weathering can lead to enrichment of heavy Mg isotopes in the saprolite because of the preferential loss of light Mg isotopes, (Brenot et al., 2008; Schmitt et al., 2012). As for the site Aroma 2540, three causes may account for the different behavior of Mg isotopes from others, i.e. isotopically lighter in the upper soil layer. First, the atmospheric deposition from Andes due to the eolian transport may play a role in the soil Mg isotope composition as this site with highest altitude is close to the Andes Mountains. The Mg isotope compositions of continental arc andesites in the Andes have a range from  $-0.26 \pm 0.05\text{‰}$  to  $-0.15 \pm 0.04\text{‰}$  with average  $\delta^{26}\text{Mg}$  of  $-0.18 \pm 0.05\text{‰}$  (Xie et al., 2018), while even isotopically lighter andesite was also reported to have a  $\delta^{26}\text{Mg}$  of  $-0.66 \pm 0.02$  (Teng et al., 2015), all of which are lighter than the soil  $\delta^{26}\text{Mg}$  in such field. Continuous accumulation of andesite from the Andes Mountains on the ground surface can thus result in a negative shift of  $\delta^{26}\text{Mg}$  relative to the deeper layers. Second, the moisture may also have the impact on soil  $\delta^{26}\text{Mg}$  at the site Aroma 2540, because northeasterly airflows from the Amazonia during the austral summer could bring convective precipitation even though it is preserved in arid climate (Garreaud et al., 2003; Huston and Hartley, 2003; MaKay et al., 2003). The sites close to the Pre-Cordillera receive  $\sim 10$  mm annual average precipitation (Houston, 2006). Since we did not collect the fog or rainwater sample, an estimated value of  $\delta^{26}\text{Mg}$  in rainwater summarized by Kimmig et al., (2018) from the available data in the present studies was used, ranging

from -0.57 to -2.22‰ with an median of -0.80‰ and an average of  $-0.93 \pm 0.41$ ‰ (SD,  $n=26$ ), close to  $\delta^{26}\text{Mg}$  of the seawater (-0.85‰; Teng, 2017). With this consideration, the precipitation then can bring light Mg isotopes that would affect the  $\delta^{26}\text{Mg}$  of the surface soil. On the other hand, biological effect seems to play a role as withered herbaceous plants like *Atriplex* sp. and cacti (*Browningia candelabris*) were present sparsely at this site with highest elevation. Biological processes, particularly the uptake of Mg by plants, fractionate Mg isotope by depleting heavy Mg isotopes in soil (Bolou-Bi et al., 2012), which also corresponds to the isotopically light Mg in upper soil layer. However, the soil in upper layer gives a lower value of CPA than the sediment, indicating a less weathering extent (Table 3.3). Such a behavior is contrary to the reported observation that presence of vegetation and microbes can enhance the weathering processes (Drever, 1994; Moulton et al., 2000). Therefore, biological effect here is suggested not to make a significant contribution to the soil Mg isotope composition.

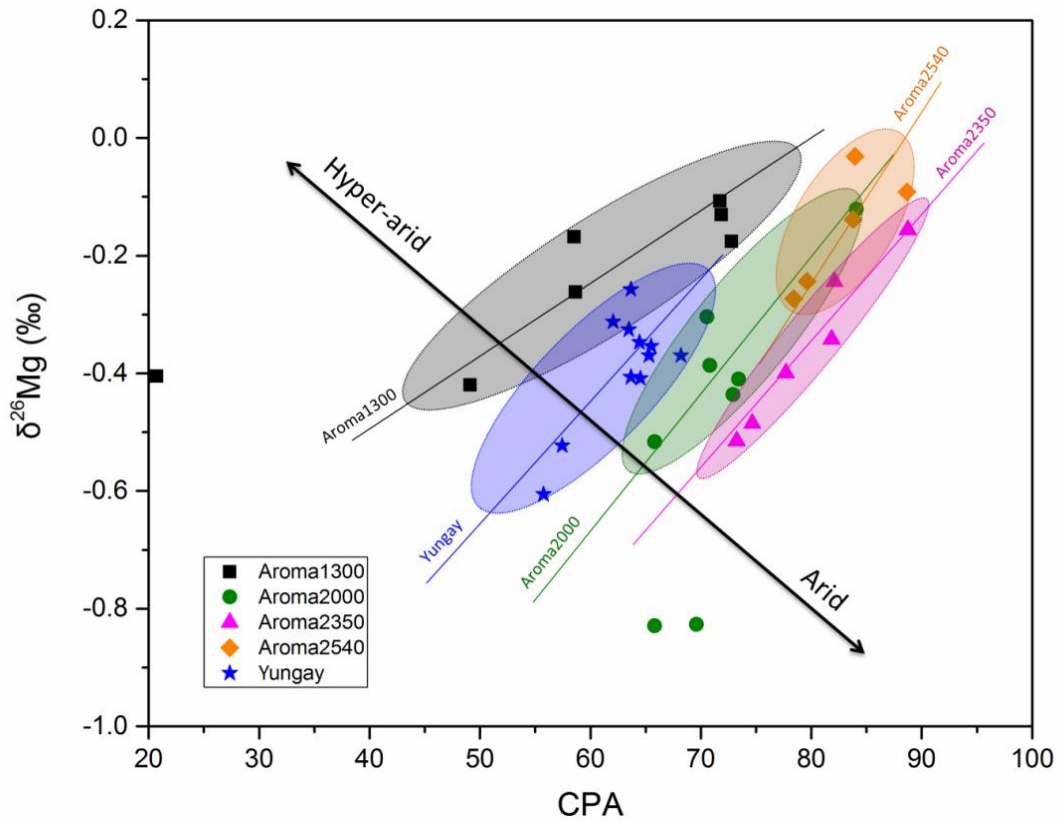


**Figure 3.18** Correlation between the CPA and  $\delta^{26}\text{Mg}$  of soil samples with profile in Aroma and Yungay regions. CPA refers to the Chemical Proxy of Alternation (Buggle et al., 2011), i.e. the molar ratio  $\text{Al}_2\text{O}_3 / (\text{Al}_2\text{O}_3 + \text{Na}_2\text{O}) \times 100$ . Outlier samples in Aroma 1300 and Aroma 2000 were ticked out in the linear analysis.

By plotting the soil  $\delta^{26}\text{Mg}$  as a function of CPA, a positive relationship was observed between the soil  $\delta^{26}\text{Mg}$  and CPA values (Figure 3.18). With increasing CPA values, i.e. stronger degree of weathering, pit soil samples intended to enrich heavy Mg isotopes regardless the elevation of the site, supporting the studies that, light Mg isotopes are preferentially released during the silicate weathering (Teng, 2017). The linear analysis of each site showed a correlation along with aridity gradient (Figure 3.18). The distinct relation between weathering degree and Mg isotope compositions of soil among given

sites may reflect the paleoclimatic conditions at different elevation. In the site Aroma 1300 and Yungay which is generally considered as hyper-arid region (mean annual rainfall < 1 mm), lighter weathering extent was observed compared with others. Huang et al. (2013) reported a significant correlation between the  $\delta^{26}\text{Mg}$  of loess samples and the chemical index of alteration (CIA) and suggested that Mg isotopes implied paleoclimatic changes. However, Wimpenny et al. (2014) pointed out that the CIA may be dependent on the calcite concentration which could directly drive negative shift of  $\delta^{26}\text{Mg}$  and obscure other weathering signals. In our work, soils in the Atacama Desert exhibited quite limited concentration of carbonate (Jones et al., 2018), indicating a potential proxy of Mg isotope systematics used for improving our understanding of paleoclimate in such a hyper-arid region. Nonetheless, further studies on the combination of Mg isotope systematics with other elements such as Ca and O are highly demanded to reconstruct the paleoclimate.

# Chapter 4

## Summary and conclusions

Magnesium (Mg) stable isotope systematics has been recently suggested as a promising and powerful tool to elucidate Mg-related the biogeochemical processes in the terrestrial environment. The aims of this work were to study i) the plant-induced Mg isotope fractionation under Mg deficient supply, ii) the Mg isotope fractionation in a field-scale soil-plant system impacted by long-term anthropogenic soil practices, and iii) the Mg isotope signatures in the Atacama Desert as extreme environment of hyper-aridity.

Plant physiological activities can fractionate Mg isotopes and therefore be traced with such isotopic footprints. In the study of plant-induced Mg isotope fractionation, summer wheat was selected as the model plant and grown in the greenhouse under both sufficient (control, 1 mM MgSO<sub>4</sub>) and deficient (low-Mg, 0.05 mM MgSO<sub>4</sub>) Mg supply along with the whole growth cycle from booting to maturity. Variations of Mg isotope composition in each plant organ at different growth stage were investigated. With the pot experiments, wheat plants were found to prefer heavy Mg isotopes and discriminate against the light ones during the uptake by roots regardless of the external environmental Mg concentration. The bulk plants in control group became isotopically heavier along with the growth, whereas the Mg isotope composition of the bulk plants with low-Mg supply showed no change at different growth stage. The root uptake of Mg with different transport systems

are considered to answer for the discrepancy. In addition, wheat spikes in the low-Mg group showed continuous enrichment of light Mg isotopes with growth, which is contrast to that in the control group, reflecting a different source of Mg loading into wheat spikes. It is concluded that plant can adjust self-regulation of uptake and transport systems when living in the low-Mg environment. Magnesium isotope compositions of bulk plants and individual plant organs can thus reflect the plant response to different level of Mg supply in the external environment and be used as a proxy to trace nutrient uptake and internal transport and distribution.

In a field-scale agricultural system, soil practices may impact the soil properties and nutrient uptake by crops. Magnesium isotopes provide a pioneering insight to evaluate such anthropogenic effect. For this aim, Mg isotope compositions of soil-plant profile in a selected agricultural field with liming practice nearly 100 years were investigated (field trials were located at Berlin-Dahlem as part of SOIL<sup>3</sup> project). The Mg isotope compositions in both the soil total pool ( $Mg_{tot}$ ) and soil exchangeable pool ( $Mg_{exch}$ ) of each soil horizon along with the profile down to 1 m depth, as well as grown crops (winter rye) of experimental plots with or without liming practice were studied. Results showed no variation of  $\delta^{26}Mg_{tot}$  along with profile and no effect of liming on  $\delta^{26}Mg_{tot}$ . However, a negative shift of  $\delta Mg_{exch}$  in limed field compared with that in non-limed field at the depth of 0-50 cm was observed. It was speculated that the enrichment of light Mg isotopes in limed field are resulted from 1) the plant uptake which depletes heavy Mg isotopes in soil and 2) addition of isotopically light lime material. The relative contribution from these two processes was calculated with an isotope-mixing model. Long-term liming practice (nearly 100 years) is considered to enhance the plant uptake of Mg in the soil horizon down to 50

cm depth. This work gives a potential approach to evaluate the effect of anthropogenic activities on soil properties and crop growth with non-traditional stable isotopes in an agricultural system.

The Atacama Desert, as an analog of Mars on Earth, is one of the driest regions characterized by its hyper-arid climate and scarce precipitation. Investigation of Mg isotope signatures in such a region improves our understanding on Mg isotope composition of the extreme environment of hyper-aridity. In this study, compositions of Mg isotope in surface soil layer (0-10 cm) at sites with different elevation (from 1300 to 2700 m a.s.l.) in the Aroma transect were analyzed. Soil samples showed generally a range of  $\delta^{26}\text{Mg}$  from -0.38 to -0.03‰. In different horizons of surface layer (0-1, 1-5, 5-10 cm depth), no obvious change of  $\delta^{26}\text{Mg}$  was observed. However, with the elevation decreased, i.e. aridity increased, soils tended to accumulate light Mg isotopes. Higher value of  $\delta^{26}\text{Mg}$  at the site Ar2000 and Ar1300 indicated another Mg input or loss process. Magnesium of surface soil in the Aroma transect is considered as mixing deposition of both oceanic aerosols and the Andean inputs. In addition, Mg isotope compositions of pit soil samples collected from the Aroma transect with altitudinal gradient were found to be dependent on the weathering degree. Climatic aridity is thought to influence the weathering degree, and thus the Mg isotope signatures. Our study suggested a potential to use Mg isotopes to reconstruct the paleoclimatic changes in such extreme environment of hyper-aridity.

In conclusion, these studies on Mg isotope fractionations provided a comprehensive and innovative insight into i) Mg isotopes as a proxy in the plant physiological response to environmental nutrient shortage, ii) Mg isotopes as a proxy to evaluate the influence of anthropogenic practices on agricultural activities, and iii) Mg isotopes as a proxy to trace

soil formation and paleoclimatic changes in extreme environment (e.g. hyper-arid climate). All of these works improve our understanding on Mg biogeochemical cycles and Mg isotope systematics in different environments.



# Reference

- An, Y., and Huang, F., 2014. A review of Mg isotope analytical methods by MC-ICP-MS. *Journal of Earth Science*, 25: 822-840.
- Aucour, A.M., Pichat, S., Macnair, M.R. and Oger, P., 2011. Fractionation of Stable Zinc Isotopes in the Zinc Hyperaccumulator *Arabidopsis halleri* and Nonaccumulator *Arabidopsis petraea*. *Environmental Science & Technology*, 45(21): 9212-9217.
- Baker, A. and Brooks, R., 1989. Terrestrial higher plants which hyperaccumulate metallic elements. A review of their distribution, ecology and phytochemistry. *Biorecovery.*, 1(2): 81-126.
- Barber S.A., 1995. *Soil Nutrient Bioavailability: A Mechanistic Approach*, New York: Wiley.
- Balogh-Brunstad, Z., Kent Keller, C., Thomas Dickinson, J., Stevens, F., Li, C.Y. and Bormann, B.T., 2008. Biotite weathering and nutrient uptake by ectomycorrhizal fungus, *Suillus tomentosus*, in liquid-culture experiments. *Geochimica et Cosmochimica Acta* 72, 2601-2618.
- Bauke, S., von Sperber, C., Tamburini, F., Gocke, M., Honermeier, B., Schweitzer, K., Baumecker, M., Don, A., Sandhage-Hofmann, A., and Amelung, W. 2018. Subsoil phosphorus is affected by fertilization regime in long-term agricultural experimental trials. *European Journal of Soil Science*, 69(1): 103-112
- Billard, V., Maillard, A., Coquet, L., Jouenne, T., Cruz, F., Garcia-Mina, J.M., Yvin, J.C., Ourry, A. and Etienne, P., 2016. Mg deficiency affects leaf Mg remobilization and the proteome in *Brassica napus*. *Plant Physiology and Biochemistry*, 107: 337-343.
- Bindeman, I.N., Lundstrom, C.C., Bopp, C., Huang, F., 2013. Stable isotope fractionation by thermal diffusion through partially molten wet and dry silicate rocks. *Earth and Planetary Science Letters* 365: 51-62.

- Black, J. R., Yin, Q. Z., Casey, W. H., 2006. An experimental study of magnesium-isotope fractionation in chlorophyll-a photosynthesis. *Geochimica et cosmochimica acta*, 70(16): 4072-4079.
- Black, J. R., Yin, Q. Z., Rustad, J. R., Casey, W. H., 2007. Magnesium isotopic equilibrium in chlorophylls. *Journal of the American Chemical Society*, 129(28): 8690-8691.
- Black, J.R., Epstein, E., Rains, W.D., Yin, Q.Z. and Casey, W.H., 2008. Magnesium-isotope Fractionation During Plant Growth. *Environmental Science & Technology*, 42(21): 7831-7836.
- Blume, H.-P., Brümmer, G.W., Horn, R., Kandeler, E., Kögel-Knabner, I., Kretzschmar, R., Stahr, K. and Wilke, B.-M., 2016. Scheffer/schachtschabel: Lehrbuch der bodenkunde. Springer-Verlag.
- Bolou-Bi, E.B., Poszwa, A., Leyval, C. and Vigier, N., 2010. Experimental determination of magnesium isotope fractionation during higher plant growth. *Geochimica et Cosmochimica Acta*, 74(9): 2523-2537.
- Bolou-Bi, E.B., Vigier, N., Poszwa, A., Boudot, J.P. and Dambrine, E., 2012. Effects of biogeochemical processes on magnesium isotope variations in a forested catchment in the Vosges Mountains (France). *Geochimica et Cosmochimica Acta*, 87: 341-355.
- Bose, J., Babourina, O. and Rengel, Z., 2011. Role of magnesium in alleviation of aluminium toxicity in plants. *Journal of Experimental Botany*, 62(7): 2251-2264.
- Brenot, A., Cloquet, C., Vigier, N., Carignan, J. and France-Lanord, C., 2008. Magnesium isotope systematics of the lithologically varied Moselle river basin, France. *Geochimica Et Cosmochimica Acta*, 72(20): 5070-5089.
- Buchachenko, A. L., 2013. Mass-independent isotope effects. *The Journal of Physical Chemistry B*, 117(8): 2231-2238.
- Buggle, B., Glaser, B., Hambach, U., Gerasimenko, N., Marković, S., 2011. An evaluation of geochemical weathering indices in loess–paleosol studies. *Quaternary International*, 240(1-2): 12-21.

- Bull, A. T., Asenjo, J. A., Goodfellow, M., Gomez-Silva, B., 2016. The Atacama Desert: technical resources and the growing importance of novel microbial diversity. *Annual review of microbiology*, 70: 215-234.
- Cai, J., Chen, L., Qu, H.Y., Lian, J., Liu, W., Hu, Y.B. and Xu, G.H., 2012. Alteration of nutrient allocation and transporter genes expression in rice under N, P, K, and Mg deficiencies. *Acta Physiologiae Plantarum*, 34(3): 939-946.
- Cakmak, I., Hengeler, C. and Marschner, H., 1994. Changes in Phloem Export of Sucrose in Leaves in Response to Phosphorus, Potassium and Magnesium-Deficiency in Bean-Plants. *Journal of Experimental Botany*, 45(278): 1251-1257.
- Cakmak, I. and Kirkby, E.A., 2008. Role of magnesium in carbon partitioning and alleviating photooxidative damage. *Physiologia Plantarum*, 133(4): 692-704.
- Cakmak, I. and Yazici, A.M., 2010. Magnesium: a forgotten element in crop production. *Better Crops*, 94(2): 23-25.
- Chen, Z.C., Peng, W.T., Li, J. and Liao, H., 2018. Functional dissection and transport mechanism of magnesium in plants. *Seminars in Cell & Developmental Biology*, 74: 142-152.
- Chmielewski, F.M. and Kohn, W., 1999. The long-term agrometeorological field experiment at Berlin-Dahlem, Germany. *Agricultural and Forest Meteorology*, 96(1-3): 39-48.
- Cooke, R. U., 1970. Stone pavements in deserts. *Annals of the Association of American Geographers*, 60(3), 560-577.
- Dauphas, N., and Schauble, E. A., 2016. Mass fractionation laws, mass-independent effects, and isotopic anomalies. *Annual Review of Earth and Planetary Sciences*: 44, 709-783.
- Davis, A. M., Richter, F. M., Mendybaev, R. A., Janney, P. E., Wadhwa, M., McKeegan, K. D., 2015. Isotopic mass fractionation laws for magnesium and their effects on <sup>26</sup>Al–<sup>26</sup>Mg systematics in solar system materials. *Geochimica et Cosmochimica Acta*, 158, 245-261.

- Deng, T.H.B., Coquet, C., Tang, Y.T., Sterckeman, T., Echevarria, G., Estrade, N., Morel, J.L. and Qiu, R.L., 2014. Nickel and Zinc Isotope Fractionation in Hyperaccumulating and Nonaccumulating Plants. *Environmental Science & Technology*, 48(20): 11926-11933.
- Derry, L. A., Kurtz, A. C., Ziegler, K., Chadwick, O. A., 2005. Biological control of terrestrial silica cycling and export fluxes to watersheds. *Nature*, 433: 728.
- Dessert, C., Lajeunesse, E., Lloret, E., Clergue, C., Crispi, O., Gorge, C., Quidelleur, X., 2015. Controls on chemical weathering on a mountainous volcanic tropical island: Guadeloupe (French West Indies). *Geochimica et Cosmochimica Acta*, 171, 216-237.
- Ding, Y., Luo, W. and Xu, G., 2006. Characterisation of magnesium nutrition and interaction of magnesium and potassium in rice. *Annals of Applied Biology*, 149(2): 111-123.
- Drever, J.I., 1994, The effect of land plants on weathering rates of silicate minerals. *Geochimica et Cosmochimica Acta* 58: 2325-2332.
- Ewing, S. A., Sutter, B., Owen, J., Nishiizumi, K., Sharp, W., Cliff, S.S., Perry, K., Dietrich, W., McKay, C.P., Amundson, R., 2006. A threshold in soil formation at Earth's arid–hyperarid transition. *Geochimica et Cosmochimica Acta*, 70(21), 5293-5322.
- Evenstar, L. A., Hartley, A. J., Stuart, F. M., Mather, A. E., Rice, C. M., Chong, G., 2009. Multiphase development of the Atacama Planation Surface recorded by cosmogenic  $^3\text{He}$  exposure ages: Implications for uplift and Cenozoic climate change in western South America. *Geology*, 37(1), 27-30.
- Fahad, Z.A., Bolou-Bi, E.B., Kohler, S.J., Finlay, R.D. and Mahmood, S., 2016. Fractionation and assimilation of Mg isotopes by fungi is species dependent. *Environmental Microbiology Reports*, 8(6): 956-965.
- Galy, A., Bar-Matthews, M., Halicz, L. and O'Nions, R.K., 2002. Mg isotopic composition of carbonate: insight from speleothem formation. *Earth and Planetary Science Letters*, 201(1): 105-115.

- Galy, A., Yoffe, O., Janney, P.E., Williams, R.W., Cloquet, C., Alard, O., Halicz, L., Wadhwa, M., Hutcheon, I.D., Ramon, E. and Carignan, J., 2003. Magnesium isotope heterogeneity of the isotopic standard SRM980 and new reference materials for magnesium-isotope-ratio measurements. *Journal of Analytical Atomic Spectrometry*, 18(11): 1352-1356.
- Gao, T., Ke, S., Wang, S.J., Li, F.B., Liu, C.S., Lei, J., Liao, C.Z. and Wu, F., 2018. Contrasting Mg isotopic compositions between Fe-Mn nodules and surrounding soils: Accumulation of light Mg isotopes by Mg-depleted clay minerals and Fe oxides. *Geochimica et Cosmochimica Acta*, 237: 205-222.
- Garreaud R.D., Vuille M., Clement A.C., 2003. The climate of the Altiplano: observed current conditions and mechanisms of past changes. *Palaeogeography, Palaeoclimatology, Palaeoecology* 194: 5–22.
- Gebert, M., Meschenmoser, K., Svidova, S., Weghuber, J., Schweyen, R., Eifler, K., Lenz, H., Weyand, K. and Knoop, V., 2009. A Root-Expressed Magnesium Transporter of the MRS2/MGT Gene Family in *Arabidopsis thaliana* Allows for Growth in Low-Mg<sup>2+</sup> Environments. *Plant Cell*, 21(12): 4018-4030.
- Gransee, A. and Führes, H., 2013. Magnesium mobility in soils as a challenge for soil and plant analysis, magnesium fertilization and root uptake under adverse growth conditions. *Plant and Soil*, 368(1-2): 5-21.
- Gerendas, J. and Führes, H., 2013. The significance of magnesium for crop quality. *Plant and Soil*, 368(1-2): 101-128.
- Guo, W.L., Nazim, H., Liang, Z.S. and Yang, D.F., 2016. Magnesium deficiency in plants: An urgent problem. *Crop Journal*, 4(2): 83-91.
- Hermans, C., Conn, S.J., Chen, J.G., Xiao, Q.Y. and Verbruggen, N., 2013. An update on magnesium homeostasis mechanisms in plants. *Metallomics*, 5(9): 1170-1183.
- Hobley, E. U., and Prater, I., 2019. Estimating soil texture from vis–NIR spectra. *European journal of soil science* 70 (1): 83-95.

- Houston, J., and Hartley, A. J., 2003. The central Andean west-slope rainshadow and its potential contribution to the origin of hyper-aridity in the Atacama Desert. *International Journal of Climatology: A Journal of the Royal Meteorological Society*, 23(12), 1453-1464.
- Houston, J., 2006. Variability of precipitation in the Atacama Desert: its causes and hydrological impact. *International Journal of Climatology: A Journal of the Royal Meteorological Society*, 26(15), 2181-2198.
- Huang, K. J., Teng, F. Z., Wei, G. J., Ma, J. L. and Bao, Z. Y., 2012. Adsorption- and desorption-controlled magnesium isotope fractionation during extreme weathering of basalt in Hainan Island, China. *Earth and Planetary Science Letters*, 359: 73-83.
- Huang, K. J., Teng, F. Z., Elsenouy, A., Li, W. Y., Bao, Z. Y., 2013. Magnesium isotopic variations in loess: Origins and implications. *Earth and Planetary Science Letters*: 374, 60-70.
- IUSS Working Group WRB. (2014). World Reference Base for Soil Resources. International soil classification system for naming soils and creating legends for soil maps. World Soil Resources Reports, No. 106. FAO, Rome.
- Immenhauser, A., Buhl, D., Richter, D., Niedermayr, A., Riechelmann, D., Dietzel, M., Schulte, U., 2010. Magnesium-isotope fractionation during low-Mg calcite precipitation in a limestone cave—Field study and experiments. *Geochimica et Cosmochimica Acta*, 74(15): 4346-4364.
- Johnson, C.M., Beard, B.L., Albarède, F., 2004. Overview and General Concepts. *Reviews in Mineralogy and Geochemistry* 55, 1-24.
- Jones, D. L., Olivera-Ardid, S., Klumpp, E., Knief, C., Hill, P. W., Lehndorff, E., Bol, R., 2018. Moisture activation and carbon use efficiency of soil microbial communities along an aridity gradient in the Atacama Desert. *Soil Biology and Biochemistry*, 117, 68-71.
- Jouvin, D., Weiss, D. J., Mason, T. F. M., Bravin, M. N., Louvat, P., Zhao, F., Ferec, F., Hinsinger, P., Benedetti, M. F., 2012. Stable isotopes of Cu and Zn in higher plants: evidence for Cu reduction at the root surface and two conceptual models for

isotopic fractionation processes. *Environmental science & technology*, 46(5), 2652-2660.

Kautz, T., Amelung, W., Ewert, F., Gaiser, T., Horn, R., Jahn, R., Javaux, M., Kemna, A., Kuzyakov, Y., Munch, J.C., Patzold, S., Peth, S., Scherer, H.W., Schlöter, M., Schneider, H., Vanderborght, J., Vetterlein, D., Walter, A., Wiesenberger, G.L.B. and Kopke, U., 2013. Nutrient acquisition from arable subsoils in temperate climates: A review. *Soil Biology & Biochemistry*, 57: 1003-1022.

Kelly, J.M. and Barber, S.A., 1991. Magnesium Uptake Kinetics in Loblolly-Pine Seedlings. *Plant and Soil*, 134(2): 227-232.

Kimmig, S.R., Holmden, C. and Belanger, N., 2018. Biogeochemical cycling of Mg and its isotopes in a sugar maple forest in Quebec. *Geochimica et Cosmochimica Acta*, 230: 60-82.

Kobayashi, N.I. and Tanoi, K., 2015. Critical Issues in the Study of Magnesium Transport Systems and Magnesium Deficiency Symptoms in Plants. *International Journal of Molecular Sciences*, 16(9): 23076-23093.

Köhn, W. and Ellmer, F., 2009. Dauerfeldversuche in Brandenburg und Berlin. Beiträge für eine nachhaltige Landwirtschaftliche Bodennutzung (Long-term field tests in Brandenburg and Berlin. Contributions to sustainable agricultural land use). State Office for Consumer Protection, Agriculture and Land Consolidation, Department of Agriculture and Horticulture, Series in Agriculture, 10, 216

Komai, Y. Studies on the absorption of cations by barley roots with special references to magnesium. *Bull. Univ. Osaka Prefecture B Agric. Biol.*, 14 (1962), pp. 99-126.

Kuhlmann, H. and Baumgartel, G., 1991. Potential Importance of the Subsoil for the P and Mg Nutrition of Wheat. *Plant and Soil*, 137(2): 259-266.

Lara, M.C., Buss, H.L., von Strandmann, P.A.E.P., Schuessler, J.A. and Moore, O.W., 2017. The influence of critical zone processes on the Mg isotope budget in a tropical, highly weathered andesitic catchment. *Geochimica Et Cosmochimica Acta*, 202: 77-100.

- Li, H.X., Chen, Z.J., Zhou, T., Liu, Y., Raza, S. and Zhou, J.B., 2018. Effects of High Potassium and Low Temperature on the Growth and Magnesium Nutrition of Different Tomato Cultivars. *Hortscience*, 53(5): 710-714.
- Li, H.Y., Du, H.M., Huang, K.F., Chen, X., Liu, T.Y., Gao, S.B., Liu, H.L., Tang, Q.L., Rong, T.Z. and Zhang, S.Z., 2016. Identification, and Functional and Expression Analyses of the CorA/MRS2/MGT-Type Magnesium Transporter Family in Maize. *Plant and Cell Physiology*, 57(6): 1153-1168.
- Li, L.G., Tutone, A.F., Drummond, R.S.M., Gardner, R.C. and Luan, S., 2001. A novel family of magnesium transport genes in Arabidopsis. *Plant Cell*, 13(12): 2761-2775.
- Li, W.Q., Beard, B.L., Li, C.X. and Johnson, C.M., 2014. Magnesium isotope fractionation between brucite [Mg(OH)(2)] and Mg aqueous species: Implications for silicate weathering and biogeochemical processes. *Earth and Planetary Science Letters*, 394: 82-93.
- Li, W.Q., Chakraborty, S., Beard, B.L., Romanek, C.S. and Johnson, C.M., 2012. Magnesium isotope fractionation during precipitation of inorganic calcite under laboratory conditions. *Earth and Planetary Science Letters*, 333: 304-316.
- Liu, X.M., Teng, F.Z., Rudnick, R.L., McDonough, W.F. and Cummings, M.L., 2014. Massive magnesium depletion and isotope fractionation in weathered basalts. *Geochimica Et Cosmochimica Acta*, 135: 336-349.
- Ma, L., Teng, F.Z., Jin, L., Ke, S., Yang, W., Gu, H.O. and Brantley, S.L., 2015. Magnesium isotope fractionation during shale weathering in the Shale Hills Critical Zone Observatory: Accumulation of light Mg isotopes in soils by clay mineral transformation. *Chemical Geology*, 397: 37-50.
- Magna, T., Hu, Y., Teng, F. Z., Mezger, K., 2017. Magnesium isotope systematics in Martian meteorites. *Earth and planetary science letters*, 474, 419-426.
- Maguire, M.E. and Cowan, J.A., 2002. Magnesium chemistry and biochemistry. *Biometals*, 15(3): 203-210.



- Maroto-Valer, M.M., Fauth, D.J., Kuchta, M.E., Zhang, Y. and Andrésen, J.M., 2005. Activation of magnesium rich minerals as carbonation feedstock materials for CO<sub>2</sub> sequestration. *Fuel Processing Technology*, 86: 1627-1645.
- Marschner, H., 2011. Marschner's mineral nutrition of higher plants. Academic press.
- Martin, P., 1982. Stem Xylem as a Possible Pathway for Mineral Retranslocation from Senescing Leaves to the Ear in Wheat. *Australian Journal of Plant Physiology*, 9(2): 197-207.
- Mavromatis, V., Prokushkin, A.S., Pokrovsky, O.S., Viers, J. and Korets, M.A., 2014. Magnesium isotopes in permafrost-dominated Central Siberian larch forest watersheds. *Geochimica Et Cosmochimica Acta*, 147: 76-89.
- McKay, C. P., Friedmann, E. I., Gómez-Silva, B., Cáceres-Villanueva, L., Andersen, D. T., Landheim, R., 2003. Temperature and moisture conditions for life in the extreme arid region of the Atacama Desert: four years of observations including the El Nino of 1997–1998. *Astrobiology*, 3(2): 393-406.
- Mengutay, M., Ceylan, Y., Kutman, U.B. and Cakmak, I., 2013. Adequate magnesium nutrition mitigates adverse effects of heat stress on maize and wheat. *Plant and Soil*, 368(1-2): 57-72.
- Metson, A., 1974. Magnesium in New Zealand soils I. Some factors governing the availability of soil magnesium: a review. *New Zealand Journal of Experimental Agriculture*, 2(3): 277-319.
- Mikkelsen, R., 2010. Soil and fertilizer magnesium. *Better crops*, 94(2), 26-28.
- Mile, M. and Mitkova, T., 2013. Soil Moisture Retention Changes in Terms of Mineralogical Composition of Clays Phase. *Clay Minerals in Nature - Their Characterization, Modification and Application*: 101-118.
- Morgan, A. M., Howard, A. D., Hobley, D. E., Moore, J. M., Dietrich, W. E., Williams, R. M., Burr, D.M., et al., 2014. Sedimentology and climatic environment of alluvial fans in the martian Saheki crater and a comparison with terrestrial fans in the Atacama Desert. *Icarus*, 229, 131-156.

- Moulton, K.L., West, J. and Berner, R.A. (2000) Solute flux and mineral mass balance approaches to the quantification of plant effects on silicate weathering. *American Journal of Science* 300: 539-570.
- Oelkers, E.H., Benning, L.G., Lutz, S., Mavromatis, V., Pearce, C.R. and Plümper, O., 2015. The efficient long-term inhibition of forsterite dissolution by common soil bacteria and fungi at Earth surface conditions. *Geochimica et Cosmochimica Acta* 168, 222-235.
- Opfergelt, S., Burton, K.W., Georg, R.B., West, A.J., Guicharnaud, R.A., Sigfusson, B., Siebert, C., Gislason, S.R. and Halliday, A.N., 2014. Magnesium retention on the soil exchange complex controlling Mg isotope variations in soils, soil solutions and vegetation in volcanic soils, Iceland. *Geochimica et Cosmochimica Acta*, 125: 110-130.
- Opfergelt, S., Georg, R.B., Delvaux, B., Cabidoche, Y.M., Burton, K.W. and Halliday, A.N., 2012. Mechanisms of magnesium isotope fractionation in volcanic soil weathering sequences, Guadeloupe. *Earth and Planetary Science Letters*, 341: 176-185.
- Pasternak, K., Kocot, J. and Horecka, A., 2010. Biochemistry of Magnesium. *Journal of Elementology*, 15(3): 601-616.
- Pinto, L., Hérail, G., Moine, B., Fontan, F., Charrier, R., Dupré, B., 2004. Using geochemistry to establish the igneous provenances of the Neogene continental sedimentary rocks in the Central Depression and Altiplano, Central Andes. *Sedimentary Geology*, 166(1-2): 157-183.
- Pogge von Strandmann, P.A.E., Burton, K.W., James, R.H., van Calsteren, P., Gislason, S.R. and Sigfusson, B., 2008. The influence of weathering processes on riverine magnesium isotopes in a basaltic terrain. *Earth and Planetary Science Letters*, 276(1-2): 187-197.
- Pokharel, R., Gerrits, R., Schuessler, J.A., Floor, G.H., Gorbushina, A.A. and von Blanckenburg, F., 2017. Mg Isotope Fractionation during Uptake by a Rock-Inhabiting, Model Microcolonial Fungus *Knufia petricola* at Acidic and Neutral pH. *Environmental Science & Technology*, 51(17): 9691-9699.

- Pokharel, R., Gerrits, R., Schuessler, J.A., Frings, P.J., Sobotka, R., Gorbushina, A.A. and von Blanckenburg, F., 2018. Magnesium Stable Isotope Fractionation on a Cellular Level Explored by Cyanobacteria and Black Fungi with Implications for Higher Plants. *Environmental Science & Technology*, 52(21): 12216-12224.
- Ra, K., and Kitagawa, H., 2007. Magnesium isotope analysis of different chlorophyll forms in marine phytoplankton using multi-collector ICP-MS. *Journal of Analytical Atomic Spectrometry*, 22(7), 817-821.
- Ra, K., Kitagawa, H., Shiraiwa, Y., 2010. Mg isotopes in chlorophyll-a and coccoliths of cultured coccolithophores (*Emiliana huxleyi*) by MC-ICP-MS. *Marine Chemistry*, 122(1-4): 130-137.
- Rech, J. A., Quade, J., Hart, W. S., 2003. Isotopic evidence for the source of Ca and S in soil gypsum, anhydrite and calcite in the Atacama Desert, Chile. *Geochimica et Cosmochimica Acta*, 67(4): 575-586.
- Ryu, J.S., Vigier, N., Decarreau, A., Lee, S.W., Lee, K.S., Song, H. and Petit, S., 2016. Experimental investigation of Mg isotope fractionation during mineral dissolution and clay formation. *Chemical Geology*, 445: 135-145.
- Saenger, C., & Wang, Z., 2014. Magnesium isotope fractionation in biogenic and abiogenic carbonates: implications for paleoenvironmental proxies. *Quaternary Science Reviews*, 90: 1-21.
- Saito, T., Kobayashi, N.I., Tanoi, K., Iwata, N., Suzuki, H., Iwata, R. and Nakanishi, T.M., 2013. Expression and Functional Analysis of the CorA-MRS2-ALR-Type Magnesium Transporter Family in Rice. *Plant and Cell Physiology*, 54(10): 1673-1683.
- Schmitt, A.D., Vigier, N., Lemarchand, D., Millot, R., Stille, P. and Chabaux, F., 2012. Processes controlling the stable isotope compositions of Li, B, Mg and Ca in plants, soils and waters: A review. *Comptes Rendus Geoscience*, 344(11-12): 704-722.
- Senbayram, M., Gransee, A., Wahle, V., Thiel, H., 2016. Role of magnesium fertilisers in agriculture: plant–soil continuum. *Crop and Pasture Science*, 66(12), 1219-1229.

- Schauble, E. A., 2004. Applying stable isotope fractionation theory to new systems. *Reviews in Mineralogy and Geochemistry*, 55(1): 65-111.
- Shaul, O., 2002. Magnesium transport and function in plants: the tip of the iceberg. *Biometals*, 15(3): 309-323.
- Shaul, O., Hilgemann, D.W., de-Almeida-Engler, J., Van Montagu, M., Inze, D. and Galili, G., 1999. Cloning and characterization of a novel  $Mg^{2+}/H^{+}$  exchanger. *Embo Journal*, 18(14): 3973-3980.
- Stok, B.P., Tanczos, O.G., Kahr, M., Stuiver, C.E.E., Kylin, A. and Kuiper, P.J.C., 1981. Transport of  $Mg^{2+}$  and  $Ca^{2+}$ , and  $Mg^{2+}$ -Stimulated Adenosine-Triphosphatase Activity in Oat Roots as Affected by Mineral-Nutrition. *Physiologia Plantarum*, 52(1): 115-123.
- Sümer, M.R., 2013. Auswirkungen verschiedener Bodennutzungssysteme auf ausgewählte physiko-chemische Bodeneigenschaften und pflanzenbauliche Parameter in Berlin-Dahlem und Dedelow.
- Tang, R.J. and Luan, S., 2017. Regulation of calcium and magnesium homeostasis in plants: from transporters to signaling network. *Current Opinion in Plant Biology*, 39: 97-105.
- Tang, Y.T., Cloquet, C., Sterckeman, T., Echevarria, G., Carignan, J., Qiu, R.L. and Morel, J.L., 2012. Fractionation of Stable Zinc Isotopes in the Field-Grown Zinc Hyperaccumulator *Noccaea caerulescens* and the Zinc-Tolerant Plant *Silene vulgaris*. *Environmental Science & Technology*, 46(18): 9972-9979.
- Tang, Y. T., Cloquet, C., Deng, T. H. B., Sterckeman, T., Echevarria, G., Yang, W. J., Morel, J. L., Qiu, R. L. (2016). Zinc isotope fractionation in the hyperaccumulator *Noccaea caerulescens* and the nonaccumulating plant *Thlaspi arvense* at low and high Zn supply. *Environmental science & technology*, 50(15): 8020-8027.
- Tanoi, K., Kobayashi, N.I., Saito, T., Iwata, N., Kamada, R., Iwata, R., Suzuki, H., Hirose, A., Ohmae, Y., Sugita, R. and Nakanishi, T.M., 2014. Effects of magnesium deficiency on magnesium uptake activity of rice root, evaluated using  $^{28}Mg$  as a tracer. *Plant and Soil*, 384(1-2): 69-77.

- Tapia, J., González, R., Townley, B., Oliveros, V., Álvarez, F., Aguilar, G., Menzies, A., Calderón, M. (2018). Geology and geochemistry of the Atacama Desert. *Antonie van Leeuwenhoek*, 111(8), 1273-1291.
- Teng, F.Z., 2017. Magnesium Isotope Geochemistry. *Non-Traditional Stable Isotopes*, 82: 219-287.
- Teng, F.Z., Man, Y., Liang, S., Buerger, G., Zhu, Y.F., Han, W., Xu, P., Xiong, G.X. and Tian, Z.J., 2007. Crystal structure stability and catalytic activity of magnetoplumbite (MP) catalyst doped with Mn and Mg. *Journal of Non-Crystalline Solids*, 353(52-54): 4806-4812.
- Teng, F.Z., Li, W.Y., Rudnick, R.L. and Gardner, L.R., 2010. Contrasting lithium and magnesium isotope fractionation during continental weathering. *Earth and Planetary Science Letters*, 300(1-2): 63-71.
- Teng, F.Z., Wadhwa, M. and Helz, R.T., 2007. Investigation of magnesium isotope fractionation during basalt differentiation: Implications for a chondritic composition of the terrestrial mantle. *Earth and Planetary Science Letters*, 261(1-2): 84-92.
- Teng, F. Z., Yin, Q. Z., Ullmann, C. V., Chakrabarti, R., Pogge von Strandmann, P. A., Yang, W., Ke, S., et al., 2015. Interlaboratory comparison of magnesium isotopic compositions of 12 felsic to ultramafic igneous rock standards analyzed by MC-ICPMS. *Geochemistry, Geophysics, Geosystems*, 16(9): 3197-3209.
- Tipper, E.T., Galy, A. and Bickle, M.J., 2008. Calcium and magnesium isotope systematics in rivers draining the Himalaya-Tibetan-Plateau region: Lithological or fractionation control? *Geochimica Et Cosmochimica Acta*, 72(4): 1057-1075.
- Tipper, E.T., Galy, A., Gaillardet, J., Bickle, M.J., Elderfield, H. and Carder, E.A., 2006. The magnesium isotope budget of the modern ocean: Constraints from riverine magnesium isotope ratios. *Earth and Planetary Science Letters*, 250(1-2): 241-253.
- Tipper, E.T., Lemarchand, E., Hindshaw, R.S., Reynolds, B.C. and Bourdon, B., 2012. Seasonal sensitivity of weathering processes: Hints from magnesium isotopes in a glacial stream. *Chemical Geology*, 312: 80-92.

- Uhlig, D., Schuessler, J.A., Bouchez, J., Dixon, J.L. and von Blanckenburg, F., 2017. Quantifying nutrient uptake as driver of rock weathering in forest ecosystems by magnesium stable isotopes. *Biogeosciences*, 14(12): 3111-3128.
- van der Heijden, G., Legout, A., Midwood, A.J., Craig, C.A., Pollier, B., Ranger, J. and Dambrine, E., 2013. Mg and Ca root uptake and vertical transfer in soils assessed by an in situ ecosystem-scale multi-isotopic (Mg-26 & Ca-44) tracing experiment in a beech stand (Breuil-Chenue, France). *Plant and Soil*, 369(1-2): 33-45.
- Vanhaecke, F., Degryse, P., 2012. Isotopic analysis. Fundamentals and applications using ICP-MS. Wiley-VCH, Weinheim.
- Verbruggen, N. and Hermans, C., 2013. Physiological and molecular responses to magnesium nutritional imbalance in plants. *Plant and Soil*, 368(1-2): 87-99.
- Walter, K., Don, A., Tiemeyer, B., and Freibauer, A., 2016. Determining soil bulk density for carbon stock calculation: a systematic method comparison. *Soil Science Society of America Journal*, 80: 579–591
- Wang, F., Michalski, G., Seo, J. H., Ge, W., 2014. Geochemical, isotopic, and mineralogical constraints on atmospheric deposition in the hyper-arid Atacama Desert, Chile. *Geochimica et Cosmochimica Acta*, 135: 29-48.
- Wang, F., Michalski, G., Seo, J. H., Granger, D. E., Lifton, N., Caffee, M., 2015. Beryllium-10 concentrations in the hyper-arid soils in the Atacama Desert, Chile: Implications for arid soil formation rates and El Niño driven changes in Pliocene precipitation. *Geochimica et Cosmochimica Acta*, 160: 227-242.
- Wang, S.J., Teng, F.Z., Rudnick, R.L. and Li, S.G., 2015. The behavior of magnesium isotopes in low-grade metamorphosed mudrocks. *Geochimica Et Cosmochimica Acta*, 165: 435-448.
- White, P. J., & Brown, P. H., 2010. Plant nutrition for sustainable development and global health. *Annals of botany*, 105(7): 1073-1080.
- Wiederhold, J. G., 2015. Metal stable isotope signatures as tracers in environmental geochemistry. *Environmental science & technology* 49 (5):2606-2624.

- Willows, R.D., 2007. Chlorophyll synthesis, The structure and function of plastids. Springer, pp. 295-313.
- Wimpenny, J., Colla, C.A., Yin, Q.Z., Rustad, J.R. and Casey, W.H., 2014a. Investigating the behaviour of Mg isotopes during the formation of clay minerals. *Geochimica Et Cosmochimica Acta*, 128: 178-194.
- Wimpenny, J., Gislason, S.R., James, R.H., Gannoun, A., Pogge Von Strandmann, P.A.E. and Burton, K.W., 2010. The behaviour of Li and Mg isotopes during primary phase dissolution and secondary mineral formation in basalt. *Geochimica Et Cosmochimica Acta*, 74(18): 5259-5279.
- Wimpenny, J., Yin, Q.Z., Tollstrup, D., Xie, L.W. and Sun, J., 2014b. Using Mg isotope ratios to trace Cenozoic weathering changes: A case study from the Chinese Loess Plateau. *Chemical Geology*, 376: 31-43.
- Wombacher, F., Eisenhauer, A., Heuser, A. and Weyer, S., 2009. Separation of Mg, Ca and Fe from geological reference materials for stable isotope ratio analyses by MC-ICP-MS and double-spike TIMS. *Journal of Analytical Atomic Spectrometry*, 24(5): 627-636.
- Xie, Q., Zhang, Z., Campos, E., Cheng, Z., Fei, X., Liu, B., Qiu, Y., Santosh, M., Ke, S., Xu, L. (2018). Magnesium isotopic composition of continental arc andesites and the implications: A case study from the El Laco volcanic complex, Chile. *Lithos*, 318, 91-103.
- Young, E.D. and Galy, A., 2004. The isotope geochemistry and cosmochemistry of magnesium. *Geochemistry of Non-Traditional Stable Isotopes*, 55(1): 197-230.
- Young, E. D., Galy, A., Nagahara, H., 2002. Kinetic and equilibrium mass-dependent isotope fractionation laws in nature and their geochemical and cosmochemical significance. *Geochimica et Cosmochimica Acta*, 66(6): 1095-1104.

# List of Figures

**Figure 1.1** Magnesium isotope signatures in major extraterrestrial and terrestrial reservoirs. The vertical line represents the average Mg isotope composition of the bulk Earth ( $\delta^{26}\text{Mg} = -0.25 \pm 0.04\text{‰}$ , 2SD), adapted from Teng (2017). **6**

**Figure 1.2** Schematic illustration of kinetic (a) and equilibrium (b) isotope fractionation, adapted from Wiederhold (2015). **8**

**Figure 1.3** Magnesium three-isotope plot from terrestrial and extraterrestrial samples. Solid line (slope = 0.511) and dashed line (slope = 0.521) represents the predicted kinetic and equilibrium fractionation laws, respectively. Data are adapted from Young and Galy (2004), Bolou-Bi et al. (2012), Teng (2017) and Uhlig et al. (2017). **10**

**Figure 2.1** Field map and sampling plots with soil texture change profile (Sümer 2012). The red and blue squares represent the studied plots with or without liming practice, respectively. Subsoil displayed great heterogeneity in this investigated field. **27**

**Figure 2.2** Location of the investigated sites in the Atacama Desert. The exact sampling sites are marked in the map with labels. The red labels indicate the sites where surface samples (end with s) were collected and black ones represent the pit samples (end with p). The Yungay site is marked with blue color. **30**

**Figure 2.3** Three-isotope plot for measured values of  $\delta^{26}\text{Mg}$  and  $\delta^{25}\text{Mg}$  (relative to NIST SRM980) of plant samples in the control group (green circles) and low-Mg supply pots (red squares), as well as those of nutrient solution relicates (blue diamonds). The fitting equation with a slope of 0.512 ( $R^2 = 0.996$ ) indicates the absence of mass-independent isotope fractionation during analytical sessions (Data from section 3.1). **36**

**Figure 3.1** Plant biomass in dry weight (a) and root/shoot ratio of biomass (b) at different growth stages with different Mg supply: control, 1 mM Mg; low Mg, 0.05 mM Mg. Data are given as the mean  $\pm$  SE of four pot replicates. Different letters denote statically significant



differences between two groups at the same growth phase using ANOVA with OriginPro 2015 ( $p < 0.05$ ). 39

**Figure 3.2** Mg concentration in each plant tissue along the growth stage at different Mg supply: control, 1 mM Mg (white); low-Mg supply, 0.05 mM Mg (purple). Patterns represent different growth stage (from left to right: booting, flowering, post-flowering, maturity). Data are given as the mean  $\pm$  SE of four pot replicates. 40

**Figure 3.3** Changes of Mg isotope composition of the bulk plant along with growth stages at different Mg supply. The black solid line and blue area represent the  $\delta^{26}\text{Mg}$  values of the nutrient solution ( $-2.70 \pm 0.03\text{‰}$ , 2SD,  $n=3$ ). Plants grown under both control and low-Mg conditions showed enrichment of heavy Mg isotopes relative to the nutrient solution. Data are calculated based on mass-balance equation and given as the mean  $\pm$  SE of four pot replicates. In the horizontal axis post-fl is short for post-flowering. 44

**Figure 3.4** Evolution of Mg isotope composition in each organ of wheat plants (root, stem, leaf, spike) having grown under control (1 mM Mg) and low-Mg (0.05 mM Mg) conditions during the growth period from the booting to the full maturity. Data are given as the mean  $\pm$  SE of four pot replicates. In the horizontal axis post-fl is short for post-flowering. 45

**Figure 3.5** Rayleigh-type mass balance model to illustrate Mg isotope fractionation between root and whole plant ( $\Delta^{26}\text{Mg}_{\text{Root-Plant}}$ ) during Mg translocation, based on the mass ratio of Mg between root and plant ( $F_{\text{root}}$ , see Table 3.1). Different symbols represent different growth stages under control (filled symbols) and low-Mg supply (open symbols): booting (diamond), flowering (triangle), post-flowering (circle) and maturity (square). 52

**Figure 3.6** Depth profiles of Mg concentrations (a), stocks (b), and isotope compositions (c) in bulk soil samples collected from experimental fields with (open red) or without (solid black) liming management. Horizon designations given according to German classification are German descriptions of a representative key soil profile at the experimental site, where

Ap is the ploughed topsoil, Bv-Ael and Ael correspond to an eluvial horizon, and Ael+Bt and Bt to an argic horizon according to World Reference Base (IUSS Working Group WRB, 2015). Data are shown as mean  $\pm$  SE of three field replicates. Larger error bars in figure (a) indicate heterogeneity of Mg concentration in the upper subsoil.

**55**

**Figure 3.7** Concentration of exchangeable Mg in soil ( $[Mg]_{\text{exch}}$ ) along soil depth (diamond) and in each plant organ of winter rye (triangle) in limed (open red) and non-limed (solid black) plots. Horizon designations and descriptions are shown in Figure 3.6. Data are given as mean value  $\pm$  SE of three field replicates.

**56**

**Figure 3.8** Ratio of Mg concentration in soil exchangeable pool to bulk soil with (a) and Mg stock in soil exchangeable pool (b) with depths in study fields receiving different soil management. Data are shown as mean value  $\pm$  SE of three field replicates.

**57**

**Figure 3.9** Isotope compositions of the exchangeable Mg pool in soil (square) along soil depth and in each plant organ (star) in limed (open red) and non-limed (solid black) plots. The red arrow represents the addition of lime in limed plots with a  $\delta^{26}\text{Mg}$  of  $-1.51 \pm 0.02$  ‰ (2SD,  $n=3$ ). For horizon designations and descriptions see caption of Figure 3.6. Data are presented as mean value  $\pm$  SE of three field replicates.

**58**

**Figure 3.10** Biomass in dry weight of each plant organ of winter rye. Data are given as mean  $\pm$  SD ( $n>10$ ). No significant difference of crop biomass was shown due to liming practice.

**59**

**Figure 3.11** A schematic diagram of Mg cycles in soil-plant ecosystem. The square boxes stand for the solid phases and the oval boxes represent dissolved species. To be pointed out that this diagram is not involved all biotic/abiotic processes, e.g. clay mineral transformation, microbe-induced transformation of Mg species.

**62**

**Figure 3.12** Conceptual diagram of the isotope-mixing model to calculate the Mg isotope mass balance between plant and exchangeable Mg pool in the present agricultural system with (left) and without (right) liming practice. Soil profiles were divided into three horizons topsoil, upper subsoil and lower subsoil with soil depth of 0-30, 30-50, 50-100 cm,

respectively (blocks marked in different colors). We considered the topsoil (brown) and upper subsoil (blue) as a combined block according to the hypothesis. The Mg isotope compositions in the exchangeable Mg pools are given as range of the  $\delta^{26}\text{Mg}$  values in the combined blocks of topsoil-upper subsoil (brown and blue) and the blocks of lower subsoil (grey), respectively (Table 3.2). The  $\delta^{26}\text{Mg}$  values of the crop (green) are given as calculated mean of the whole plant  $\pm$  SE of three field replicates (Table 3.3) and the  $\delta^{26}\text{Mg}$  value of the lime product (red) is given as mean  $\pm$  2SD of sample replicates (n=3).

**70**

**Figure 3.13** Magnesium isotope compositions with altitudinal gradient in Aroma region. Symbol in each block from left to right represents the sampling soil horizon of 0-1, 1-5, 5-10 cm depth, respectively. Error bar in the figure means the standard error of three field replicates.

**75**

**Figure 3.14** The relationship between  $\delta^{26}\text{Mg}$  and  $\text{SiO}_2/\text{TiO}_2$  molar ratio of the surface soil at each site in the Aroma transect. The  $\delta^{26}\text{Mg}$  are present as the mean  $\pm$  SE of three field replicates. No significant effect of the  $\text{SiO}_2/\text{TiO}_2$  molar ratio on surface soil Mg isotope compositions was observed.

**76**

**Figure 3.15** Variation of Mg concentrations in different soil layer at each site in the Aroma transect. Data are present as the mean  $\pm$  SE of three field replicates.

**77**

**Figure 3.16**  $\delta^{26}\text{Mg}$  as a function of MgO content (wt %) in surface soil samples from the Aroma transect. Open symbols represent the soil depth of 0-1 cm, while half-solid and solid symbols correspond to the soil depth of 1-5 and 5-10 cm, respectively.

**82**

**Figure 3.17** Evolution of Mg isotope compositions with soil profiles at different altitudinal level in the Aroma and Yungay regions. Error bar represents the analytical uncertainty based on repeated measurements (2SD, n > 3).

**83**

**Figure 3.18** Correlation between the CPA and  $\delta^{26}\text{Mg}$  of soil samples with profile in Aroma and Yungay regions. CPA refers to the Chemical Proxy of Alternation (Buggle et al., 2011), i.e. the molar ratio  $\text{Al}_2\text{O}_3/(\text{Al}_2\text{O}_3 + \text{Na}_2\text{O}) \times 100$ . Outlier samples in Aroma 1300 and Aroma 2000 were ticked out in the linear analysis.

**86**

# List of Tables

<b>Table 1.1</b> Summary on Mg isotope compositions of plants and corresponding growth mediums in laboratory and field scales.	<b>16</b>
<b>Table 2.1</b> Chemical compositions of nutrient solution.	<b>24</b>
<b>Table 2.2</b> Physicochemical properties of soil samples along with depth in two investigated fields. Data are given as mean value $\pm$ SE of three field replicates.	<b>28</b>
<b>Table 2.3</b> Procedure for Mg purification.	<b>33</b>
<b>Table 2.4</b> Magnesium concentrations and isotope compositions of the in-house soil standard and the NIST SRM 1575a Pine needles for the sample validation.	<b>35</b>
<b>Table 3.1</b> Mg concentrations and isotope compositions ( $\delta^{26}\text{Mg}$ ) of all plant organs with wheat plant growth.	<b>46</b>
<b>Table 3.2</b> Magnesium concentrations, stocks, and isotope compositions in both soil total pool and exchangeable pool in the studied non-limed and limed plots.	<b>63</b>
<b>Table 3.3</b> Plant dry biomass, Mg concentration, and isotope composition of plant organs in each plot.	<b>65</b>
<b>Table 3.4</b> Major element concentrations (wt %) expressed as oxides and Mg isotope compositions of surface soil samples in the Aroma transect.	<b>78</b>
<b>Table 3.5</b> Major element concentrations (wt %) expressed as oxides and Mg isotope compositions of soil samples with profile from the Aroma and Yungay regions.	<b>80</b>

# List of Abbreviations

a.s.l.	Above sea level
ATP	Adenosinetriphosphate
Ca <sup>2+</sup>	Calcium ion
CaCO <sub>3</sub>	Calcium carbonate
CIA	Chemical index of alteration
CO <sub>2</sub>	Carbon dioxide
–COOH	Carboxyl group
CPA	Chemical proxy of alteration
DSM3	Dead Sea Magnesium
equil	Equilibrium
exch	Exchangeable
H <sub>2</sub> O <sub>2</sub>	Hydrogen peroxide
H <sub>2</sub> SO <sub>4</sub>	Sulfuric acid
HCl	Hydrochloric acid
HF	Hydrofluoric acid
HNO <sub>3</sub>	Nitric acid
ICP-MS	Inductively Coupled Plasma - Mass Spectrometry
K <sup>+</sup>	Potassium ion
kin	Kinetic
MC-ICP-MS	Multicollector - Inductively Coupled Plasma - Mass Spectrometry
Mg	Magnesium
[Mg]	Magnesium concentration
MgCO <sub>3</sub>	Magnesium carbonate
MgO	Magnesium oxide

MgSO <sub>4</sub>	Magnesium sulfate
–NH <sub>2</sub>	Amino group
NH <sub>4</sub> <sup>+</sup>	Ammonium ion
–OH	Hydroxyl group
PFA	Perfluoroalkoxy alkane
PTFE	Polytetrafluoroethylene
SD	Standard deviation
SE	Standard error
–SH	Sulfonyl group
SiO <sub>2</sub>	Silicon oxide
SO <sub>3</sub>	Sulfur trioxide
SOC	Soil organic
SRM	Standard reference material
TF	Translocation factor
TiO <sub>2</sub>	Titanium dioxide

# Acknowledgement

I would like to give my sincere appreciation to my doctoral advisor Prof. Erwin Klumpp for all of his support during my Ph.D. study. All in all, I learnt a lot from Prof. Klumpp's gentle guide, sparkling ideas, and constructive comments. His serious attitude towards science would benefit me for the rest of my life.

I sincerely appreciate to my supervisor Dr. Bei Wu. Thanks to her careful guidance on how to be an excellent scientist on all aspects with great carefulness, from doing experiment to data processing, literature reading to paper writing. And thanks to her daily care which greatly helped me have a better life during the past four years in Jülich.

I would like to greatly appreciate my supervisors Prof. Wulf Amelung and Prof. Roland Bol. Special thanks to their regular discussion on my doctoral work, their guidance on my paper writing, and their support for my external studies in Amsterdam.

Many thanks to Prof. Andreas Schäffer at RWTH Aachen University for his valuable support and discussion on my doctoral exams and research work.

I am very grateful to Anne E. Berns, Claudia Walraf, Herbert Phillipp, and David Uhlig for their assistance in my experiment, sampling, discussion, and paper writing. And I would like to show my great thanks to my friends in IBG3 and in Jülich for their company.

Finally I would like to give my deepest gratitude to my family for their unconditional love and support me whatever I needed. And thanks to my friends in China who keep in touch with me and take care of my daily life.

I give my best wishes to all of you and hope all of you a wonderful life in the future.

# Curriculum Vitae

**Yi Wang**, Ph.D. student

Male; Date of Birth: May 1991

Institute of Bio- and Geosciences: Agrosphere (IBG-3), Forschungszentrum Jülich, D-52425 Jülich, Germany

Tel: +49(0)2461-61 9037

Email: [yi.wang@fz-juelich.de](mailto:yi.wang@fz-juelich.de)

## **EDUCATION**

10.2015–present PhD student, RWTH Aachen University / Forschungszentrum Jülich

09.2012–06.2015 M.E., Environmental Engineering, Zhejiang University, P.R. China

09.2008–06.2012 B.E., Environmental Engineering, Wuhan University of Technology, P.R. China

## **RESEARCH FIELD**

Biogeochemical cycle of Mg; Mg stable isotopes in terrestrial environment; Abiotic- and biotic-induced Mg isotope fractionation; mass spectrometry techniques (e.g. ICP-MS, MC-ICP-MS); theory and technology of contaminated soil remediation.

## **CONFERENCES**

- The 14th Stable Isotope Mass Spectrometry User Group (SIMSUG) meeting, in July 2017, Nottingham, UK. (Poster)
- International Conference Goldschmidt 2018, in August 2018, Boston, USA. (Poster)

## **SELECTED PUBLICATIONS**

**Wang, Y.**, Wu, B., Berns, A., Xing, Y., Kuhn, A., Amelung, W.. Magnesium isotope fractionation reflects plant response to magnesium deficiency: a greenhouse study with wheat. Submitted to Plant and Soil, 2019

**Wang, Y.**, Wu, B., Berns, A., Bol, R., Wombacher, F., Ellmer, F., Amelung, W.. Magnesium isotope signatures trace liming effects on crop nutrient uptake in long-term agricultural field trial. Submitted to Geoderma, 2019

**Wang, Y.**, Bol, R., Moradi, G., Wu, B., Sun, Y., van Hall, R., Amelung, W., Klumpp, E., Weathering degree in hyper-arid area of the Atacama Desert, Chile as revealed by magnesium isotope signatures. In preparation, 2019.

**Wang, Y.**, Peng, C., Fang, H.X., Sun, L.J., Zhang, H., Feng, J.B., Duan, D.C., Liu, T.T. and Shi, J.Y.. Mitigation Of Cu(II) Phytotoxicity to Rice (*Oryza Sativa*) In The Presence Of TiO<sub>2</sub> and CeO<sub>2</sub> Nanoparticles Combined With Humic Acid. Environmental Toxicology and Chemistry, 2015, 34(7): 1588-1596.